TWO-PHOTON 3D OPTICAL DATA STORAGE *VIA* FLUORESCENCE MODULATION OF FLUORENE DYES BY PHOTOCHROMIC DIARYLETHENES

by

CLAUDIA C. CORREDOR
B.S. Universidad Nacional de Colombia, 1994
M. S. University of Central Florida, 2003

A dissertation submitted in partial fulfillment of the requirements
for the degree of Doctor of Philosophy
in the Department of Chemistry
in the College of Sciences
at the University of Central Florida
Orlando, Florida

Spring Term
2007

Major Advisor: Kevin D. Belfield

ABSTRACT

Three-dimensional (3D) optical data storage based on two-photon processes provides highly confined excitation in a recording medium and a mechanism for writing and reading data with less cross talk between multiple memory layers, due to the quadratic dependence of two-photon absorption (2PA) on the incident light intensity. The capacity for highly confined excitation and intrinsic 3D resolution affords immense information storage capacity (up to 10^{12} bits/cm^3). Recently, the use of photochromic materials for 3D memory has received intense interest because of several major advantages over current optical systems, including their erasable/rewritable capability, high resolution, and high sensitivity. This work demonstrates a novel two-photon 3D optical storage system based on the modulation of the fluorescence emission of a highly efficient two-photon absorbing fluorescent dye (fluorene derivative) and a photochromic compound (diarylethene). The feasibility of using efficient *intermolecular* Förster Resonance Energy Transfer (RET) from the non-covalently linked two-photon absorbing fluorescent fluorene derivative to the photochromic diarylethene as a novel read-out method in a two-photon optical data storage system was explored.

For the purpose of the development of this novel two-photon 3D optical storage system, linear and two-photon spectroscopic characterization of commercial diarylethenes in solution and in a polymer film and evidence of their cyclization (O→C) and cycloreversion (C→O) reactions induced by two-photon excitation were undertaken.

For the development of a readout method, Resonance Energy Transfer (RET) from two-photon absorbing fluorene derivatives to photochromic compounds was investigated under one- and two-photon excitation. The Förster's distances and critical acceptor concentrations were determined for non-bound donor-acceptor pairs in homogeneous molecular ensembles. To the best of my knowledge, modulation of the two-photon fluorescence emission of a dye by a photochromic diarylethene has not been reported as a mechanism to read the recorded information in a 3D optical data storage system. This system was demonstrated to be highly stable and suitable for recording data in thick storage media. The proposed RET-based readout method proved to be non-destructive (exhibiting a loss of the initial fluorescence emission less than 20% of the initial emission after 10,000 readout cycles). Potential application of this system in a rewritable-erasable optical data storage system was proved.

As part of the strategy for the development of diarylethenes optimized for 3D optical data storage, derivatives containing π-conjugated fluorene molecules were synthesized and characterized. The final part of this reasearch demonstrated the photostability of fluorene derivatives showing strong molecular polarizability and high fluorescence quantum yields. These compounds are quite promising for application in RET-based two-photon 3D optical data storage. Hence, the photostability of these fluorene derivatives is a key parameter to establish, and facilitates their full utility in critical applications.

To Celmira Martinez and Alonso Corredor- my guide

To Luz, Alvaro, Daniel and Elisa Corena and Lina Corredor- my pride and joy

To Martin Nunez- my soulmate

To Guillermo Anzola- my inspiration

ACKNOWLEDGMENTS

I would like to thank my advisor, Dr. Kevin D. Belfield, for his wise advice and guidance. I am deeply indebted for his personal support during good times and difficult times. I appreciate his nomination to the Graduate Student Summer Research Fellowship at UCF and the Summer Research Scholarships that gave me economic support during the months that I did not teach.

It was a great pleasure to be part of the photochemistry, polymer, organic and materials chemistry Group at UCF. I enjoyed working with my lab-coworker and best friend Alma Morales including numerous passionate discussions and continuous exchange of ideas. I am thankful to present and past group members Sheng Yao, Katherine J. Schafer-Hales, Ciceron Yanez, Carolina Andrade, Shilong Bao, Stephen Andrasik, Sanchita Biswas, Mohammed Daoudi, Dao Nguyen, Mykhailo V. Bondar, Zhenli-Huang, Gheorge Luchita, for a friendly collaborative atmosphere.

This dissertation was the result of a truly interdisciplinary and collaborative effort. I want to express my sincere thanks to Alma Morales and Sheg Yao for providing me the fluorene derivatives studied in this dissertation. I am deeply indebted to Mykhailo V. Bondar from whom I learned a lot. His way of explaining complicated concepts in an understandable manner is remarkable. It was him who helped me with photophysical experiments and did experimental work on the two-photon absorption measurements. I am going to miss his coffee breaks. Thank you, Mike!

I also thank Zhenli-Huang for his efforts on refining and updating the two-photon laser scanning microscope for our 3D data storage experiments and for his work in 3D data storage and imaging simulations. I would like to thank F. E. Hernandez and I. Cohanoschi at the Plasmonic and Materials Design Laboratory at UCF for Z-scan experimental data on diarylethene **2** and for fruitful discussions. Especial thanks to Michael Sigman at the Forensic Trace Analysis Laboratory at UCF for their collaboration in the analysis of photoproducts of fluorene derivatives by HPLC-MS. All the collaborations have truly been rewarding and contributed to the interdisciplinary nature of this work.

I wish to thank the Bristol-Myers Squibb Pharmaceutical Research Institute for its generous Doctorate Fellowship. Without the BMS support it would had been imposible to return to UCF to finish my degree. Thank you very much for giving me the time and the economic support that I needed. I would like to thank past and present members of the Institute that believed in my potential: Paul Kurtulik, Joel Young, Mark Powell, Frank Tomasella, Tom Raglione, David K Lloyd and Ruben Lozano.

TABLE OF CONTENTS

LIST OF FIGURES

LIST OF TABLES

LIST OF ACRONYMS/ABBREVIATIONS

δ_{2PA}	Two-photon absorption cross-section
1PA	One-photon absorption
1PE	One-photon excitation
2PA	Two-photon absorption
2PE	Two-photon excitation
3D	Three dimensional
A	Acceptor
AP	Anti-parallel
BER	Bit Error Rate
C or C-form	Closed isomer of a diarylethene
CD-R	Compact Disk Recordable
CD-RW	Compact Disk Rewritable
D	Donor
DIC	Diferential Interfereance Contrast
DVD	Digital Versatile Disk
GB	Gigabyte
GM	Göppert-Mayer or 1×10^{-50} cm^4 sec photon^{-1} molecule^{-1}
HCD	Hot carrier diffusion
NA	Numerical Aperture
NLO	Nonlinear optics
O or O-form	Open isomer of a diarylethene

P	Parallel
PMMA	Poly(methylmethacrylate)
RET	Förster Resonance Energy Transfer
TB	Terabyte

CHAPTER 1. INTRODUCTION

The main motivation for the development of digital data storage (CD-R, CD-RW) has been the improvement in play-back quality and increased storage capacity. Two approaches to increase storage capacity are the arrangement of several layers in a DVD (such as the DVD 18 format with 4 layers) and the reduction of the bit size by using laser diodes with emission wavelengths in the blue (such in the case of the Blue-Ray® disc, the new optical disc format developed by the Blu-ray Disc Association). The use of blue laser diodes is based on the observation that, with conventional optics, a laser beam spot size is limited by the diffraction limit and dependent on the wavelength (λ) and the numerical aperture (NA) [1, 2]. However, both approaches have their limitations. In the first approach, the construction of several layers requires the arrangement of bubble-free bonding layers that are difficult to produce and penetration depth of the light is limited [1]. In the second approach, the high optical excitation energy and small optical focus size characteristic of blue laser data storage formats lead to significant hot carrier diffusion (HCD) prior to the energy transfer to the Ge-Sb-Te crystal lattice. Therefore, the fundamental limit of resolution for re-writable optical storage systems is no longer determined by the laser focus size alone, but also by additional nonequilibrium HCD effects [3].

One of the most attractive alternatives to increase storage capacity is to store bits throughout all three dimensions of the storage material (multilayer storage) by the use of two-

photon absorbing optical materials [4-7]. Two-photon 3D memories offer increased storage capacity by using volume storage, in a manner similar to the multilayer optical disk systems but with the advantages of simpler media fabrication, many more layers, and potentially lower raw bit error rates (BER) [7a]. Two-photon optical materials nonlinearly absorb the incident light, confining the absorption at the focus to a volume of order λ^3 (where λ is the laser wavelength), thus affording immense information storage capacity (researchers in 3D bit optical data storage have experimentally achieved GBs of information per disk, the theoretical capacity being calculated to be 2.5 TB). Section 2.1 of the background chapter will introduce the phenomenon of two-photon absorption and its contribution to recent advances in high density 3D optical data storage.

Multilayer two-photon data storage has been demonstrated by using photochromic compounds [4, 7]. Photochromism is a reversible transformation of a single chemical species between two states having different absorption spectra, such change being induced in one or both directions by electromagnetic radiation. Among many known photochromic systems, diarylethenes (developed by Irie *et. al.* [8] and Lehn *et. al*. [9]) are promising candidates for applications because of their excellent fatigue resistance, picosecond switching time, high photoisomerization quantum yields, and absence of thermal isomerization [10]. Although extensively characterized by one-photon excitation (1PE), much less is known about the photochromism of diarylethenes induced by two-photon excitation (2PE). 2PE can be used to induce photochromic transformations under intense laser excitation (such as mode-locked femtosecond Ti:sapphire laser irradiation). In this case, photochromic molecules simultaneously absorb two photons, and the transition probability is proportional to the square of the incident

laser intensity. Section 2.2 will give an account of the photochromic materials (especially diarylethenes) used in two-photon 3D optical data storage.

An important requirement of 3D optical data storage is a non-destructive read-out method. Section 2.3 will discuss different reading methods that do not erase the stored information, and the advantages of fluorescence read-out. The conceptual reading/writing system based on *intramolecular* Förster Resonance Energy Transfer (RET) from a donor to an acceptor to build fluorescent molecules is discussed in detail. The feasibility of using efficient *intermolecular* RET from non-covalently linked two-photon absorbing fluorescent dyes to photochromic diarylethenes as a novel method to retrieve the stored information in a data storage system is explored. Section 2.4 introduces the fluorene derivatives used as fluorescent donors in this novel storage system. A summary of the extensive nonlinear optical (NLO) data collected on these π-conjugated compounds will be presented.

1.1 Research Objective

The purpose of this research is to establish the foundation of a novel two-photon 3D optical storage system based on the modulation of the fluorescence emission of a fluorene derivative by a photochromic diarylethene (nondestructive readout). This research effort was comprised of several steps. First, a complete photophysical characterization of two commercial diarylethenes under one- and two-photon excitation was pursued. Studies in this phase include determination of the cyclization ($\Phi_{O\rightarrow C}$) and cycloreversion ($\Phi_{C\rightarrow O}$) reaction quantum yields of diarylethenes at different excitation wavelengths, two-photon absorption cross-sections (δ_{2PA}) of

their open (**O)** and closed (**C)** photoisomers, two-photon isomerization in solution and in polymer films, fluorescence quantum yields, steady-state excitation anisotropy, and photochemical stability.

Second, the preparation of more efficient 2PA photochromic diarylethenes was attempted in order to increase their two-photon absorption cross-sections (δ_{2PA}). For this purpose, two strategies were investigated: 1) chemical modification of the photochromic molecule by covalent attachment of an efficient 2PA chromophore (fluorene derivative) to the photochromic diarylethene and 2) use of intermolecular RET from an efficient 2PA fluorene derivative to the photochromic diarylethene (without chemical modification) in order to increase the nonlinear optical properties of the diarylethene. Results from these studies provide guidance for subsequent studies in polymer films. Two-photon 3D optical data storage based on photochromic diarylethenes and fluorene derivatives was demonstrated. Possibilities for recording data by two-photon excitation in polymer composites containing diarylethenes were explored. Appropriate non-destructive readout methods were evaluated. In particular, the feasibility of using RET from non-covalently attached fluorene derivatives to diarylethenes as a novel readout method in 3D optical data storage was demonstrated. Suitable fluorene derivatives were selected for RET studies, based on their δ_{2PA} values, fluorescence quantum yields, and the degree of overlap of their emission spectra with the absorption spectra of the isomers of the photochromic diarylethenes. Finally, for practical applications of fluorene derivatives in 3D optical data storage, high photostability under intense laser excitation is required. Single- and two-photon photostability studies of two new fluorene derivatives with potential practical applications in 3D optical data storage are presented.

1.2 Research Outline

This work is structured as follows: a summary of the recent contributions of two-photon absorption to high density optical data storage are presented in the background chapter (chapter 2). This chapter also gives background information on diarylethenes for applications in 3D optical data storage and different non-destructive read-out methods, such as fluorescence read-out. Applications of Förster Resonance Energy Transfer (RET) as a mechanism to read stored information are also presented in this chapter. This will lead into chapter 3 which provides details of the photophysical characterization and photochemical dynamics of two diarylethenes under one- and two-photon excitation. Chapter 4 will present the synthesis of diarylethenes containing fluorene moieties, including the synthetic methodology and details of their characterization, followed by results on an additional strategy to enhance the nonlinear optical properties of diarylethenes by using intermolecular Förster Resonance Energy Transfer in Chapter 5. Chapter 6 provides experimental results on a novel RET-based two-photon 3D optical data storage system with non-destructive readout *via* fluorescence modulation of an efficient fluorene dye by a photochromic diarylethene. Photostability studies of two new fluorene derivatives, attractive for applications in RET-based two-photon 3D optical data storage are presented in chapter 7. Chapter 8 provides a synopsis of results and suggest some future directions for research in this area.

CHAPTER 2. BACKGROUND

2.1 Two-Photon Absorption and its Contribution to Recent Advances in High Density 3D Optical Data Storage

Two-photon absorption (2PA) involves the concerted absorption of two photons that combine to produce an electronic excitation that is conventionally caused by one-photon absorption (1PA) at a correspondingly shorter wavelength. Under suitable excitation conditions, the initial excitation transition that occurs in one-photon excitation (1PE) may also proceed via a two-photon process. The history of 2PA began in 1931 when Göppert-Mayer predicted the possibility of the 2PA [11]. It was observed experimentally in the 1960´s owing to the advent of high-intensity lasers [12]. It was not until the mid-1990´s, with the increased availability of high-intensity lasers and the discovery of new chromophores exhibiting very large effective 2PA cross-section (δ_{2PA}) values, that the door to 2PA applications in photonics and biophotonics was opened. δ_{2PA} measures the efficiency of a molecule to absorb two photons under intense pulsed laser excitation. δ_{2PA} is defined as the two-photon absorption cross-section and is typically expressed in Göppert-Mayer or GM units ($1\ GM = 10^{-50}\ cm^4\ sec\ photon^{-1}\ molecule^{-1}$), in recognition of Maria Göppert-Mayer. The two-photon phenomenon is being pursued in many fields such as two-photon optical power limiting [13], fluorescence microscopic imaging [14], 3D microfabrication [15], and photodynamic therapy [16].

The 2PA process depends on both the spatial and temporal overlap (proximity) of the incident photons. In the single-photon process, the rate of photon absorption is directly proportional to the incident intensity (I). Contrary to this, as two photons are required in the 2PA process, the rate of absorption takes on a quadratic dependency on the incident intensity (I^2). This quadratic, or nonlinear, dependence of 2PA on the intensity of the incident light has substantial implications, as demonstrated in our laboratory in Figure 2.1. The quartz cuvette in Figure 2.1 contains a fluorescent chromophore especially designed to be a good two-photon absorber (fluorene **1,** Figure 2.1). The output from a tunable Coherent Mira 900 Ti:Sapphire laser (tuned to 760 nm, 200 fs pulse width, 76 MHz repetition rate) was focused into the cuvette by a 10x objective (upper side), providing 2PE. A second-harmonic generator was used to double the frequency of 760 nm light (λ_{exc}: 380 nm), which was used as the 1PE source (as shown in the lower part of the cuvette).

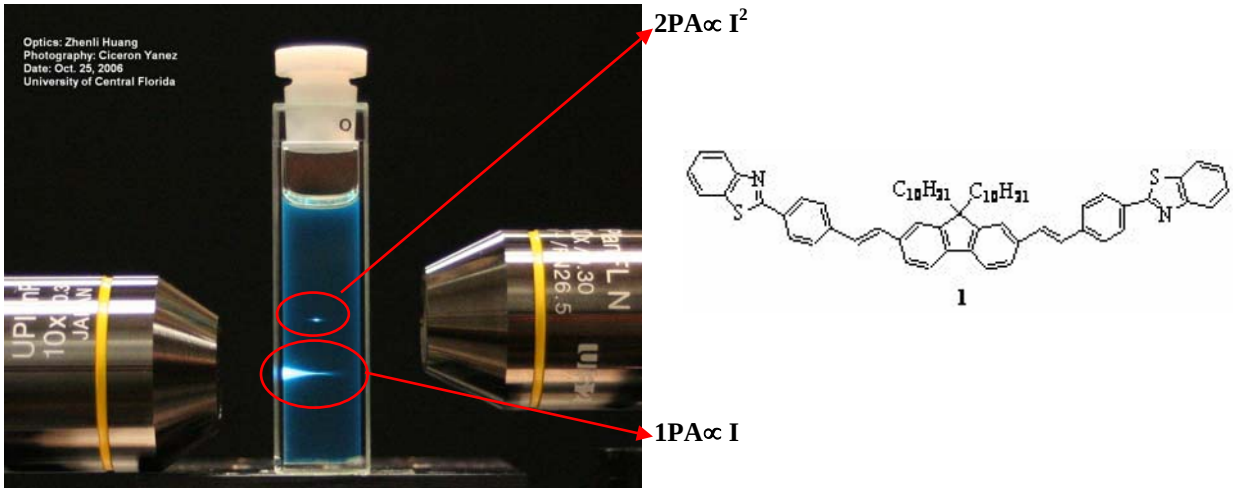

Figure 2.1. Photograph demonstrating the spatial selectivity of one-photon excitation vs. two-photon excitation in a CH_2Cl_2 solution of fluorene **1**.

Due to the direct proportionality of the rate of photon absorption on the incident intensity, linear excitation is not a highly localized process and significant absorption occurs all along the

path of a focused beam (Figure 2.1, bottom). This can lead to excitation outside the focal volume. Moreover, excitation using UV light can be damaging to polymers and provides poor penetration through thick samples because of light scattering. Nonspecific excitation of the sample produces background noise and crosstalk and gradual depletion of the photochrome, associated with increased fatigue in photochromic materials.

In a two-photon process, the extent to which the excitation falls off with distance from the focal point, is dramatically improved due to the quadratic dependence of the absorption probability on the light intensity in combination with the strong focusing of the beam (confining the majority of all excitations to a volume of $<1\ \mu m^3$ around the focal point). Irradiance in the vicinity of the focus falls off as $I \propto z^{-2}$ (where z is the axial propagation distance) which implies that 2PA decreases as z^{-4} [17]. Some advantages of the use of two-photon excitation are: a capacity for highly confined excitation, deep penetration depth (using longer wavelength light) intrinsic three-dimensional spatial resolution, random access, parallel addressing, immense information storage capacity (up to 10^{12} bits/cm^3), very fast optical writing and reading speed, minimal crosstalk between adjacent bits, high reading sensitivity, and low cost [4-7, 17].

In comparison with 1PE, simultaneous 2PE generally has a relatively small cross-section due to the low probability that two photons will be simultaneously absorbed by a media. This probability may be dramatically increased with the use of a source having a high irradiance, such as the mode-locked titanium:sapphire laser. Comprehensive treatment of the physics of non-linear optics (NLO) originating from interaction of atoms and molecules with light can be found elsewhere [18].

The first attempt of the application of 2PE in 3D optical data storage was reported in 1989 by Parthenopolus and Rentzepis using a spirobenzopyran/polymer system [4].

Spirobenzopyran is a photochromic molecule which normally absorbs only in the UV region of the spectrum, and upon excitation, transforms to a merocyanine form which absorbs in the green-red region of the spectrum (Figure 2.2). The merocyanine form also emits red-shifted fluorescence when excited with green light. Two-photon recording was accomplished by excitation of the spirobenzopyran form provided by the simultaneous absorption of one photon at 1064 nm and one at 532 nm (nondegenerate 2PA). The two wavelengths were obtained from a mode-locked and frequency doubled Nd:YAG laser.

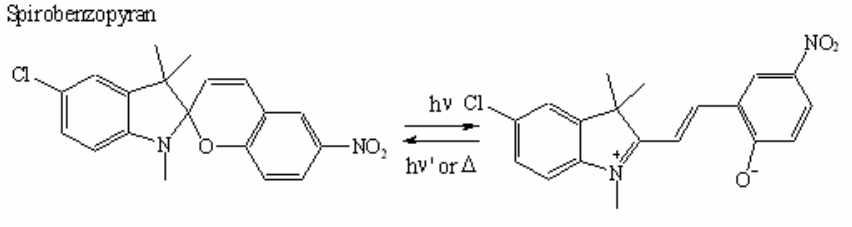

Figure 2.2. Photoisomerization of a spirobenzopyran derivative

Early photochromes fell far short of satisfying the requirements of the computer industry due to poor stability and back (thermal) isomerization in the dark. Besides, methods to retrieve the written information tended to cause its destruction. Consequently, a large research effort was undertaken by many groups to identify new photochromic systems that could better address the demands of the data storage industry. Since Rentzepis's original paper, a large number of articles and reviews have been published that propose materials that may be used in two-photon volumetric optical data storage. Denk *et al.* demonstrated recording by two-photon photobleaching in a latex bed and read-out by using a two-photon confocal microscopy [14a]. Strickler and Webb demonstrated optical data storage by means of two-photon photoactivation of a fluorescent dye that was non-fluorescent until photochemically modified [19].

The same authors later showed 3D recording by two-photon induced photopolymerization of a liquid acrylate ester blend [5]. Ueki and Kawata *et al.* proposed a new technique for achieving 3D bit-type optical memory recording and reading in photorefractive materials [20]. Toriumi *et al.* induced two-photon recording onto a PMMA containing a photochromic diarylethene by laser excitation [21]. Day and Gu *et al.* reported the use of photorefractive polymers in erasable-rewritable 3D optical data storage [22]. Pudavar *et al.* showed two-photon recording and two-photon read-out in a PMMA polymer block doped with a two-photon chromophore (AF240) [23]. Work by Belfield et al. demonstrated two-photon write-once read-many (WORM) data storage by 2PE of a photoacid generator and two-photon fluorescent readout of the neutral and protonated 2PA fluorescent dyes [24]. Continued work by Rentzepis followed this by demonstrating a WORM material consisting of Rhodamine B base dye precursor and a two-photon acid photogenerator (AG) dispersed in PMMA, and a rewritable 3D data storage based on 2-indolylfulgides [7].

An illustration of bit-oriented 3D optical memory is shown in Figure 2.3. Conceptually, a volumetric media contains a homogeneous dispersion of a data storage chromophore. The writing of data is achieved by focusing one or more light beams at a given point in the media, causing a change in state (switching) of the data storage chromophores at that point (and only at that point). By 3D scanning of the focus spot in the medium, a data bit is recorded in the medium in three dimensions. Data is then read back by similarly probing desired areas in the media in such a way that written and unwritten forms of the chromophore will return different signals (such as fluorescence, phosphorescence, burning or destruction of the original forms or refractive index change) [4,7,10] .

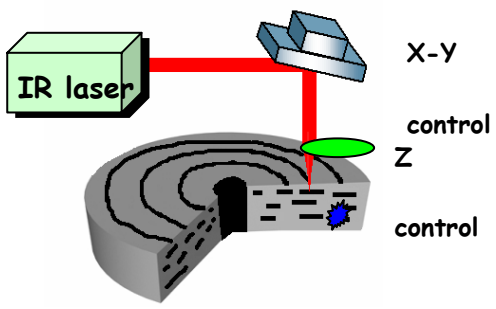

Figure 2.3. Illustration of bit-oriented 3D optical memory.

2.2 Diarylethenes for Applications in Two-Photon 3D Optical Data Storage

Photochromism is referred to as a light-induced reversible transformation of a chemical species between two isomers having different absorption spectra. The two isomers differ from one another not only in the absorption spectra but also in various physical and chemical properties such as refractive indices, dielectric constants, oxidation–reduction potentials and geometrical structures [25]. For utilization in optical storage media, one of the isomers is assigned to "0" in the computer binary code while the other form becomes "1". Hirshberg *et al.* first demonstrated reversible change in the molecular structure of spiropyrans during light irradiation and proposed a memory model based on this change [26]. Many other compounds exhibit photochromism including spirooxazines, fulgides, and azobenzenes. (Figure 2.4) [27].

In spite of multiple studies, organic photochromic compounds have found little application in commercial optical data storage due to serious problems with their thermal and photochemical stability. For example, many spirobenzopyrans, spironaphthooxazines, and naphthopyrans undergo thermally reversible photochromic reactions (the photogenerated isomers return to the initial isomers even in the dark) [25]. On the contrary, thermally irreversible photochromic compounds are potential candidates for optical memory. Diarylethenes and

furylfulgides are among photochromic compounds that exhibit thermally stable photochromic reactions. Among the wide variety of thermally irreversible photochromic molecules, diarylethenes (Figure 2.4) are, perhaps, the most promising ones.

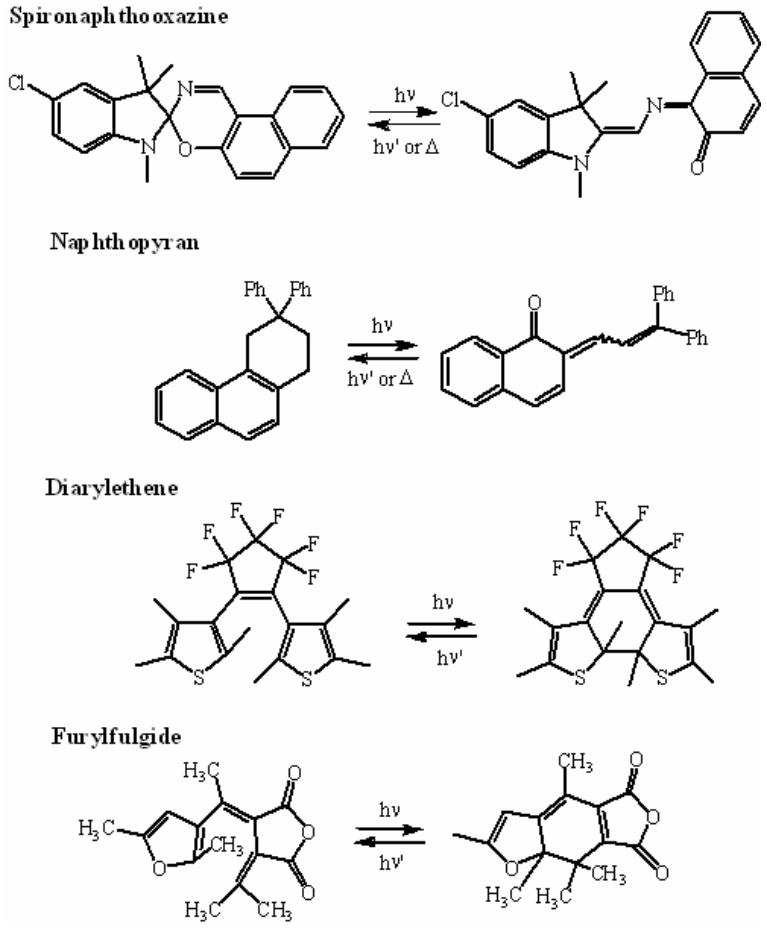

Figure 2.4. Typical photochromic compounds

Diarylethenes have been found to display highly desirable photochromic properties: excellent fatigue resistance, short response time, high quantum yields, absence of thermal isomerization, and large changes in the absorption wavelength between the two isomers. Some diarylethenes have no thermochromicity even at 300 °C, the colored forms are stable for more than three months at 80 °C, and the cyclization and cycloreversion reactions can be repeated

more than 10^4 times while keeping adequate photochromic functions [28]. Diarylethenes have being extensively studied over the last two decades. Several excellent reviews have been written considering the molecular design, synthesis, properties and applications of diarylethenes in memories and switches [8, 10, 25, 28, 31].

In this section important photophysical characteristics of two particular diarylethenes, pertinent to the development of the two-photon 3D optical data storage system proposed in this dissertation, are discussed. One of the most studied diarylethenes is 2,3-bis(2,4,5-trimethyl-3-thienyl)-2,5,-furandione (**1**) (Figure 2.5a) [28] . The absorption spectrum of the open (**O**) and closed (**C**) isomers of **1** are shown in Figure 2.5b. The **O** isomer is transparent in the visible spectral range and undergoes electrocyclic ring closure under UV irradiation, resulting in the formation of the colored **C** form [28b].

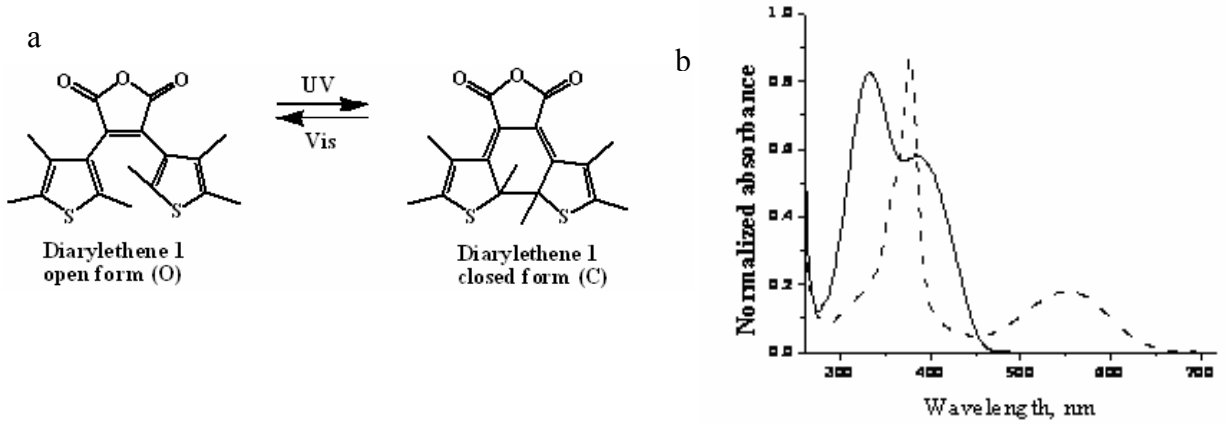

Figure 2.5. a). Schematic diagram of the cyclization and cycloreversion photochromic (isomerization) reactions of **1** b. Absorption spectra of the **O** (—) and **C** (---) isomers of diarylethene **1** in hexane.

The cycloreversion reaction **C** → **O** proceeds under visible and UV light irradiation resulting in the "bleached" **O** isomer. The photochromic electrocyclic reaction of this class of photochromic compounds is understood to obey the Woodward–Hoffmann orbital symmetry rules [8]. As predicted by these rules, ring opening and ring closure reactions of diarylethene **1**

occur photochemically in the conrotatory mode, while the thermally induced ground-state reaction, predicted to take place in the disrotatory mode, is sterically hindered [8].

A measurement of the efficiency of the photocyclization and cyclization reactions is given by the respective quantum yield. The *quantum yield* is defined as the number of photoconverted molecules of the respective isomer (open or closed) per number of photons absorbed [8]. Irie *et al.* measured the photocyclization ($\Phi_{O\rightarrow C}$) and cycloreversion ($\Phi_{C\rightarrow O}$) quantum yields along with the fluorescence properties of both isomers in different solvents [29-30]. These studies revealed that at least two types of conformers exist in the excited state of diarylethene **1**. One was described as a more planar conformer with C_2 symmetry (so-called "antiparallel" **AP**) which undergoes ring closure, whereas another one is a twisted conformer with S_2 symmetry (so-called "parallel" **P**) which possesses intramolecular charge transfer character and exhibits no photochromic transformation (Figure 2.6) [29]. The relative amount of **P** and **AP** conformers in the ground state depends on solvent polarity, with less polar solvents corresponding to an increased amount of **AP** conformer [29, 30].

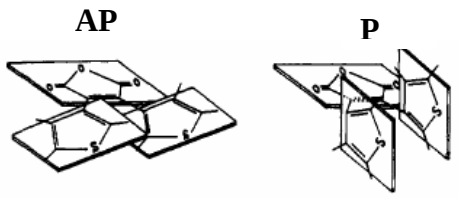

Figure 2.6. "Antiparallel" (**AP**) and "parallel" (**P**) conformers of diarylethene 1

Theoretical studies by Cho and Cheong revealed several similar types of conformers can exist in the ground state of **1**, and only **AP** conformers undergo photochemical reaction [28c]. In general, the population ratio of the two conformations is 1:1. Therefore, the cyclization quantum yield cannot exceed 0.5 [8].

Photochromic reactions are always accompanied by rearrangement of chemical bonds. During the rearrangement, undesirable side reactions may occur to some extent. Irie *et al.* defined *fatigue resistance* as the number of photochromic cycles at which the absorbance change of the open-ring isomer (or the closed-ring isomer) decreases to 80% of the first cycle. The best diarylethene derivatives can be cycled 10,000 times with no more than 20% decrease of the initial absorbance [8]. Thus, nondestructive readout is defined as loss of no more than 20% of the original properties after 10,000 readout cycles. Irie *et al.* reported more than 100 photocyclization and cycloreversion cycles of diarylethene **1** under 1PE in air (480 cycles in vacuum) [28b]. Miyasaka *et al.* reported the direct observation of the photochromic transformation of diarylethene **1** under one-photon excitation, and time constants of the ring-closure and ring-opening processes of < 10 ps [29a].

Uchida *et al.* [31] reported studies on diarylethene **2** (1,2-bis (2-methylbenzo[b]thiophen-3-yl) hexafluoro-cyclopentene), depicted in Figure 2.7. Diarylethene **2** is especially well suited for data storage due to its high cyclization and cycloreversion photoisomerization reaction quantum yields ($\Phi_{O\rightarrow C}$: 0.35 at 313 nm and $\Phi_{C\rightarrow O}$: 0.35 at 517 nm in hexane). Diarylethene **2** is thermally stable (the **C** form is stable for more than 12 h at 80 °C) and can be cycled more than 10,000 times [8]. Diarylethene **2** was found photochemically inactive in the single crystalline phase [31]. Neither the **O** nor the **C** forms of **2** displayed significant fluorescence (Φ_f: open form = 0.02 and closed form < 0.02) [31a]. As a consequence, fluorescence-based read-out systems are not viable. However, Jeong *et al.* recently synthesized sulfonyl derivatives of diarylethene **2** ($BTFO_4$) that have high fluorescent quantum yield upon photocyclization [31d].

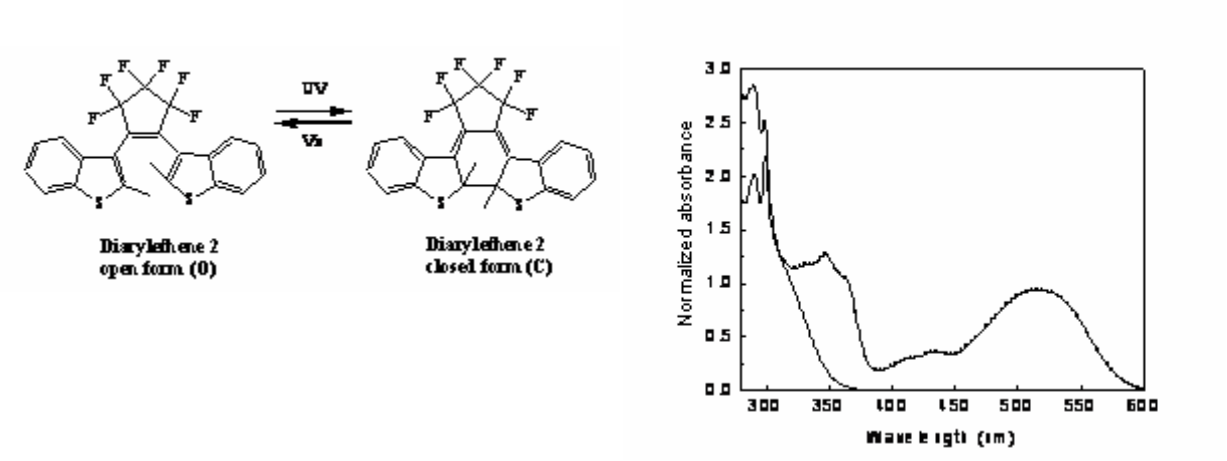

Figure 2.7. a). Schematic diagram of the cyclization and cycloreversion photochromic (isomerization) reactions of **2** b. Absorption spectra of the **O** (—) and photostationary state (a mixture of open and closed forms) (■) of diarylethene **2** in hexane.

2.2.1 Nonlinear Properties of Diarylethenes

Although extensively characterized by linear excitation, much less is known about the nonlinear properties (NLO) properties of diarylethenes. Atassi *et al.* determined the product of the dipole moment, μ, and first order hyperpolarisability, β (βμ), of the isomers of diarylethene **2** in their open and closed forms ($\beta\mu_{open}$= 13x10^{-48} esu, $\beta\mu_{closed}$= 55x10^{-48} esu), and showed a large increase of βμ in going from the **O** to the **C** isomer [32a]. Experimental evidence of two-photon isomerization of diarylethene **1** in PMMA films was reported by Sekkat *et al.* [33]. The same dye-doped photochromic medium was investigated under two-photon excitation by Toriumi *et al.* for the development of a reflection confocal microscopy-based readout system for 3D optical memory [21b]. Although some progress had been made in the search for a suitable diarylethene-based chromophore for 3D data storage, the key element of two-photon excitation had not been addressed. Two-photon excitation is a weak phenomenon, and most organic molecules do not possess a suitable 2PA cross-section (δ_{2PA}) to allow their substantial excitation by weak lasers

(such as are available for use in consumer electronics devices). For efficient recording by two-photon excitation, the write photoisomer should have a high δ_{2PA} at the writing wavelength and high photoisomerization quantum yield for the write to read conversion. Therefore photochromes would need to be re-engineered to be useful in real-world devices, but it was only recently that chemists began to understand how molecular design may be used to optimize third-order nonlinear optical properties [17]. As demonstrated by Irie *et al.*, a method to develop more efficient 2PA photochromic materials is to covalently attach an efficient 2PA chromophore to a photochromic molecule [34]. However, covalent attachment of the 2PA chromophore often perturbs the electronic distribution and conformation of the photochrome, resulting in loss of desirable photochromic properties or decreased cyclization and cycloreversion quantum yields relative to the parent diarylethene. Another difficulty is the low solubility of some derivatives in useful organic solvents, posing a challenge in device fabrication [34]. Clearly, a deeper understanding of the two-photon properties of diarylethenes is required.

2.3 Read-Out Systems in Optical Data Storage: Applications of Förster Resonance Energy Transfer (RET)

As described in section 2.1, the stored information is accessed by detection of a property characteristic of the written form such as fluorescence, phosphorescence, refractive index change, optical rotation, IR absorption, etc. [4,7,10]. An important issue that impaired the progress of 3D photochromic data storage to date is the matter of the ‘‘destructive reading’’ of data. In order to have a truly “non-destructive” readout method, the write, read and erase wavelengths should be well separated from each other [7]. For example, using luminescence readout, the wavelengths of light used to produce the luminescence (excitation wavelengths $\lambda_{exc.}$)

and the resulting emission wavelengths ($\lambda_{em.}$) must reside outside the spectral regions where the photochromic reactions are induced.

Besides the issue of the destructive reading, some readout methods have characteristic disadvantages. Changes in refractive index have the disadvantage that the changes between both isomers are small, severely limiting sensitivity. IR readout has the disadvantage that the IR bands have normally very weak absorption cross sections, and polymer matrices usually absorb at the excitation wavelengths, also decreasing the readout sensitivity [35a]. Among many different read-out methods, photoluminescence is one of the most attractive ones because of the high sensitivity afforded by fluorescence technologies and the ability for non-destructive "all optical" read-write-erase cycles. In general, the photochromic parent compounds do not display significant luminescence, but several systems appended with various chromophores have shown reversible changes in emission intensity (fluorescent switch) [35].

Fluorescent switches are composed of two distinct molecules that are chemically bonded to each other to form a single molecule with unique properties. One component is a photochromic compound (for example a fulgimide or a diarylethene) and the other is a strongly fluorescing dye (for example an oxazine or an anthryl). In this approach, the composite molecule is specifically designed and synthesized to display, under specific conditions, both the photochromic functions of the first component and the fluorescence properties of the dye. Excellent reviews on the topic by Irie and Tian have been recently published [8, 35c, 35d]. An example of the versatility of this approach was illustrated by Liang *et al.*. They synthesized a fluorescent switch by using a photochromic N-(4-aminophenyl) fulgide, and a highly fluorescent oxazine dye (Figure 2.8a) [35a].

a

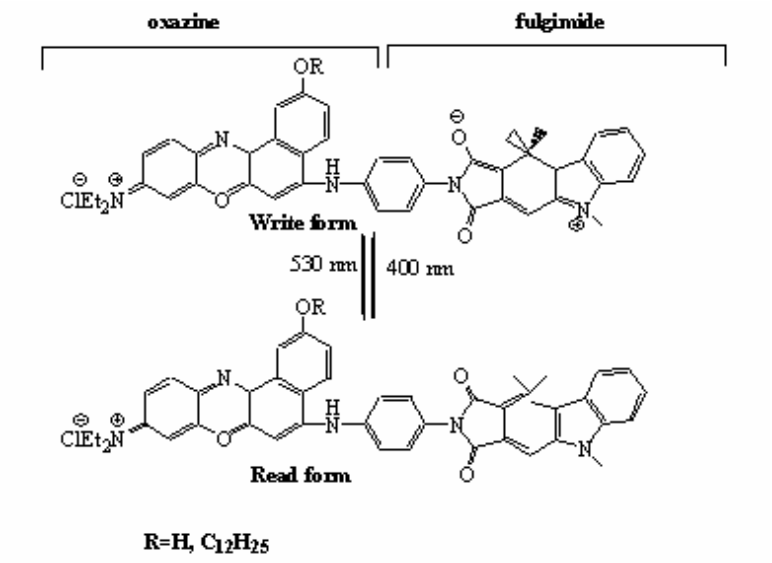

b

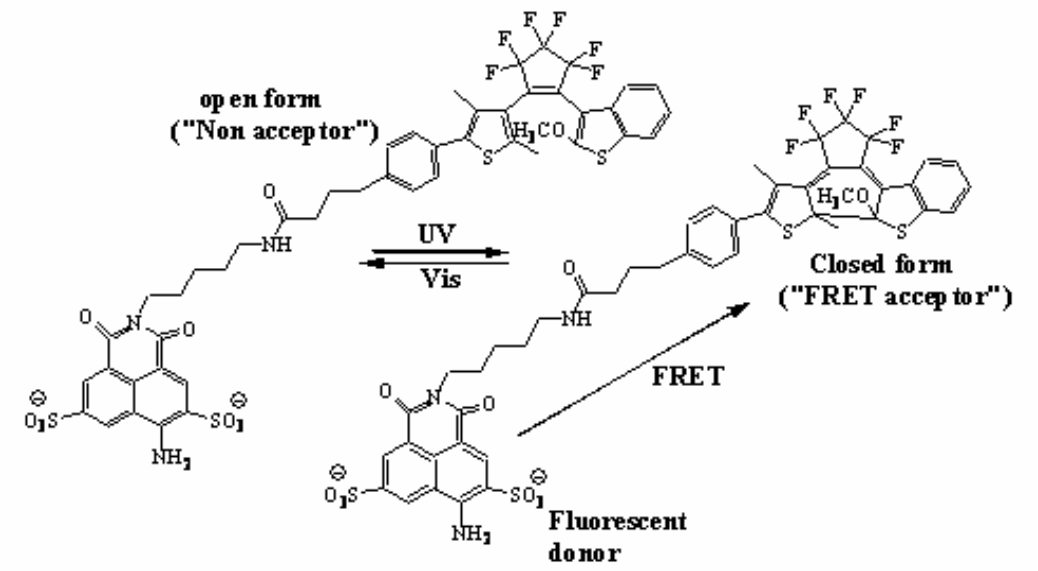

Figure 2.8. a) Structure of the composite molecule of N-(4-aminophenyl)fulgide and oxazine dye in their read and write forms. b) Lucifer Yellow (donor) covalently attached to a bis(thienyl)ethane (acceptor) through a spacer

To store information, the polar, **C** form of the photochromic component is illuminated with 530-nm light, which converts it to the open, nonpolar form. The information is accessed by excitation at the 650-nm band of the oxazine dye component, causing the dye to fluoresce.

However, the dye emits intense fluorescence in a nonpolar environment, which is attained only when the fulgimide component is in its open, nonpolar structure. A key aspect in this design is to attach dyes that display fluorescence that do not overlap the absorption spectrum (if fluorescence overlaps the absorption the energy can be reabsorbed producing destructive readout). Förster Resonance Energy Transfer (RET) from a fluorescent donor to a photochromic acceptor has also been proposed in order to prepare fluorescent switches [36]. RET is a physical process by which energy is transferred nonradiatively from an excited molecular fluorophore (donor, D) to another chromophore (acceptor, A) *via* long-range dipole-dipole coupling. The RET efficiency varies with the 6th power of the donor-acceptor separation over the range of ~1.5-10 nm, a range of distances corresponding to most biologically significant molecular interactions within cells [36, 37]. As an example of a fluorescent switch, Jares-Erijman and Irie *et al.* (2002) used Lucifer Yellow I (D) and bis(thienyl)ethane (A) to build fluorescent molecules in order to develop a general conceptual reading/writing system based on RET, where they found that the single-photon fluorescence emission of D is reversibly modulated by cyclical transformations of the photochromic A upon irradiation of appropriate UV and visible light, respectively (Figure 2.8b) [36a].

Instead of chemical modification, an intriguing alternative is to employ a mixture of the fluorescent dye and the photochromic compound. Kozlov and Castellano (2004) [36b] demonstrated the ability of this approach to produce fluorescent switches by using the **O** and **C** isomers of the diarylethene **2**, as a photochromic energy transfer quencher of the metal-to-ligand charge transfer (MLCT) based luminescence in $[Ru(dpp)_3]^{2+}$ (dpp : 4,7-diphenyl-1,10-phenanthroline). Only the **C** isomer of diarylethene **2** serves as a quencher for the MLCT luminescence, and the read (390 nm), write ($\lambda < 360$ nm), and erase ($\lambda > 500$ nm) wavelengths

are well-separated. Brousmiche (2003) and Gvishi (2005) suggested the use of RET in order to enhance the nonlinear optical performance of organic materials [37]. The approach consists of the use of a mixture of an efficient 2PA dye and photochromic molecules. The 2PA dye serves as a donor (**D**) and the photochromic compound as an acceptor (**A**), combining efficient two-photon excitation with intermolecular RET to a photochromic compound. Brousmiche *et al.* demonstrated RET from a two-photon absorbing chromophore to a nile red derivative when excited by either high-intensity IR (two-photon) or UV-visible (single-photon) radiation. Through RET, the two-photon absorbing moiety effectively imparted a large two-photon absorption (2PA) cross-section to the nile red acceptor and permitted its excitation upon irradiation of the 2PA dye with high intensity IR light [37b, 37c]. The intriguing possibility of using RET to increase the nonlinear optical performance of diarylethenes and also as a read out method in two-photon 3D optical data storage device was explored in this research.

2.4 Nonlinear Optical Properties and Photostability of Fluorene Derivatives

Fluorene derivatives with large two-photon absorption (2PA) cross-sections exhibit desirable properties for the development of new nonlinear optical and photonic technologies, particularly in the fields of 3D microfabrication [38a], optical power limiting [38b], and two-photon fluorescence imaging [38c]. Fluorene is an aromatic ring system, characterized by two benzene rings joined together by a fused five-member ring, providing high electron delocalization through good overlap of π molecular orbitals between the rings. The π-conjugated system allows for facile synthetic manipulation as it can be functionalized at the 2, 4, 7, and/or 9

positions (Figure 2.9), facilitating the systematic preparation of derivatives with varying electronic character.

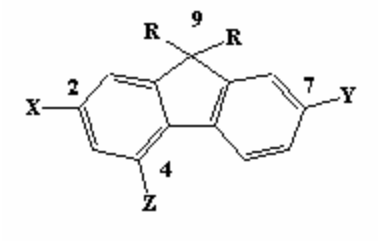

Figure 2.9 Basic π-conjugated fluorenyl ring system

Modifications can be such that X = Donor (D), Y = Acceptor (A), or X = Y of either D or A, Z is either D or A, and R = n-alkyl, alcoxy or carboxylic acid groups. Structures of some of the fluorene derivatives are shown in Figure 2.10, with blue representing electron-donating (D) groups, red representing electron-withdrawing groups (A), and black indicating π-conjugated linking groups (π). One paradigm for a chromophore to exhibit high 2PA is an extended π-conjugation system with various electron acceptor (A) or donor (D) groups attached in specific locations of a molecule in either symmetrical (D-π-D, A-π-A, D-π-A-π-D, A-π-D-π-A) or unsymmetrical (D-π-A) architectures. The A or D groups facilitate photo-induced charge transfer along the conjugation path upon excitation, consequently, achieving large optical nonlinearity. The stronger D or A is the higher the nonlinear response. Besides the strength of D or A groups, another major factor is the number of the π-electrons (or extent of conjugation) [17, 18, 39, 40].

Different designs in chemical architecture allowed investigation of the effects of symmetry, solvism, donor-acceptor strengths, conjugation length, and multi-branched geometries on the two-photon absorbing properties of these molecules [39].

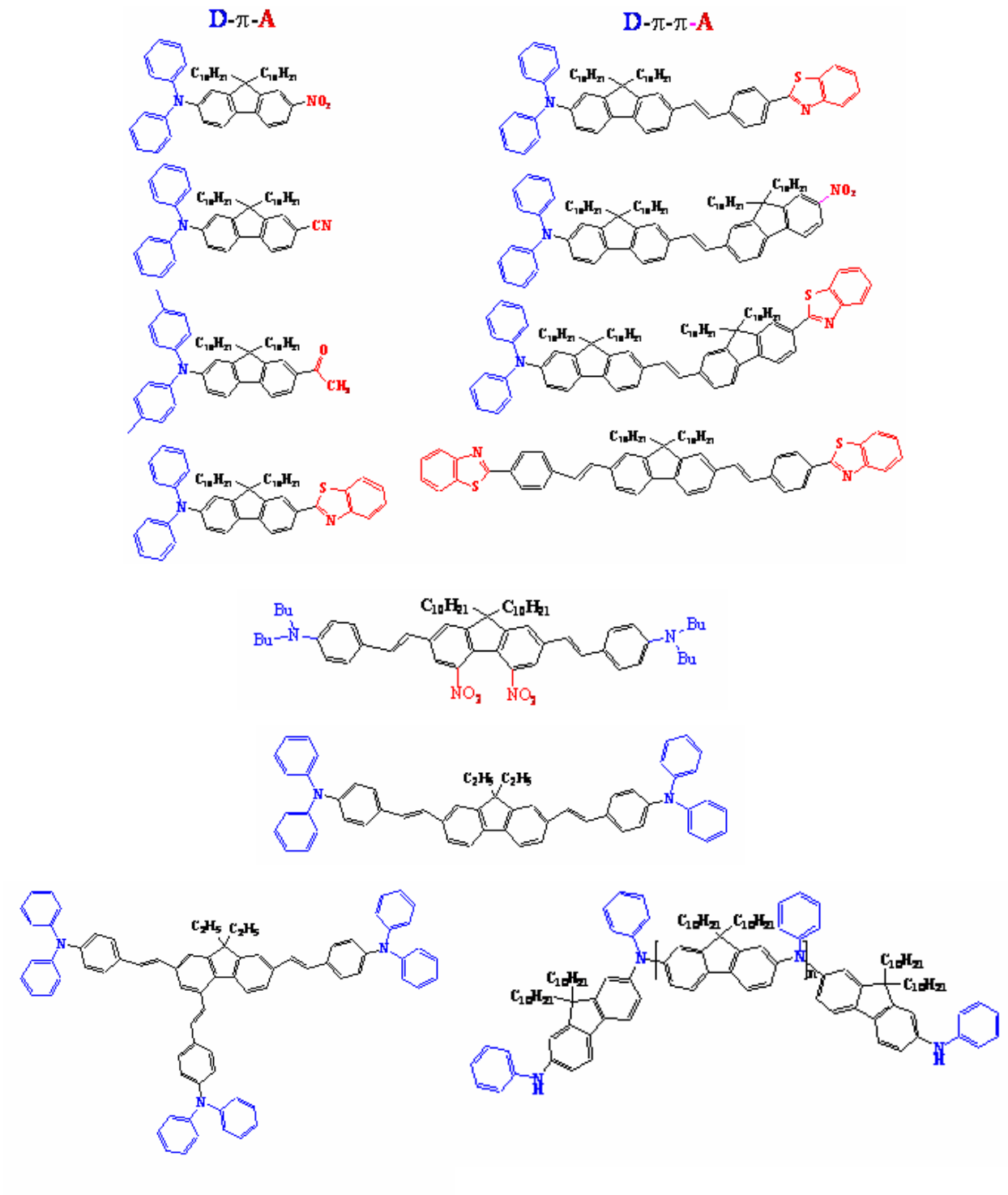

Figure 2.10 Representative fluorene derivatives characterized as highly efficient 2PA materials

As observed with other organic compounds, the delocalization of the π-electrons in these systems gives rise to a strong polarizability, which is known to accentuate a molecule's linear and NLO responses [39].

Extending the π-conjugation length, as for instance with a styryl linking bridge, in dipolar and in symmetric systems shows a considerable improvement in peak nonlinearities, particularly for some symmetric systems (of the A-π-π-A and D-π-π-D), when compared to its shorter counterpart (of the A-π-A and D-π-D) [39]. Styryl groups also extend the two-photon absorption out to longer wavelengths. Symmetrically substituted fluorene derivatives exhibit negligible 2PA into the first excited state (S_1) but strong absorption into the first two-photon allowed state, reminiscent of true centrosymmetric systems. Unsymmetrical derivatives clearly indicate that significant 2PA is possible into nearly any excited state (formally forbidden or allowed) [39].

Photodecomposition (the irreversible light-induced destruction of a dye) is one of the main limitations of many organic dyes for their applications in photonics and nonlinear optical technologies [41]. Hence, photochemical stability of fluorene derivatives under one- and two-photon excitation is critical for a number of emerging nonlinear optical applications. Photochemical decomposition under two-photon excitation may well be different from the reactions induced by low intensity irradiation [41a]. Even in the case when the same excited state of the molecule is populated under one- and two-photon excitation, additional photochemical processes such as photoionization and bond fission are possible for the latter type of excitation due to high irradiation intensities [41b]. Thus, the one- and two-photon photochemical decomposition (or stability) of select efficient 2PA fluorene dyes was the subject of one part of this dissertation.

CHAPTER 3. PHOTOPHYSICAL CHARACTERIZATION OF DIARYLETHENES UNDER ONE- AND TWO-PHOTON EXCITATION

In this chapter the photophysical characterization of two diarylethenes (3,4-bis-(2,4,5-trimethyl-thiophen-3-yl)furan-2,5-dione (**1**) and 1,2-bis(2-methylbenzo[b]thiophen-3-yl)hexafluorocyclopentene (**2**) will be discussed (Figure 3.1.).

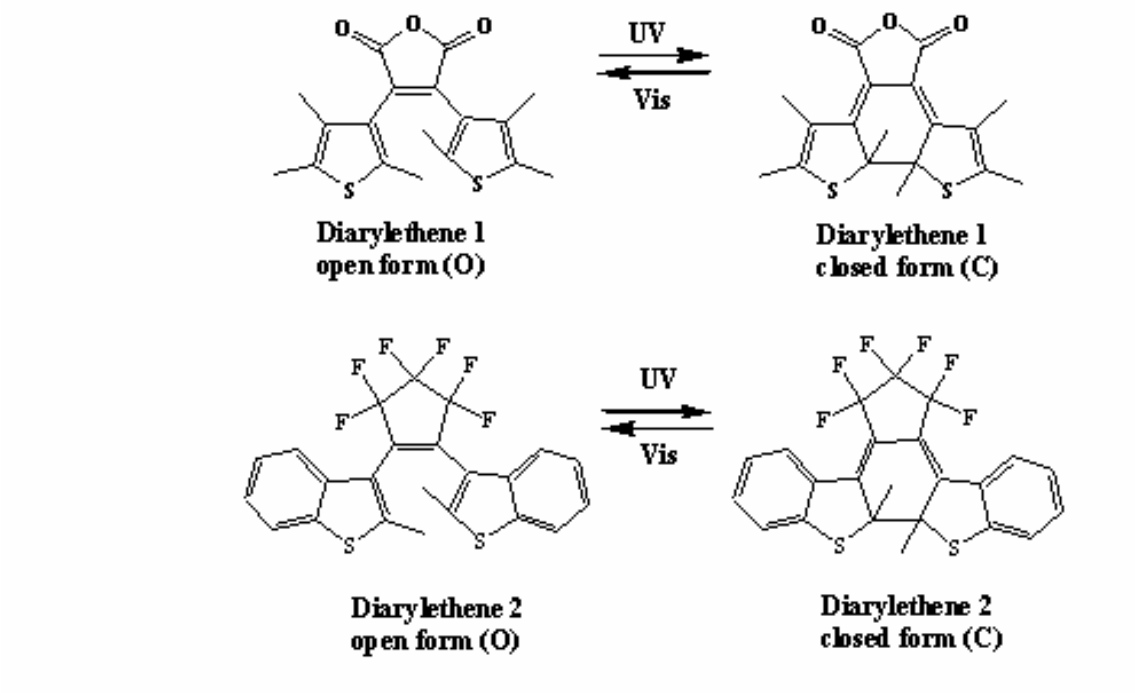

Figure 3.1. a). schematic diagram of the cyclization and cycloreversion photochromic (isomerization) reactions of diarylethenes **1** and **2**

Details of the spectral characterization in solution at room temperature under 1PE and 2PE will be given. Results of the photophysical characterization under linear excitation, such as

absorption and emission spectra of the **O** and **C** isomers, fluorescence quantum yields, steady-state excitation anisotropy, quantum yields of cyclization and cycloreversion reactions and photochemical stability will be presented. Results of the photophysical characterization under 2PE, such as δ_{2PA} of the open and closed isomers of **1** and **2** will be discussed. The main goal of the experiments discussed in this chapter is to provide a deeper understanding of the photochromic and photodecomposition processes of two diarylethenes under one- and two-photon excitation in order to provide the basis to develop high quality 3D-data storage materials and optimize their write-read conditions.

3.1 General Comment on Materials, Methods, and Instruments

Diarylethenes **1** and **2** were purchased from TCI America and used without further purification. Spectroscopic grade hexane (Alfa Aesar) and THF (Acros) were used as a solvent. The absorption spectra of the **O**-form and mixtures of **O**-**C**-forms of **1** were recorded with an UV-visible Agilent 8453 spectrophotometer. The pure **C**-form was separated from a mixture of open and closed forms in the photostationary state by normal phase HPLC, using a Waters HPLC instrument equipped with a binary pump (1525), an in-line degasser, a PDA detector (2996) and a manual injector (7725I). The best chromatographic separation was achieved by using a silical gel (4.6 x 150 mm, particle size 5 μm, pore size 100 Å) analytical column, with a mobile phase of 97:3 hexane:ethyl acetate under isocratic flow. The flow rate was 0.5 mL/min, the injection volume was 50 μL, the column temperature was 30 °C and the run time was 10 minutes.

Steady-state fluorescence and excitation anisotropy spectra were measured with a PTI Quantamaster spectrofluorimeter in the photon-counting regime of the PMT using an L-format

configuration [42]. All fluorescence measurements were performed in 10 mm fluorometric quartz cuvettes for the concentrations, $C \leq 5 \times 10^{-6}$ M. The fluorescence quantum yield of **1**, $\Phi_{FL} \approx 0.003$, was determined by a standard method, relative to 9,10-diphenylanthracene in cyclohexane [42], corresponding well with data reported in Ref. 43.

The quantum yields of the direct, $\Phi_{O \rightarrow C}$, and reverse, $\Phi_{C \rightarrow O}$, photochromic reactions (**O** $\rightarrow$ **C** and **C** $\rightarrow$ **O** reactions, respectively), were determined from the temporal changes in the corresponding absorption spectra under steady–state Xe-lamp irradiation passing through the excitation monochromator of the PTI Quantamaster spectrofluorimeter. All measurements were performed at room temperature in the dark. The values of $\Phi_{O \rightarrow C}$ and $\Phi_{C \rightarrow O}$ were obtained by the absorption method described in detailed in reference [44] for air-saturated and degassed solutions prepared by repeated freeze-pump-thaw cycles. Briefly, this absorption method is based on measurement of the temporal changes in the optical density D (λ, t) at the long wavelength maximum of the **C**-form of the diarylethene (for example, 553 nm for diarylethene **1**), and optical density at the excitation wavelength, D(λ_{exc}, t), during irradiation. The **O** isomer of the diarylethene has no absorption at 553 nm and, thus, it is straightforward to determine the number of reacted molecules, whereas the number of absorbed photons by the **O** isomer (for $\Phi_{O \rightarrow C}$) or **C** isomer (for $\Phi_{C \rightarrow O}$) at λ_{exc}, was recalculated from the dependences D (λ_{exc}, t), taking into account the individual spectral shapes of the corresponding forms of **1**. Hexane solutions (2 mL) of **1** with concentrations, $C \sim (1.5 - 2) \times 10^{-5}$ M, were placed into a 10 x 10 x 35 mm quartz cuvette and carefully sealed to avoid solvent evaporation during experiments. The entire volume of the solution was irradiated with light irradiance 0.05 – 0.3 mW/cm^2 in the 270 – 610 nm spectral range. The irradiation power was measured with a Laserstar powermeter (Ophir Optronics Inc.)

with sensitivity in the nW range. The changes in the absorption spectra during irradiation were measured with an UV-visible Agilent 8453 spectrophotometer. A probe beam in this spectrophotometer was attenuated over 10-fold by neutral density filters in order to reduce photocyclization process during the measurements.

The quantum yields of the photochemical reactions under one-photon excitation, Φ, were determined by the equation [44]:

$$\Phi = \{[D(\lambda, 0) - D(\lambda, t_{ir})]\, N_A\} / \{10^3\, \varepsilon(\lambda) \int_\lambda \int_0^{tir} I_0(\lambda)\, [1 - 10^{-D(\lambda, t)}]\, d\lambda dt\}, \qquad (1)$$

where $D(\lambda, 0)$, $D(\lambda, t_{ir})$, $\varepsilon(\lambda)$, t, and λ are the initial and final optical density of the solution, extinction coefficient ($M^{-1}cm^{-1}$), irradiation time t (s), and excitation wavelength λ (cm), respectively; N_A is Avogadro's number; t_{ir} is the total irradiation time; and $I_0(\lambda)$ is the spectral distribution of the excitation irradiance. The same method was used for the determination of the photodecomposition quantum yields, Φ_{Ph}, of diarylethene **1** under one-photon excitation. First, an equilibrium between two forms was reached at the corresponding λ_{exc}, and then the values of Φ_{Ph} were determined from the temporal changes in equilibrium spectra upon irradiation over a longer period of time.

The 2PA spectrum of the **O** isomer of **1** was measured by the up-converted fluorescence method [45] using a femtosecond laser system (Clark-MXR 2010 Ti:Sapphire amplified, second harmonic of an erbium-doped fiber ring oscillator system (output 775 nm) pumped an optical parametric generator/amplifiers (TOPAS, Light Conversion), with pulse duration, $\tau_P \approx 140$ fs, (FWHM), 1 kHz repetition rate, tuning range 560 - 2100 nm, and maximum average power ≈ 25

mW). The upconverted fluorescence of the **O** isomer of **1** was detected for solutions in 10 mm quartz cuvettes ($C \approx 4.4 \times 10^{-4}$ M) with a PTI Quantamaster spectrofluorimeter in the analog regime of the PMT, relative to fluorescein in water (pH = 11) [45]. In order to decrease reabsorption effects, the laser beam excited solutions near the exit surface of the cuvette from which fluorescence was observed. The number of reacted molecules during these measurements was negligible. The two-photon induced cyclization reaction of **1** was observed under high intensity excitation with a picosecond Nd:YAG laser (PL 2143 B Ekspla) coupled to an optical parametric generator (OPG 401/SH) with pulse duration, $\tau_P \approx 35$ ps (FWHM), pulse energy, $E_P \leq 100$ μJ, at the wavelength, $\lambda_{exc} = 810$ nm, and repetition rate, f = 10 Hz. The excitation laser beam was focused into a 1 mm quartz cell of **1** in hexanes (the volume of solution was ~ 40 μL; $C \sim 4.3 \times 10^{-3}$ M) to a waist of radius ≈ 0.12 mm. An appearance of the **C** isomer of **1** was detected spectrophotometrically at $\lambda_{max} = 553$ nm.

The 2PA cross-sections of the **O** and **C** isomers of diarylethene **2** were measured by a open-aperture Z-scan method [46] using a picosecond Nd:YAG laser (PL 2143 B Ekspla) coupled to an optical parametric generator (OPG 401/SH) with pulse duration ≈ 25 ps (FWHM), operating at a 10 Hz repetition rate.

3.2 Spectral Characterization of Diarylethene 1

3.2.1. Steady-State Spectral Properties

Individual absorption spectra of the **O** and **C** isomers of **1** in hexane are shown in Figure 2.3b. Corresponding extinction coefficients of the **O** and **C** isomers at λ_{max} were 7.2×10^3 M^{-}

$^{1}cm^{-1}$ (331 nm) and 2.7 x 10^{4} $M^{-1}cm^{-1}$ (377 nm), respectively. The nature of the broad **O** isomer absorption spectrum of **1** (Figure 2.5b) was analyzed by excitation anisotropy. The excitation anisotropy spectrum of **1** in silicon oil is shown in Figure 3.2, curve 5.

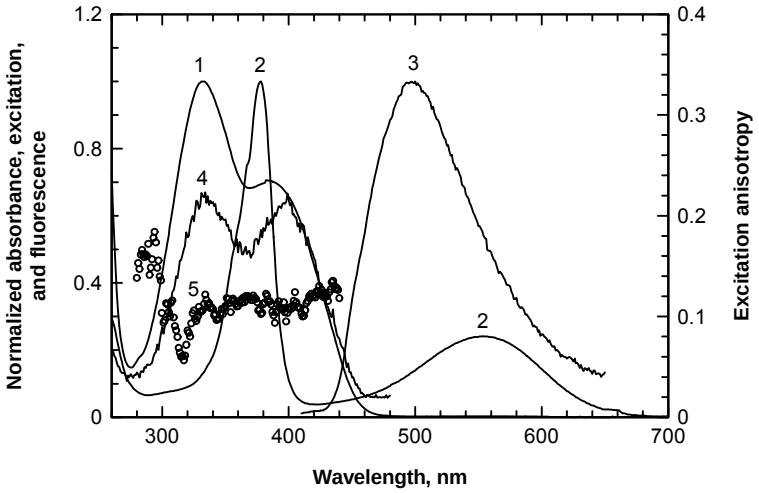

Figure 3.2 Normalized absorption (1, 2), corrected excitation (4) and fluorescence (3), and excitation anisotropy (5) spectra of the **O** isomer (1, 3-5) and **C** isomer (2) of **1** in hexane. λ_{obs} = 490 nm is the wavelength of the observation of the excitation and anisotropy spectra (4, 5),. Excitation spectrum (4) is normalized to the absorption spectrum (1) at 400 nm.

In viscous silicon oil at room temperature, no fast rotation of **1,** and corresponding depolarization effects, occurs during the fluorescence lifetime ($\tau_{FL} \approx 360$ ps) [29], and excitation anisotropy, r, reaches its maximum value [42]:

$$r = (3\cos^2\alpha - 1)/5 \qquad (2)$$

where α is the angle between absorption, $S_0 \rightarrow S_n$, and emission, $S_1 \rightarrow S_0$, transition dipoles (S_0, S_1, S_n are the ground, first excited, and higher excited electronic states, respectively). Changes in r at $\lambda < 320$ nm (Figure 3.2, curve 5) reveal the spectral position of different electronic transition in the broad absorption spectrum of the **O** isomer. In the spectral range $\lambda > 300$ nm the values of

r did not exceed 0.14. Relatively low values of r at the long wavelength edge of the absorption band (Figure 3.2, curve 1) may be explained by assuming strong overlap of several nonparallel absorption electronic transitions. High molecular symmetry as a contributing reason for the reduced anisotropy in the long wavelength absorption band [47] is less probable, because the symmetry of the reactable **O** isomer (anti-parallel) conformer of **1** is not very high (symmetry C_2). The excitation spectrum of the **O** isomer (Figure 3.2, curve 4) did not coincide with corresponding absorption curve 1, which indicated a decrease in the fluorescence quantum yield, Φ_{FL}, in the short wavelength part of the absorption spectrum, confirming a complicated electronic structure of the absorption band of the **O** isomer.

3.2.2. Quantum Yields of the Photochromic Reactions under One-Photon Excitation

The kinetic changes in the absorption spectra of **1** (hexane solutions) under the steady-state irradiation at λ_{exc} = 330 nm and 550 nm are shown in Figures 3.3a and 3.3b, respectively. Observed isobestic points of the absorption spectral changes reveal no photochemical products can arise during the irradiation and affect the photoisomerization kinetics. The initial slopes of the dependences $N_{mol} = f(N_{ph})$, (where N_{mol} and N_{ph} are the number of reacted molecules and the number of absorbed photons, respectively) are shown in the inserts of Figure 3.3. These measurements were performed for different λ_{exc} in the absorption band of **1**, and the spectral dependences of the cyclization and cycloreversion reaction quantum yields were obtained (Figure 3.4).

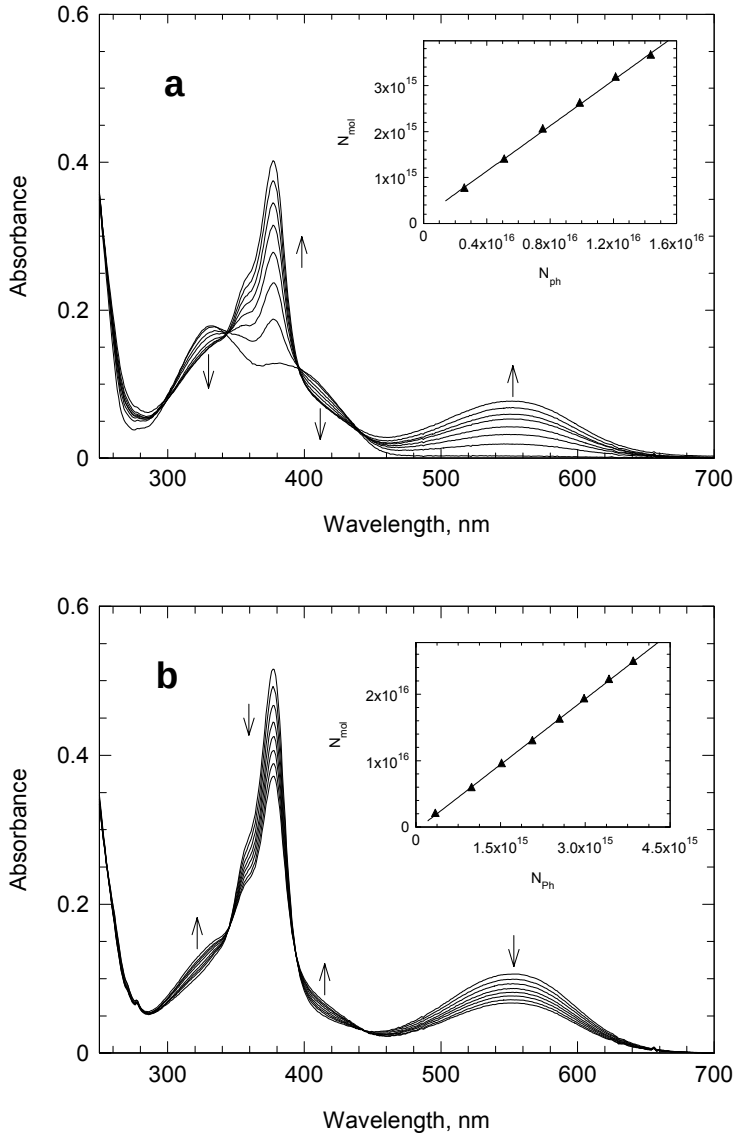

Figure 3.3 Kinetic changes in the absorption spectra of **1** in hexane (C ≈ 2.5 x 10^{-5} M) under irradiation at (a) λ_{exc} = 330 nm and (b) λ_{exc} = 550 nm (temporal step between two adjacent spectra, Δt = 100 s, irradiance of the excitation ≈ 0.140 mW/cm^2 (a) and ≈ 0.100 mW/cm^2 (b)). The initial spectrum in (a) is an original **O** isomer absorption and subsequent spectra show the photostationary state under the irradiation at λ_{exc} = 415 nm.

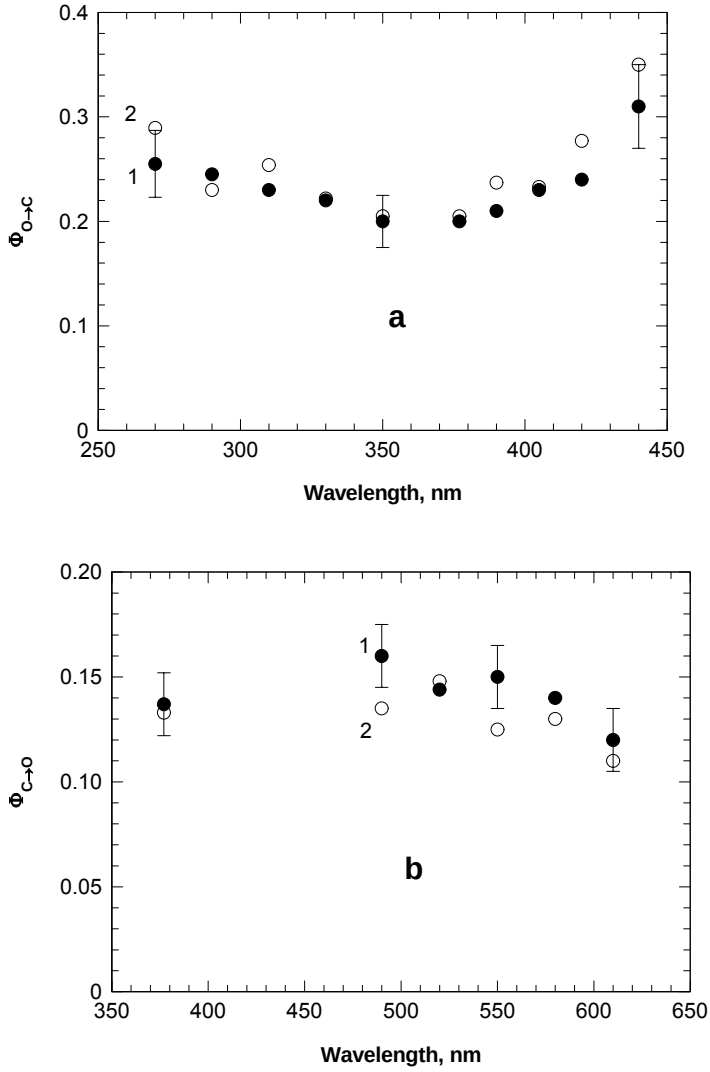

Figure 3.4 Spectral dependences of the photocyclization , $\Phi_{O\rightarrow C}$ (a), and cycloreversion, $\Phi_{C\rightarrow O}$ (b), reaction quantum yields of **1** for air saturated (1) and deoxygenated (2) hexane solutions.

From these data, a weak spectral dependence of $\Phi_{O\rightarrow C}$ and $\Phi_{C\rightarrow O}$ was observed. The values of $\Phi_{O\rightarrow C}$ were in the range 0.2 – 0.35 and differed by ca. a factor of two from previously reported data ($\Phi_{O\rightarrow C} \approx 0.13$) [29a]. The cycloreversion quantum yields of **1**, $\Phi_{C\rightarrow O} \approx 0.1 - 0.16$, were in good agreement with previously reported data [29b, 30a]. Air-saturated and deoxygenated solutions of **1** exhibited nearly the same reaction efficiencies for both forms.

This suggests that molecular oxygen did not affect the fast picosecond photoisomerization processes of **1**. A simplified electronic model of **1** (Figure 3.5) is proposed on the basis of spectral properties (Figure 3.2) and also on the experimental and theoretical data reported by Irie *et al.* [28b, 29, 30a]. A distinctive feature of the photochromic transformations of **1** is a fast rate of the cyclization and cycloreversion processes: $\{1/k_{32}, 1/k_{31}\} \leq 10$ ps; $1/k_{10} \leq 2$ - 3 ps, demonstrated *via* picosecond transient absorption spectroscopy [29a].

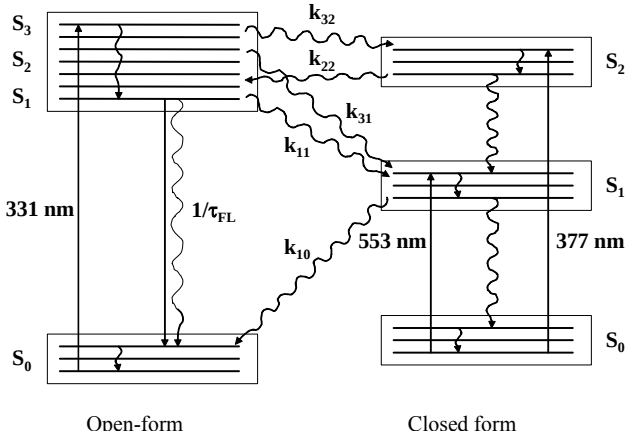

Figure 3.5 Schematic representation of the electronic structures of the open and closed isomers of **1**.

Upon examination of the spectral dependence (Figure 3.4a), an increase in the value of $\Phi_{O\rightarrow C}$ at $\lambda_{exc} = 440$ nm reveals an efficient cyclization reaction **O** $\rightarrow$ **C** from the fluorescent state of the **O** isomer with lifetime, $\tau_{FL} \approx 360$ ps. This is consistent with the results of transient absorption measurements of **1** in hexane [29b]. Nearly the same values of $\Phi_{C\rightarrow O}$ at $\lambda_{exc} = 377$ nm and $\lambda_{exc} = 550$ nm (Figure 3.4b) indicate the cycloreversion processes occurring at these wavelengths are similar in nature. This suggests that the probable reaction pathway proceeds through the S_1 state of **C** isomer (i.e. S_0 state of the **C** isomer was excited to the S_2 state, then relaxed to the S_1 state and transformed to the S_0 state of the **O** isomer with the corresponding

velocity constant, k_{10} (Figure 3.5) rather than possible direct transformation **C** → **O** from the S_2 state with velocity constant k_{22}.

3.2.3. Kinetic Analysis

The kinetics of the photochromic transformations of **1** under steady-state irradiation were calculated for different λ_{exc} in order to determine the optimized writing conditions for possible data recording. These calculations were performed with the differential equation:

$$dN_{CF}(t)/dt = -\sigma_{CF} \cdot I_0 \cdot N_{CF}(t) \cdot \Phi_{C \rightarrow O} + \sigma_{OF} \cdot I_0 \cdot N_{OF}(t) \cdot \Phi_{O \rightarrow C} \qquad (3)$$

where $N_{OF}(t)$, $N_{CF}(t)$, σ_{OF}, and σ_{CF} are the concentrations and one-photon absorption cross-sections of the **O** and **C** isomers, respectively; I_0 is the irradiance of the excitation light (in phot·cm^{-2}·s^{-1}). Equation 3 was solved numerically using the constant field approximation ($I_0 \approx$ constant in the entire irradiation volume), and with the start conditions: $N_{CF}(0) = 0$, $N_{OF}(0) = N_0$ (where $N_0 = N_{CF}(t) + N_{OF}(t)$ is the total molecular concentration of **1**, assumed to be constant). The concentration of the incipient **C** isomer was calculated over a broad spectral range for various steady-state irradiation conditions. These calculations were based on the known photophysical parameters of **1** and obtained spectral dependence of $\Phi_{O \rightarrow C}$ (the average value of $\Phi_{C \rightarrow O} \approx 0.14$, was considered constant over the entire spectral range). The spectral curves of the normalized values, N_{mol} / N_0 are shown in Figure 3.6. $\lambda_{exc} \approx 330$ nm and $\lambda_{exc} \approx 400$ - 405 nm were found to be the most efficient excitation wavelengths for the irradiation dose, $F \leq 10^{17}$ phot·cm^{-2}, with maximum efficiency at 330 nm. Irradiation conditions in which $F \geq 5 \times 10^{17}$ phot·cm^{-2} corresponded to the most effective writing wavelengths at $\lambda_{exc} \approx 320$ -325 nm and λ_{exc}

≈ 410-420 nm, with maximum efficiency at the peak of long wavelength absorption band. All calculated processes corresponded to linear excitation (were independent of light irradiance).

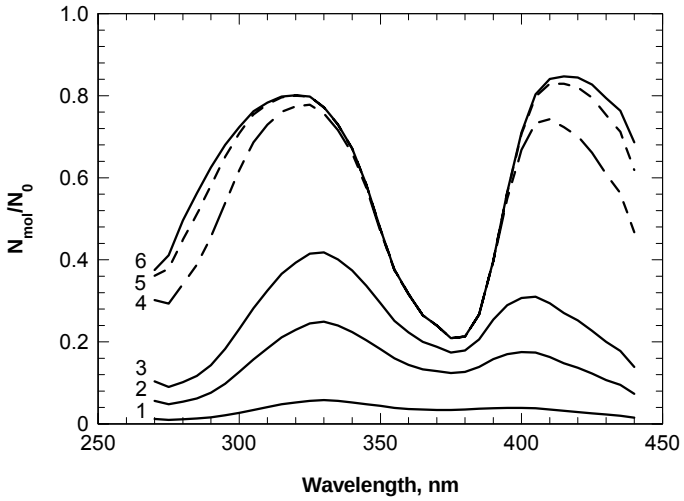

Figure 3.6 Calculated spectral dependencies of the normalized concentration of the C-form of **1**, N_{mol} / N_0, forming with total irradiation dose (1) F = 10^{16} phot·cm^{-2}, (2) 5 x 10^{16}, (3) 10^{17}, (4) 5 x 10^{17}, (5)10^{18}, (6) 2 x10^{18}.

3.2.4. Photochemical Stability

Photodecomposition quantum yields of **1**, Φ_{Ph}, were determined in hexane solution at room temperature under steady-state irradiation over a broad spectral range (Figure 3.7, curve 1). As can be seen, there was a strong spectral dependence of Φ_{Ph}. The values of $\Phi_{Ph} << \{\Phi_{C\rightarrow O}, \Phi_{O\rightarrow C}\}$ revealed slow photochemical processes (velocity constants ~ 10^8-10^9 s^{-1}) relative to the fast photochromic transformation (~ 10^{11}-10^{12} s^{-1}) [29a], demonstrating that photodecomposition of **1** proceeds under the constant equilibrium between two forms. The excited states of the O and C isomers undergo photodecomposition simultaneously. It was difficult to separate, quantitatively, the quantum yields of these processes in the 270– 440 nm spectral range from the experimental values of Φ_{Ph} due to unknown lifetimes of the excited states of **1**.

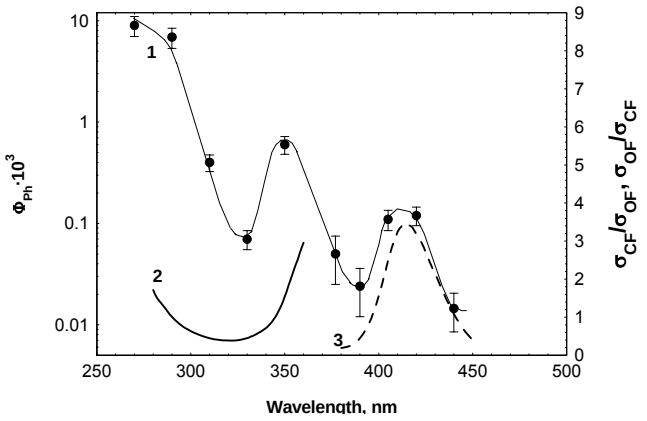

Figure 3.7 Spectral dependences of the photodecomposition quantum yield $\Phi_{Ph}(\lambda)$ of **1** in (1) hexane, (2) the ratio of the absorption cross-sections σ_{CF}/σ_{OF} and (3) σ_{OF}/σ_{CF}. The solid line in (1) is presented as a guide.

The kinetic analysis of the possible photodecomposition processes was performed for the equilibrium state of **1** for different excitation wavelengths and reaction pathways. From this analysis, the value of Φ_{Ph} should be independent of the absorption cross-sections σ_{OF} and σ_{CF}, in the case of the first-order photochemical reactions proceeding from the lowest electronic excited state of the **O** and **C** isomers. Nevertheless, the experimentally observed spectral dependence of Φ_{Ph} (Figure 3.7, curve 1) was strong and exhibited two peaks at $\lambda_{exc} \approx 350$ nm and ≈ 410 nm. The spectral behaviour of Φ_{Ph} was similar to the corresponding dependence of the ratio, σ_{CF}/σ_{OF} in the range $\lambda_{exc} \leq 350$ nm (curve 2), and to the reverse ratio σ_{OF}/σ_{CF}, at $\lambda_{exc} \geq 390$ nm. This suggests relatively complex photochemical reactions simultaneously proceed from different excited electronic states of the **O** and **C** isomers and cannot be described by first-order photoreactions. From the data in Figure 3.7, one can see the highest photochemical stability of **1** in hexane corresponded to the excitation wavelengths $\lambda_{exc} \approx 390$ nm and $\lambda_{exc} \approx 440$ nm ($\Phi_{Ph} \sim (1.5 – 2) \times 10^{-5}$), which can be used for optimization of the writing process, increasing the fatigue resistance.

3.2.5. Two-Photon Absorption Cross-Sections and Two-Photon Cyclization Quantum Yield

The 2PA spectrum of the **O** isomer of **1** is shown in Figure 3.8 (curve 2). The maximum of the 2PA spectrum corresponded to λ_{max} = 337 nm with the 2PA cross-section ≈ 80 GM, being relatively large compared to other diarylethene derivatives, e. g., for B1536 the reported values was < 1GM) [33], and, thus, promising for practical applications.

.

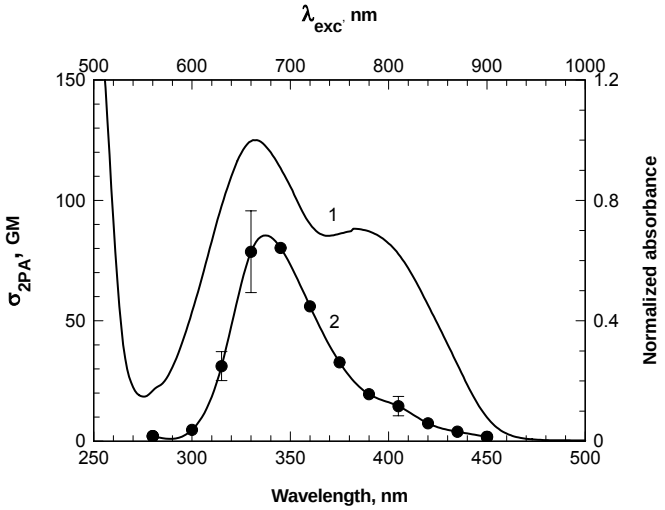

Figure 3.8 Normalized (1) linear absorption, and (2) 2PA spectra of the O isomer of **1** in hexane.

According to the anisotropy experiments, the observed 2PA band corresponds to the $S_0 \rightarrow S_2$ two-photon allowed transition in the **O** isomer. It can be assumed that the shoulder in the 2PA spectrum at ≈ 405 nm is due to the long wavelength, lower energy transition in the **O**-form, $S_0 \rightarrow S_1$. Evidence of the two-photon induced photochromic cyclization reaction **O** → **C** of **1** under picosecond irradiation is shown in Figure 3.9. The changes in the absorption spectrum of the **O** isomer during irradiation were sufficiently small, ensuring that no reverse reactions occured in the excitation volume (the concentration of the **C** isomer in the solution was negligible). In this case the quantum yield of the cyclization reaction of **1** under two-photon

excitation, $\Phi_{2PA}^{O\rightarrow C}$, can be estimated from the 2PA spectrum of the **O** isomer (Figure 3.8, curve 2) and a Gaussian spatial and temporal beam profile approximation. The value of $\Phi_{2PA}^{O\rightarrow C} \approx 0.22 \pm 0.05$ was obtained at λ_{exc} = 810 nm, comparable to the corresponding one-photon cyclization reaction quantum yield $\Phi_{O\rightarrow C} \approx 0.23 \pm 0.02$ at λ_{exc} = 405 nm (Figure 3.4a, curve 1). Good agreement of these values strongly supports the similar nature of the cyclization process of this diarylethene derivative under both one- and two-photon excitation.

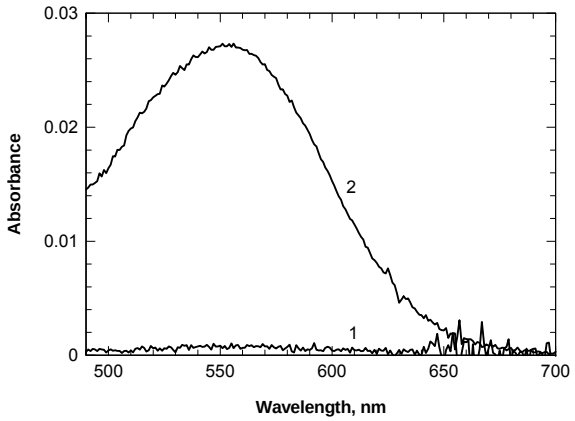

Figure 3.9 Absorption spectra of **1** in hexane (C ≈ 4.3 x 10^{-3} M): (1) before and (2) after irradiation for 300 min at λ_{exc} = 810 nm, with $\tau_p \approx 35$ ps (FWHM), $E_P \approx 25$ μJ, and f = 10 Hz.

3.3 Spectral Characterization of Diarylethene 2

3.3.1. Steady-State Spectral Properties

Individual absorption spectra of the open and closed forms of diarylethene derivative **2** in hexane are shown in Figure 3.10. The absorption spectrum of **2** in the photostationary state in hexane is shown in Figure 3.10 (3). Diarylethene **2** is especially well suited for data storage due to its high cyclization ($\Phi_{O\rightarrow C}$) and cycloreversion ($\Phi_{C\rightarrow O}$) photoisomerization reaction quantum yields ($\Phi_{O\rightarrow C}$: 0.35 at 313 nm and $\Phi_{C\rightarrow O}$: 0.35 at 517 nm in hexane). Neither the open nor the

closed forms display significant fluorescence (fluorescence quantum yields: open form = 0.02 and closed form < 0.006). The kinetic changes in the absorption spectra of the hexane solutions of **2** under the steady-state irradiation at λ_{exc} = 313 nm and 517 nm are shown in Figure 3.11 (a and c, respectively). The initial slopes of the dependences $N_{mol} = f(N_{ph})$, (where N_{mol} and N_{ph} are the number of reacted molecules and the number of absorbed photons, respectively) are shown in Figure 3.11b and 3.11d.

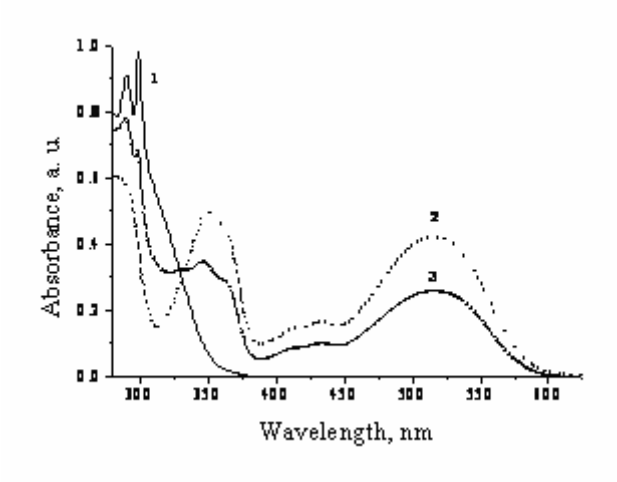

Figure 3.10 Absorption spectra of the (1) open form (O) (extinction coefficient at λ_{max} (258 nm):1.5 x 10^4 $M^{-1}cm^{-1}$), (2) closed form (C) (extinction coefficient at 517 nm: 9.9 x 10^3 $M^{-1}cm^{-1}$), and (3) photostationary state of diarylethene 1 in hexane (λ_{exc}: 254 nm).

The temporal step between two adjacent spectra in Figures 3.11a and 3.11c is 15 s (excitation irradiance = 0.167 mW/cm^2 in Figure 3.10a and = 0.10 mW/cm^2 in Figure 3.10c). These measurements were performed for different λ_{exc} in the main absorption band of **2**, resulting in determination of the spectral dependences of the cyclization and cycloreversion reaction quantum yields.

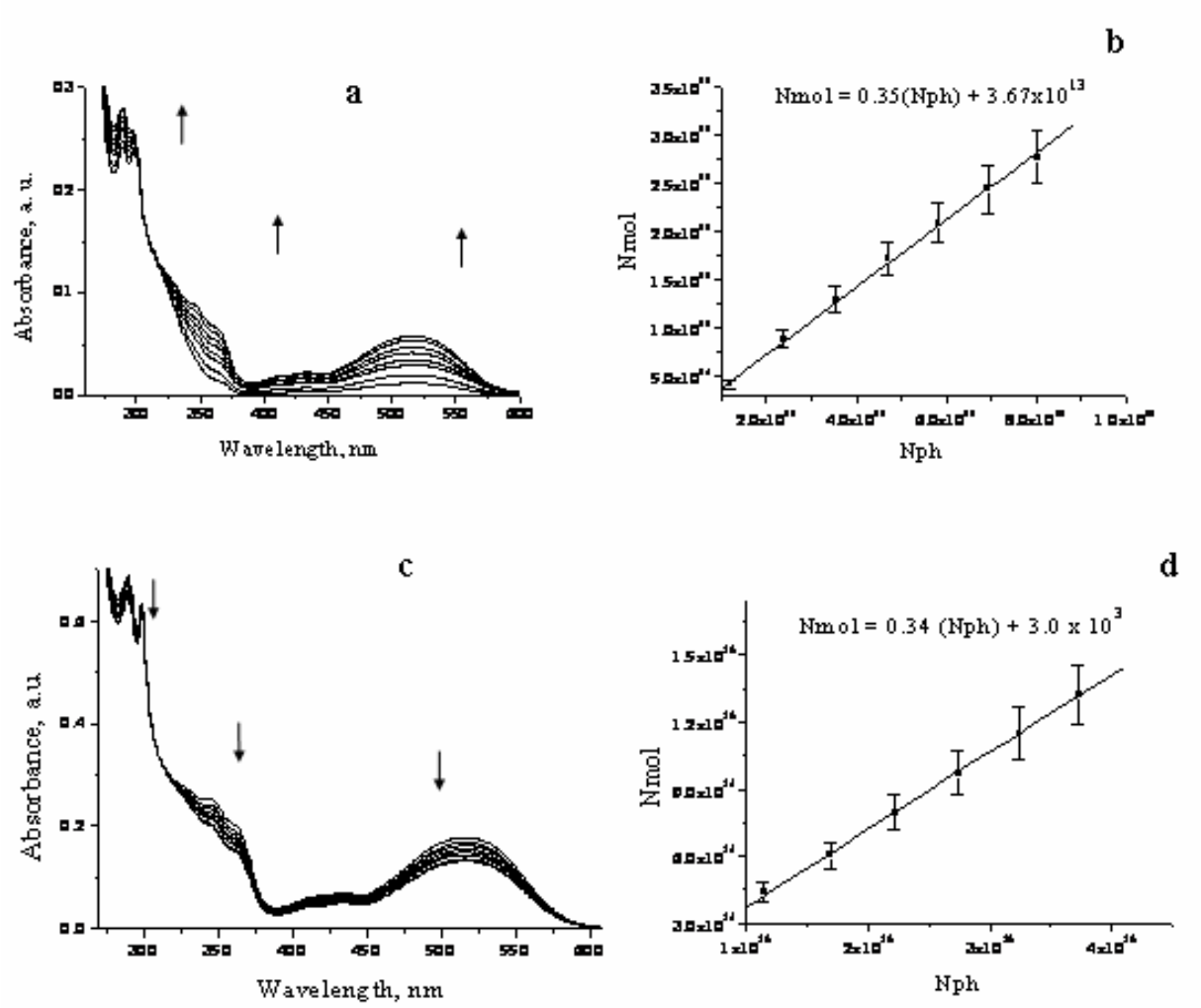

Figure 3.11. Kinetic changes in the absorption spectra of **2** in hexane (C ≈ 4.0 x 10^{-5} M): (a) initial spectrum corresponds to the open isomer and subsequent spectra show changes in absorption under irradiation at λ_{exc} = 313 nm, (b) N_{mol} vs. N_{ph} plot for determination of $\Phi_{O\rightarrow C}$ at 313 nm, (c) initial spectrum corresponds to the photostationary state and subsequent spectra show changes in absorption under irradiation at λ_{exc} = 517 nm, and (d) N_{mol} vs. N_{ph} plot for determination of $\Phi_{C\rightarrow O}$ at 517 nm.

The spectral dependences of the photocyclization ($\Phi_{O\rightarrow C}$) and cycloreversion ($\Phi_{C\rightarrow O}$) reaction quantum yields are shown in Figure 3.12. Only a very weak spectral dependence of $\Phi_{O\rightarrow C}$ and $\Phi_{C\rightarrow O}$ was observed. The values of $\Phi_{O\rightarrow C}$ were in the range 0.24 – 0.37.

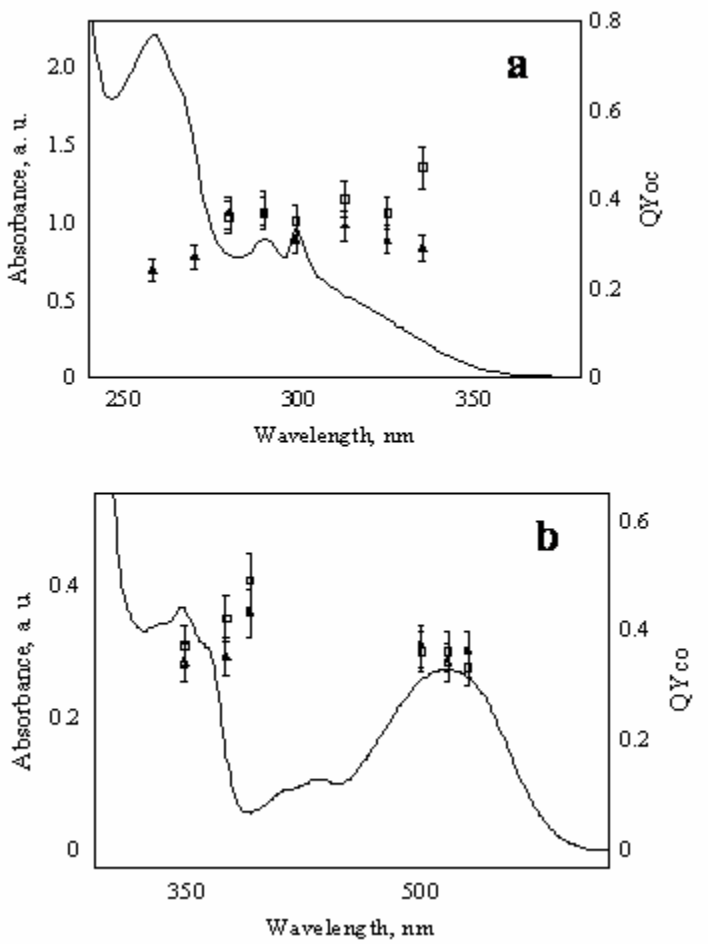

Figure 3.12. Spectral dependences of the photocyclization , ΦO→C (a), and cycloreversion, ΦC→O (b), reaction quantum yields of **2** for air saturated (▲) and deoxygenated (□) hexane solutions.

3.3.2. Two-Photon Absorption Cross-Sections

To ascertain the optimized experimental conditions for two-photon recording and readout, two-photon absorption cross-sections (δ_{2PA}) of the open and closed forms of diarylethene **2** in ethyl acetate were determined by an open aperture Z-scan method, using a picosecond laser as the excitation source [46]. The δ_{2PA} of the open form at 520 nm (corresponding to 260 nm of single photon excitation) was 85 GM, comparable to δ_{2PA} reported for structurally related diarylethenes [34]. However, Z-scan signals of the closed form at 1040 nm (corresponding to

the λ_{max} of absorption at ~ 517 nm) were too weak to give reliable δ_{2PA}. According to symmetry rules, the two-photon allowed transition of the closed form of diarylethene **2** (a molecule of relatively high symmetry), is expected to be located at shorter wavelengths (in the $S_0 \rightarrow S_2$ or higher transition bands) than the single-photon allowed absorption band ($S_0 \rightarrow S_1$ band). When exciting the closed form of diarylethene **1** at wavelengths shorter than 900 nm, Z-scan signals were clearly observed. The δ_{2PA} of the closed form of diarylethene **2** at 680, 750, and 800 nm was 150, 145, and 120 GM, respectively. Typical Z-scan plots obtained are shown in Figure 3.13.

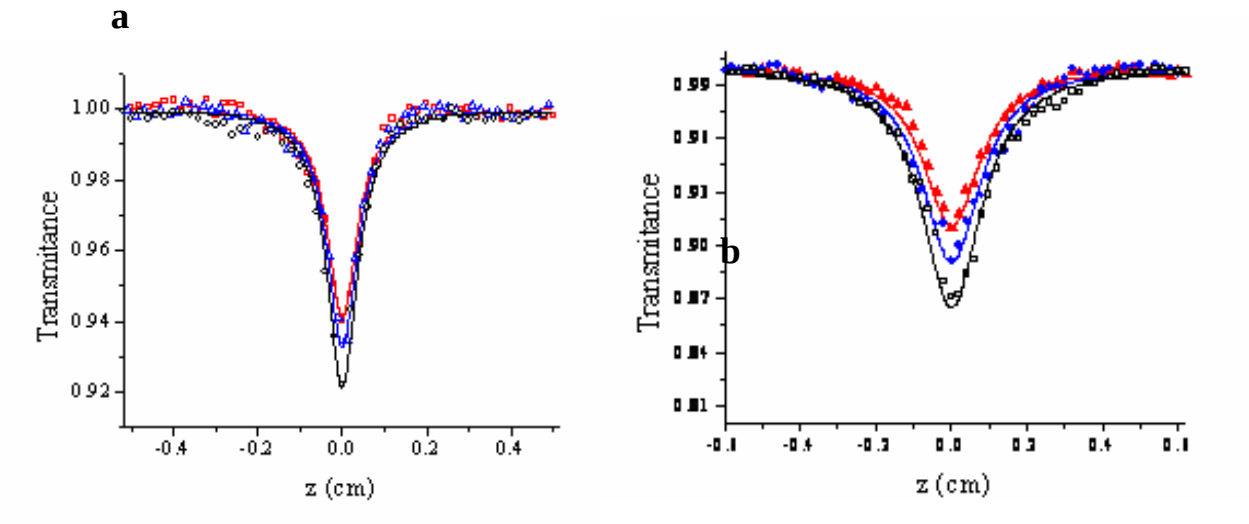

Figure 3.13 a) Open aperture Z-scan curve of the open form of diarylethene derivative **2** at 520 nm at three different input energies (E_{in}): 3.5 (□), 3.9 (Δ), and 4.3 μJ (○) and b) open aperture Z-scan curve of the closed form of diarylethene derivative **2** at 750 nm at three different input energies (E_{in}): 13.0 (▲), 16.0 (•), and 20.0 μJ (□)

CHAPTER 4. EFFICIENT DIARYLETHENES FOR TWO-PHOTON 3D OPTICAL DATA STORAGE: ENHANCEMENT OF NONLINEAR OPTICAL PROPERTIES BY CHEMICAL MODIFICATION

For efficient applications of diarylethenes in two-photon 3D optical data storage, the diarylethene isomers should have a relatively high 2PA cross-section (δ_{2PA}) at the excitation wavelength, high photoisomerization quantum yield, and a non-destructive readout method. As demonstrated in chapter 3, diarylethenes **1** and **2** are not optimized for two-photon excitation. Two-photon absorption cross-sections for both isomers range from 80 to 150 GM. These are moderate values, and these photochromic materials, by themselves, may not meet application requirements due to insufficient nonlinear absorption (long excitation time or high irradiance may be required for two-photon photoisomerization). Moreover, since any of the photoisomers of diarylethenes **1** and **2** have significant fluorescence, their emission can not be used as a readout method. One of the goals of this research is to develop more efficient 2PA photochromic diarylethenes for applications in 3D optical data storage and to provide a non-destructive readout method. For this purpose, two strategies were attempted: 1) chemical modification of the diarylethene by covalent attachment of an efficient 2PA fluorescent chromophore (fluorene derivative) and 2) use of intermolecular RET from an efficient 2PA fluorene derivative to the photochromic diarylethene (non-covalently attached). In this chapter the synthetic strategy used to prepare diarylethenes incorporating fluorene derivatives will be discussed.

4.1 Materials, Methods, and Instruments

Reactions were conducted under N_2 or Ar. Benzothiazole was distilled under reduced pressure prior to use. THF was distilled over $NaBH_4$ followed by sodium before use. All solvents and reagents were used as obtained from commercial sources unless specified. ^{1}H NMR spectra were recorded on a Varian Mercury-300 NMR (300 MHz) spectrometer using TMS (δ = 0.0 ppm) as the internal standard. Chemical shifts (δ) of all ^{1}H NMR spectra are reported in parts per million (ppm) and the respective spectra of fluorene compounds prepared in this project can be viewed in Appendix A. ^{13}C NMR spectra were recorded on the same spectrometer (75 MHz) using the carbon signal of the deuterated solvent ($CDCl_3$ δ = 77.4 ppm) as the internal standard. FT-IR spectra were recorded on a Perkin-Elmer Spectrum One spectrometer. Fluorene (**1**) was recrystallized in hexanes prior to use. Synthesis of 2-nitrofluorene (**2**), 2-iodo-7-nitro-fluorene (**3**), 7-iodo-9,9-didecyl-2- nitrofluorene (**4**), 2-(tri-*n*-butylstannyl)benzothiazole (**5**), 2-(9,9-didecyl-7-nitrofluoren-2-yl)benzothiazole (**6**), 7-benzothiazol-2-yl-9,9-didecylfluoren-2-ylamine (**7**) were previously prepared and characterized [47]. These compounds were freshly prepared and characterized following established procedures but a brief description on their preparation will be presented. ^{13}C NMR spectra of previously synthesized derivatives were used for characterization purposes and are not included.

4.2. Synthesis of Diarylethenes Containing Fluorene Derivatives

This study is an attempt to construct N-substituted maleimide diarylethenes containing fluorene fragments, by reacting diarylethene **1** with fluorene derivatives containing primary amines. The maleimide fragment is widely used in photochromic diarylethenes as a bridge. The transformation of 1,2-dihetarylmaleic anhydrides into maleimides containing an unsubstituted nitrogen atom (on treatment with ammonium acetate or hexamethyldisilazane HMDS) or into N-alkylmaleimides (using aliphatic and aromatic amines) has been reported (Figure 4.1) [48a]. This synthetic approach has also been used in the preparation of new copolymers having photochromic units as pendant groups (Figure 4.2a) [48b, 48c].

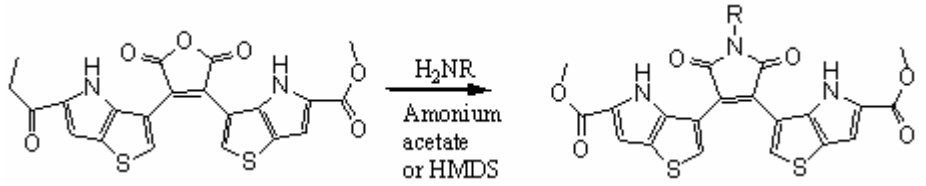

Figure 4.1. Photochromic compounds containing thieno[3,2-b]pyrroles fragments linked by a maleimide bridge

Our synthetic approach is different from the one reported by Li and Tian, which recently incorporated two diarylethenes units into the 9,9′ positions of one fluorene unit to obtain a monomer that was subsequently polymerized by typical palladium-catalyzed Suzuki coupling reaction (Figure 4.2b) [48d].

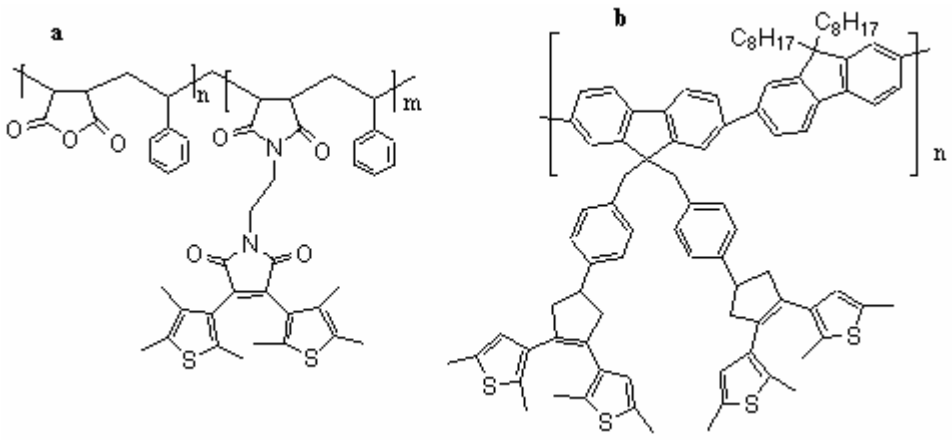

Figure 4.2. a) copolymer having a photochromic unit as pendant group b) fluorene polymer containing two photochromic pendant groups

Details of the synthetic strategy for the functionalization of fluorene derivatives into the core of diarylethene **1** are given in Figures 4.3, 4.4 and 4.5 and at the end of this chapter. Preparation of key intermediates was efficient from readily available fluorene. Nitration of fluorene (**1**) with nitric acid yielded 2-nitrofluorene (**2**) (Figure 4.3) following a literature procedure (melting point 158 °C was in good agreement with that of the literature value 157- 160 °C) [47]. This was followed by iodination of **2**, to yield the key intermediate 2-iodo-7-nitrofluorene (**3**) (melting point 245 °C was consistent with that of the literature value 244-245 °C). Dialkylation of **3** was accomplished by generation of the fluorenyl anion with KOH in DMSO and subsequent didecylation with 1-bromodecane in the presence of KI at room temperature. 2-Iodo-9,9-didecyl-7-nitrofluorene (**4**) was obtained as a yellow solid in 77% isolated yield after column chromatography. Pd-catalyzed Stille coupling was subsequently performed between **4** and (2-tri-n-butylstannyl)benzothiazole (**5**) in refluxing toluene with dichlorobis(triphenylphosphine)-palladium(II). 2-(9,9-Didecyl-7-nitrofluoren-2-yl) benzothia zole (**6**) was obtained as yellow crystals in 55% isolated yield after column chromatography [47].

Quantitative reduction of **6** was achieved using hydrazine hydrate and 10% Pd/C in a 1:1 mixture of EtOH and THF at 70 °C (Figure 4.3), providing 7-benzothiazole-9,9-didecylfluoren-2-ylamine (**7**) as a bright yellow viscous oil [47].

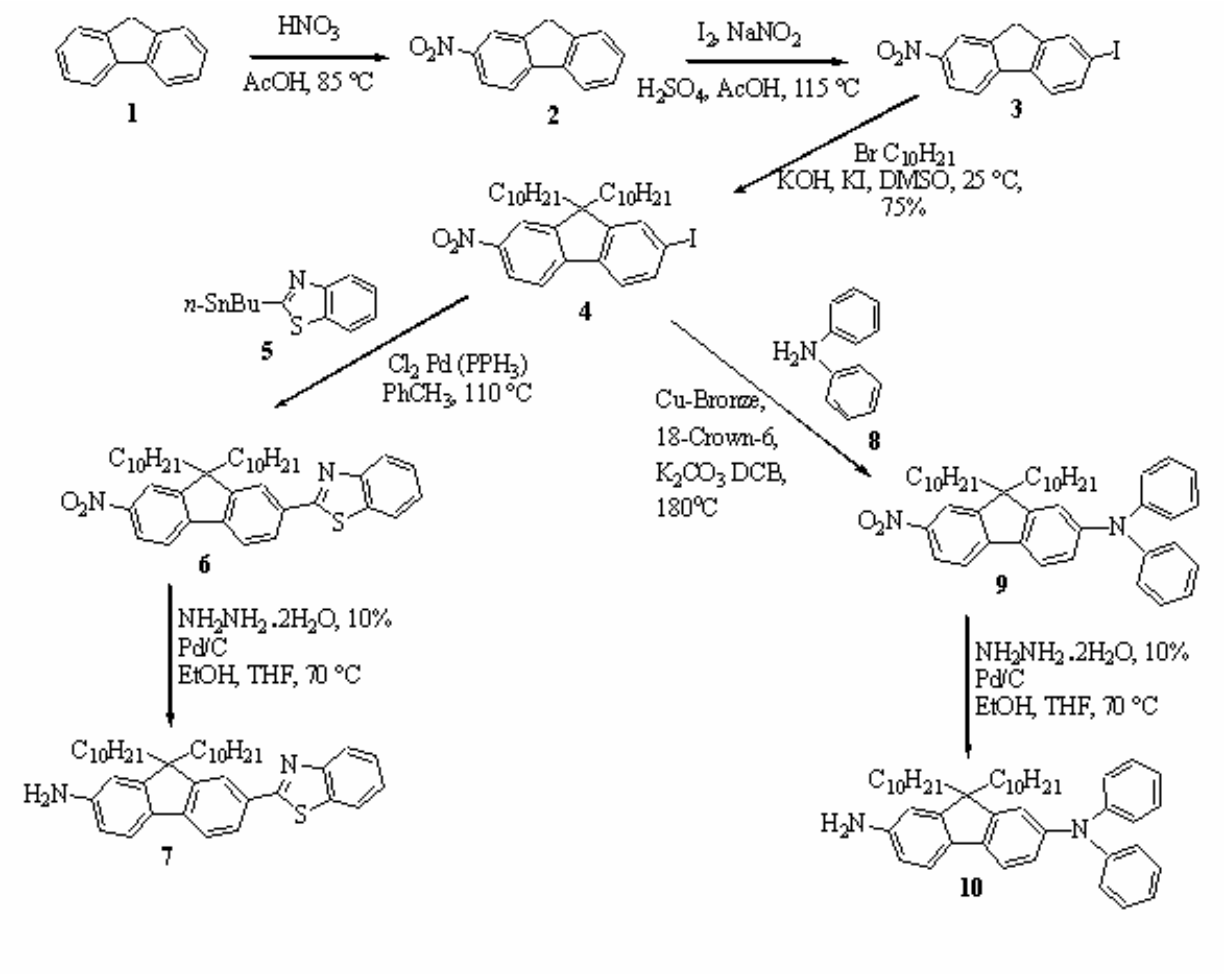

Figure 4.3. Synthesis of key intermediates of fluorene derivatives **7** and **10**

Amine **7** was used directly in subsequent steps due to its oxidative lability (as shown in Figure 4.5). (9,9-didecyl-7-nitro-fluoren-2-yl)diphenylamine **9** was obtained via a Cu-mediated Ullmann condensation of diphenylamine (**8**) with **4** in o-dichlorobenzene using K_2CO_3 as base and 18-crown-6 at 180 °C (orange oil after column chromatographic purification, 80% yield).

Quantitative reduction of **9** was also achieved using hydrazine hydrate and 10% Pd/C in a 1:1 mixture of EtOH and THF at 70 °C, providing 7-diphenylamine-9,9-didecylfluoren-2-ylamine (**10**) as a bright yellow viscous oil [47]. Amine **10** was also used directly in subsequent steps due to its fast oxidative lability (as shown in Figure 4.5). In order to test the ability of the fluorene derivatives **7** and **10** to react with diarylethene **14**, a model reaction was previously attempted (Figure 4.4).

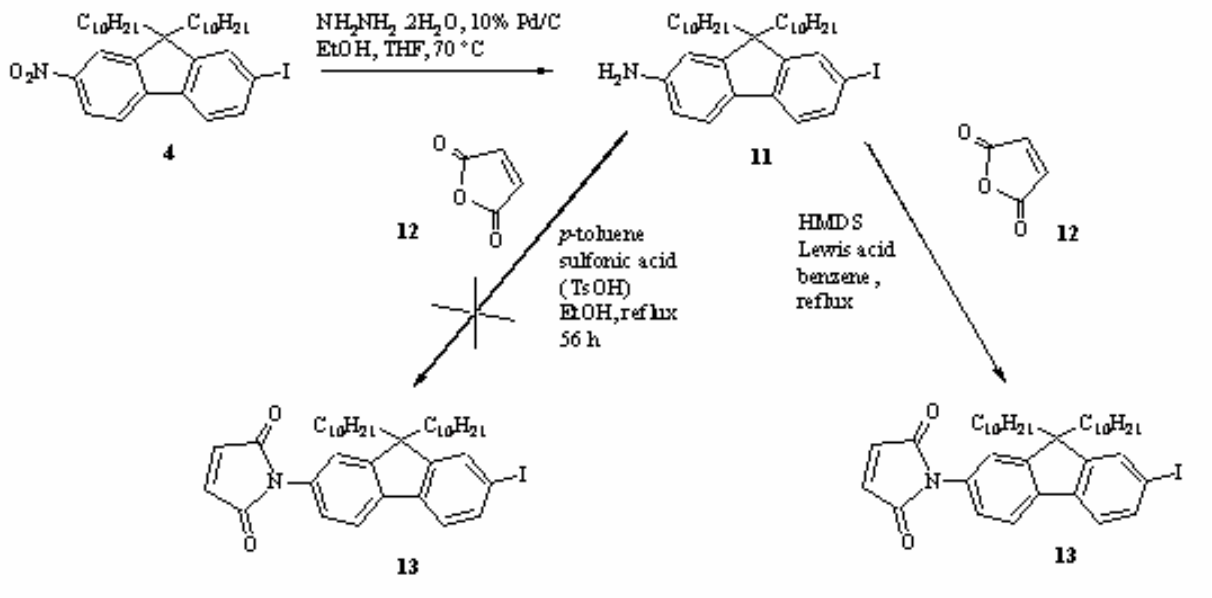

Figure 4.4. Synthesis of intermediate **8** and model reaction with maleic anhydride

Quantitative reduction of 7-Iodo-9,9-didecyl-2-nitrofluorene (**4**) was achieved using hydrazine hydrate, providing 7-iodo-9,9-didecylfluoren-2-ylamine (**11**) as a light yellow solid. As shown in Figure 4.4, the first synthetic methodology attempted for the preparation of the N-arylmaleimide **13** was the one reported by Krayushkin *et al.* using *p*-toluenesulfonic acid in ethanol materials [48a]. At 80 hours of reaction only starting materials were present, and the

target compound **13** was not recovered. An alternative synthetic methodology was attempted, using a hexamethyldisilazane (HMDS)-mediated reaction of the maleic anhydride (**12**) with 7-iodo-9,9-didecylfluoren-2-ylamine (**11**) and subsequent *in situ* cyclization of the resulting amic acid in the presence of a Lewis acid (Figure 4.4) that afforded **13** as a light yellow solid (85% yield) [48b]. In the model reaction, a higher yield (91%) and shorter reaction time (26 hours) was observed when $ZnBr_2$ was used as the Lewis acid (^{1}H NMR spectra shown in Appendix 1). These preliminary results encouraged subsequent reactions of arylamines **7** and **10** with diarylethene **14** *via* HMDS-mediated reactions in the presence of $ZnBr_2$ as the Lewis acid. (Figure 4.5).

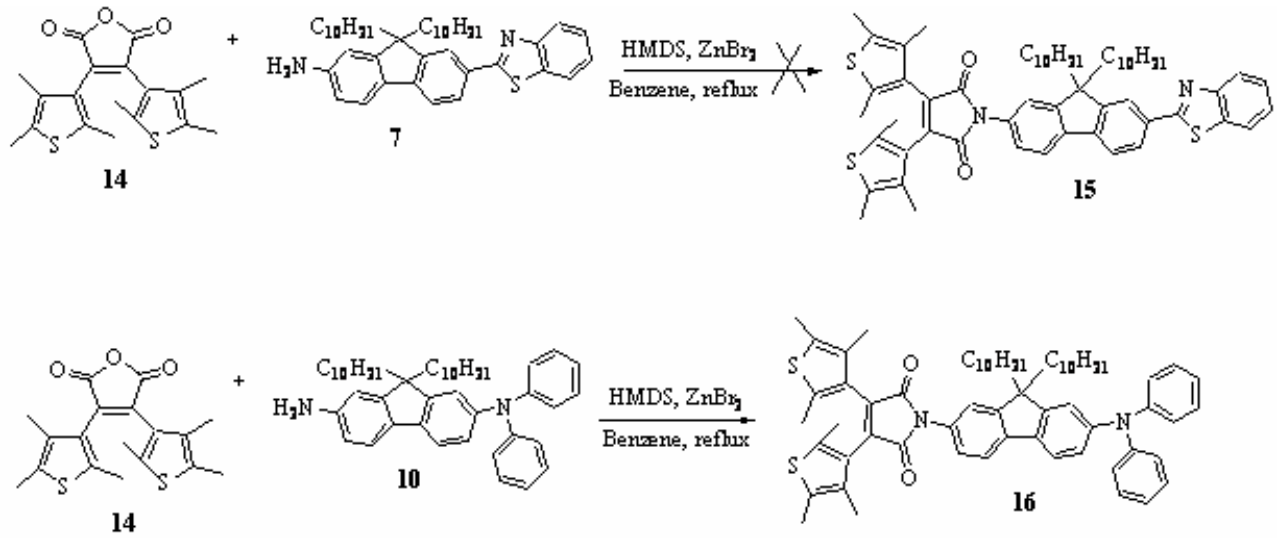

Figure 4.5. Synthesis of diarylethene **15** and **16** with substituted fluorene derivatives

The synthesis of fluorene derivatives **15** and **16** (shown in Figure 4.5) were not successful. In the case fluorene derivative **15**, after 80 hours of reaction mostly starting materials were present. The fact that the reaction between amine **7** and diarylethene **14** did not occur under the experimental conditions may be due to the low reactivity of this amine due to the presence of the electron-withdrawing benzothiazole group.

The same reaction conditions were used in the reaction of amine **10** with diarylethene **14**. In this case, the reaction was left under reflux for 36 hours, until the starting materials completely reacted (as followed by TLC hexanes: ethyl acetate 10:1). Amine derivative **10** was very reactive in the presence of oxygen and got oxidized quite rapidly, probably due to the presence of the diphenylamine electrodonating group in the fluorene core. Reaction was done inmmediately after preparation of the amine derivative and under N_2 atmosphere. The reaction afforded many products that were difficult to separate. ^{1}H NMR of the crude product confirmed the presence of the target product at low yield.

With the purpose of developing new synthetic routes to diarylethenes **15** and **16**, and to overcome the issues of the reactivity of the fluorene moiety due to the presence of electro-donating or electro-withdrawing groups, the reaction of an unsubstituted fluorene compound with diarylethene **14** was attempted (as depicted in Figure 4.6).

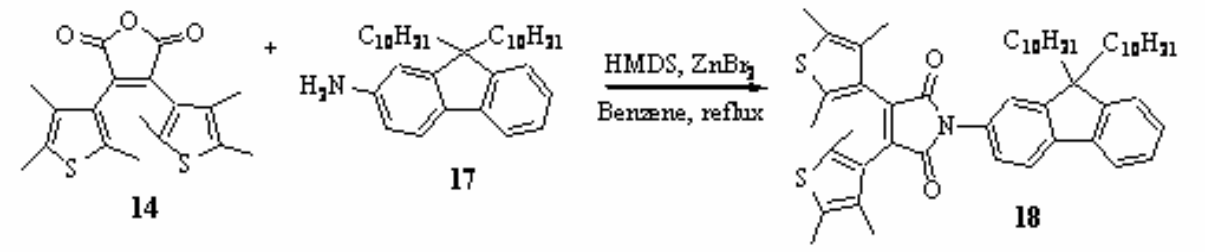

Figure 4.6. Synthesis of diarylethene **18** with unsubstituted fluorene derivative **17**

Hexamethyldisilazane (HMDS)-mediated reaction of the diarylethene **14** with 2-amine-9,9-didecylfluorene (**17**) and subsequent *in situ* cyclization of the resulting amic acid in the presence of a Lewis acid (Figure 4.6) afforded **18** as a light orange oil (76% yield). ^{1}H and ^{13}C NMR corresponded to the predicted signals of diarylethene **18** (Appendix A). The absorption

spectrum of diarylethene **18** in THF is shown in Figure 4.7. In the same figure, the absorption spectra of the open and closed forms of **14** are shown for comparison.

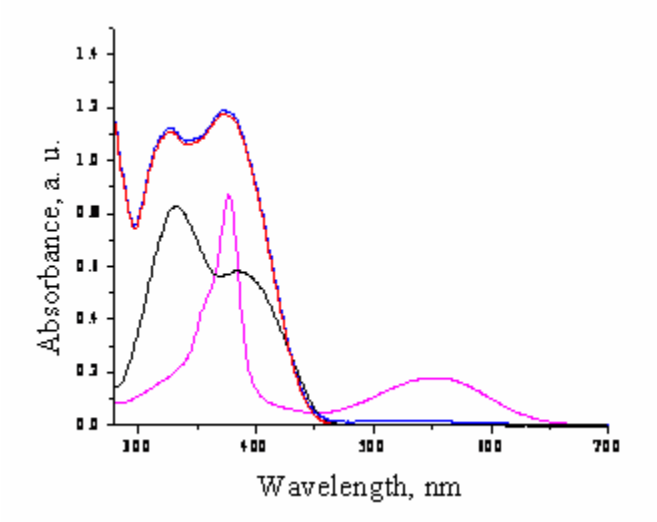

Figure 4.7. Absorption specta of the open (black) and closed isomers (magenta) of diarylethene **14** in THF, of the open form of diarylethene **18** (red) in THF, and diarylethene **18** in THF after irradiation at 300 nm for 10 minutes (irradiance ≈ 0.140 mW/cm^2).

An increased molar absorptivity from 350 to 450 nm was observed in diarylethene **18** when compared to the parent diarylethene **14**, expected due to the contribution of the fluorene derivative. The photochromism of diarylethene **18** was determined by excitation of its open form at 300 nm. The kinetic changes in the absorption spectra (C ≈ 2.5 x 10^{-5} M) of diarylethene **18** at temporal intervals of 100 s and excitation irradiance of ≈ 0.140 mW/cm^2 were recorded. After the first irradiace interval of 100 s, a new absorption band between 475 and 650 nm was observed. This absorption band is characteristic of the closed form of diarylethenes. However, subsequent irradiance demonstrated that this absorption band did not increase with subsequent irradiance intervals. For comparative purposes, solutions of equal molar concentrations (C ≈ 2.5 x 10^{-5} M) of diarylethenes **14** and **18** were irradiated for 100 s and the absorption spectra of the solutions were compared (Figure 4.8). The maximum absorption of diarylethene **18** in the visible

region corresponded to only 7% of the maximum absorption of diaylethene **14** in the same wavelength region.

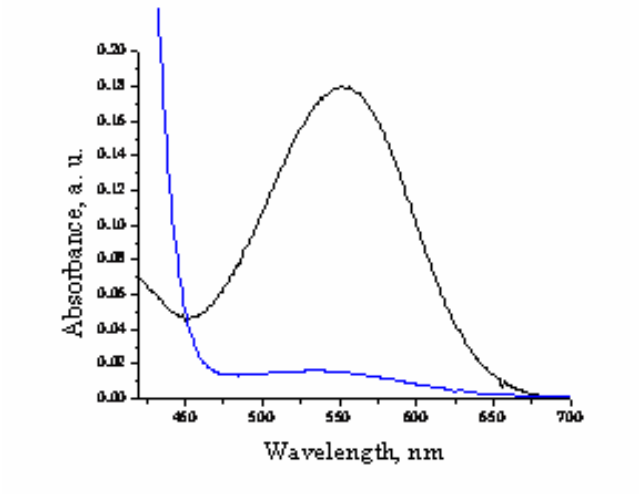

Figure 4.8. Absorption spectra of the closed form (black) of diarylethene **14** in THF and the closed form of diarylethene **18** (blue) in THF after irradiation at 350 nm.

Although quantitative analysis was not pursued to determine the photocyclization quantum yield of diarylethene **18**, these results suggest that this derivative loses most of the photochromic activity of the parent diarylethene (as depicted in Figure 4.9).

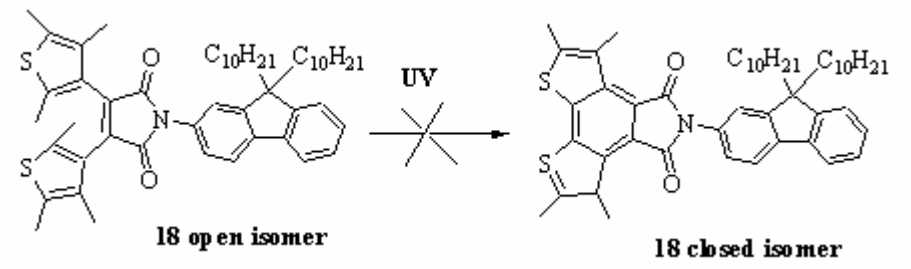

Figure 4.9. Schematic representation of the photocyclization reaction of diarylethene **18**

4.2.1 Synthesis of 2-nitrofluorene (2)

Fluorene (**1**) (15g, 90.2 mmol) and glacial acetic acid (150 mL) were added together into a three-neck round bottom flask (fitted with a mechanical stirrer, addition funnel and a

thermometer), and heated to 85 °C under N_2. Nitric acid (60%, 20 mL) was slowly added over a period of 20 min via the addition funnel, maintaining the temperature at 85 °C. The reaction was cooled to room temperature over 2 h, resulting in a thick yellow precipitate which was filtered, and washed with 300 mg of potassium acetate dissolved in 12 mL of acetic acid. The solid was transferred into 250 mL of distilled H_2O, stirred, and vacuum filtered. The yellow product was dissolved in absolute EtOH, and pale orange crystals were collected, washed with cold EtOH and dried, yielding 15.4 g of product (80% yield). m.p. 152-153 °C (lit 157 °C).

4.2.2 Synthesis of 2-iodo-7-nitrofluorene (3)

2-Nitrofluorene (**2**) (12 g, 56.87 mmol) and acetic acid (350 mL) were placed into a 500 mL three-neck flask fitted with a condenser, N_2 inlet and thermometer. I_2 (7.23 g, 28.49 mmol) was added and the reaction mixture was stirred for 30 min turning the orange, inhomogeneous solution to a dark orange-brown in coloration. $NaNO_2$ (4.4 g, 63.77 mmol), followed by concentrated H_2SO_4 (37.5 mL) was added and the reaction heated to 115-120 °C for 2 h. A pale yellow precipitate resulted. The suspension was cooled down to room temperature, poured into 500 g of ice, filtered and dried in a vacuum oven. The crude was recrystallized in a mixture of 1/1 (v/v) of EtOH/THF (1000 mL) resulting in the collection of yellow crystals (15.34 g, 80% yield). m.p. 245-246 °C (lit 244-245 °C).

4.2.3 Synthesis of 2-iodo-9,9-didecyl-7-nitrofluorene (4)

2-iodo-7-nitrofluorene (**3**) (9.6 g, 28 mmol), 1-bromodecane (12.58 g, 57.0 mmol), KI (0.49 g, 3 mmol), and DMSO (65 mL) were placed in a 250 mL 3-necked flask containing a stir

bar at room temperature. To the stirred solution, freshly powdered KOH (6.65 g, 119 mmol) was slowly added, turning the yellow reaction mixture dark green. The reaction was followed to completion via TLC (10:1 hexanes/EtOAc). The reaction mixture was poured into distilled water and its organic components extracted with hexanes. The organic extract was washed with water, dried over $MgSO_4$, and concentrated, affording 16.0 g of a viscous dark orange oil that crystallized upon standing. The resulting filtered and concentrated dark orange oil was purified via silica gel column chromatography (40:1 hexanes/EtOAc, 12.97g, 75% yield). ^{1}H NMR (300 MHz, $CDCl_3$) δ: 8.25 (d, 1H, ArH), 8.18 (d, 1H, ArH), 7.79 (s, 1H, ArH), 7.72 (m, 2H, ArH), 7.53 (d, 1H, ArH), 1.99 (m, 4H, CH_2), 1.18 (bm, 14H, CH_2), 1.05 (bm, 14H, CH_2), 0.83 (t, 6H, CH_3), 0.56 (m, 4H, CH_2).

4.2.4 Synthesis of 2-(tri-*n*-butylstannyl)benzothiazole (5)

Freshly distilled benzothiazole (20 g, 148 mmol) was added under N_2 via syringe into freshly prepared anhydrous THF (150 mL) in a 500 mL three-neck flask fitted with a low-temperature thermometer. The clear solution was cooled to -75 °C and *n*-BuLi (111 mL 1.6 M in hexanes) was slowly added, over 50 min, via an addition funnel, into the cooled solution (maintaining the temperature < -65 °C), gradually turning the solution a deep orange color. *n*-Bu_3SnCl (58 g, 178 mmol) was slowly added through an addition funnel into the cooled reaction mixture. Upon complete addition, the reaction was gradually allowed to warm to -10 °C and stirred for 1 h, turning the mixture green. After ~1 h, the reaction was gradually warmed to 0 °C and aqueous KF (3%, 100 mL) was gradually added, turning the solution bright yellow, which was then stirred at 10 °C for 1 h. The organic layer was diluted with toluene, separated, dried

over $MgSO_4$, filtered, and concentrated to give an orange-brown liquid. A light pale yellow liquid was collected (50g, 80%) under vacuum distillation at 144-146 °C/0.1 mm Hg (lit. 144-146 °C/0.15 mm Hg).

4.2.5 Synthesis of 2-(9,9-didecyl-7-nitrofluoren-2-yl)benzothiazole (6)

2-iodo-9,9-didecyl-7-nitrofluorene (**4**) (5.0 g, 8 mmol) and 2-(tri-*n*-butylstannyl)benzothiazole (**5)** (4.25 g, 10 mmol) were dissolved in 100 mL of toluene, degassed, and placed under Ar. To the clear yellow solution, $Pd(PPh_3)_4$ (0.235 g, 0.2 mmol) was added and degassed. The reaction was heated to 110 °C. The reaction was followed by TLC (10:1 (v/v) hexanes/ethyl acetate), and found to be complete after 5 h, during which time the mixture turned black in color. Toluene was removed *in vacuum*, and the resulting dark orange oil was purified via silica column chromatography using 30/1 (v/v) hexanes/ethyl acetate, and recrystallized from hexanes (3.0 g, 60 % yield). ^{1}H NMR (300 MHz, $CDCl_3$) δ: 8.32, 8.37 (dd, 1H, ArH), 8.24, 8.18 (dd, 1H, ArH), 8.14 (m, 1H, ArH), 8.10 (m, 1H, ArH), 7.96, 7.92 (dm, 1H, ArH), 7.91, 7.88 (dd, 1H, ArH), 7.87, 7.84 (dd, 1H, ArH), 7.57, 7.38 (dd, 1H, ArH), 7.53, 7.42 (dm, 1H, ArH), 7.49, 7.46 (dd, 1H, ArH), 2.14 (m, 4H, CH_2), 1.14 (bm, 14H, CH_2), 1.04 (bm, 14H, CH_2), 0.81 (t, 6H, CH_3), 0.62 (m, 4H, CH_2).

4.2.6 Synthesis of 7-benzothiazol-2-yl-9,9-didecyl-fluoren-2-ylamine (7)

2-(9,9-Didecyl-7-nitrofluoren-2-yl)benzothiazole (**6**) (940 mg, 1.5 mmol) was dissolved into a mixture of 1/1 (v/v) EtOH/THF mixture (10 mL) after which 10% Pd/C (940 mg) was

added. The reaction was heated to 70 °C under N_2 and hydrazine monohydrate 98% (753 mg, 0.73 mL, 15 mmol) was added dropwise and the reaction mixture was allowed to stir overnight. Upon completion (10 h, monitored by TLC: 10/1 (v/v) hexanes/ethyl acetate), the reaction was passed through a silica gel plug (under N_2), washed with THF and concentrated. A viscous sticky yellow oil was isolated (758 mg, 85% yield). ^{1}H NMR (300 MHz, $CDCl_3$) δ: 8.03, 8.00 (dm, 1H, ArH), 7.98 (d, 1H, ArH), 7.97, 7.95 (dd, 1H, ArH), 7.90, 7.86 (dd, 1H, ArH), 7.63, 7.59, 7.56, 7.51 (dd, 1H, ArH), 7.51, 7.44, 7.39, 7.32, (dq, 1H, ArH), 7.48, 7.35 (dm, 1H, ArH), 7.19 (m, 1H, ArH), 6.67 (M, 2H, ArH), 3.82 (bs, 2H, NH_2), 1.98 (m, 4H, CH_2), 1.15 (bm, 14H, CH_2), 1.04 (bm, 14H, CH_2), 0.82 (t, 6H, CH_3), 0.66 (m, 4H, CH_2).

4.2.7 Synthesis of 2-(9,9-didecyl-7-nitrofluoren-2-yl)diphenylamine (9)

2-Iodo-9,9-didecyl-7-nitrofluorene (**4**) (3.0 g, 4.86 mmol) was dissolved in 30 mL of 1,2-dichlorobenzene at room temperature under N_2. To this K_2CO_3 (5.37 g, 38.86 mmol), 18-crown-6 (256 mg, 0.97 mmol), and copper bronze (1.39 g, 21.86 mmol) were added at room temperature, resulting in an orange solution. Diphenylamine (0.82 g, 4.86 mmol) was added and the reaction mixture was heated to 180 °C for 43 h. TLC (5:1 hexanes:EtOAc) was employed to monitor the reaction, and upon completion, the dark brown mixture was filtered hot through a short silica gel plug (10:1 hexanes:EtOAc). The yellow solution was concentrated, resulting in a yellow-orange oil. The high boiling solvent 1,2-dichlorobenzene was removed under reduced pressure. The orange oil was further purified by column chromathography on silica gel using first 10:1:3 hexanes/EtOAc/THF, followed by 15:1 hexanes/EtOAc, resulting in a bright yellow-orange oil (2.56 g, 80% yield); ^{1}H NMR spectrum of **9** shown in the appendix). ^{1}H NMR (300

MHz, $CDCl_3$) δ: 8.25, 8.22 (dd, 1H, ArH), 8.14 (d, 1H, ArH), 7.67 (d, 1H, ArH), 7.62 (d, 1H, ArH), 7.32, 7.29 (dd, 4H, ArH), 7.16 (d, 1H, ArH), 7.10 (m, 2H, ArH), 7.06 (dm, 1H, ArH), 7.03 (dm, 4H, ArH), 1.85 (m, 4H, CH_2), 1.20 (bm, 14H, CH_2), 1.05 (bm, 14H, CH_2), 0.85 (t, 6H, CH_3), 0.65 (m, 4H, CH_2).

4.2.8 Synthesis of 9,9-didecyl-N,N-diphenyl-fluorene-2, 7-diamine (10)

2-(9,9-Didecyl-7-nitro-fluoren-2-yl)diphenylamine (**9**) (1.77 g, 2.68 mmol) was dissolved into a mixture of 1/1 (v/v) EtOH/THF mixture 20 mL) after which 10% Pd/C (1.8 g) was added. The reaction was heated to 70 °C under N_2 and hydrazine monohydrate 98% (1.34 g, 1.3 mL, 26.8 mmol) was added dropwise, and the reaction mixture was allowed to stir overnight. Upon completion (12 h) (TLC: 10/1 (v/v) hexanes/ethyl acetate), the reaction was passed through a silica gel plug (under N_2), washed with hexanes and concentrated (under N_2). A viscous sticky yellow oil was isolated (1.52 g, 90% yield). The crude oil was used immediately in the next step, due to its high reactivity. ^{1}H NMR (300 MHz, $CDCl_3$) δ: 7.6, 7.4 (dm, 4H, ArH), 7.2 (m, 4H, ArH), 7.15 (t, 4H, ArH), 6.9 (d, 2H, ArH), 6.6 (d, 2H, ArH), 1.85 (m, 4H, CH_2), 1.20 (bm, 14H, CH_2), 1.05 (bm, 14H, CH_2), 0.85 (t, 6H, CH_3), 0.65 (m, 4H, CH_2).

4.2.9 Synthesis of 2-amino-7-iodo-fluorene (11)

2-Iodo-7-nitrofluorene (**4**) (2.0 g, 3.24 mmol) was dissolved into a mixture of 1/1 (v/v) EtOH/THF mixture (20 mL) after which 10% Pd/C (2.0 g) was added. The reaction was heated to 70 °C under N_2 and hydrazine monohydrate 98% (1.62 g, d: 1.032. 1.58 mL, 32.4 mmol) was added dropwise and the reaction mixture was allowed to stir overnight. Upon completion (16 h)

(TLC: 10/1 (v/v) hexanes/ethyl acetate), the reaction was passed through a silica gel plug (under N_2), washed with hexanes and concentrated. A light brown solid was isolated (1.66 g, 87 % yield). ^{1}H NMR (500 MHz, $CDCl_3$) δ: 7.5 (d, 1H, ArH), 7.45 (d, 1H, ArH), 7.25, 7.19 (dm, 2H, ArH), 6.6 (d, 2H, ArH), 1.88 (m, 4H, CH_2), 1.10 (bm, 14H, CH_2), 0.96 (bm, 14H, CH_2), 0.83 (t, 6H, CH_3), 0.60 (m, 4H, CH_2).

4.2.10 Synthesis of 1-(9,9-bis-didecyl-7-iodo-9H-fluoren-2-yl)-pyrrole-2,5-dione (13)

A solution of 7-iodo-9,9-didecylfluoren-2-ylamine (**11**) (0.255 mmol, 150 mg) in dry benzene (5 mL) was added dropwise to a stirred solution of maleic anhydride (**12**) (0.255 mmol, 25 mg) in dry benzene (5 mL) was added dropwise at room temperature. After the addition was completed the solution turned yellow, without precipitates. The solution was stirred for 1 hour and then recrystallized $ZnCl_2$ (0.255 mmol, 34.8 mg) was added in one portion. While the resulting reaction mixture was heated (80 °C), a solution of HMDS (0.383 mmol, 80 μL) in dry benzene (2 mL) was added slowly, and the reaction mixture was refluxed. After 12 hours, starting materials were still present. An excess of 20% of $ZnCl_2$ and HMDS were added to drive the reaction to completion. The mixture was refluxed for another 36 hours after the starting materials reacted completely. The reaction mixture was cooled to room temperature and poured into 0.5 N HCl (10 mL). The aqueous phase was extracted with ethyl acetate (3 x 10 mL). The combined organic extracts were washed successively with 10 mL of saturated $NaHCO_3$ and brine and dried over Na_2SO_4. The solution was concentrated under reduced pressure to leave the residue which was purified by column chromatography (silica gel, 90:10 hexane/EtOAc) to afford **13** as a light yellow solid (144.6 mg, 85% yield). A higher yield (91%) and shorter

reaction time (26 hours) was observed when $ZnBr_2$ was used as the Lewis acid (^{1}H NMR spectra shown in A`ppendix 1). ^{1}H NMR (300 MHz, $CDCl_3$). δ: 7.62, 7.59 (dm, 2H, ArH), 7.25 (m, 4H, ArH), 6.75 (t, 4H, ArH), 1.85 (m, 4H, CH_2), 1.20 (bm, 14H, CH_2), 1.05 (bm, 14H, CH_2), 0.85 (t, 6H, CH_3), 0.65 (m, 4H, CH_2).

4.2.11 Synthesis of 11-(9,9-Bis-decyl-9H-fluoren-2-yl)-3,4-bis-(2,4,5-trimethyl-thiophen-3-yl)-pyrrole-2,5-dione (18)

Diarylethene **14** (0.6 mmol, 208 mg) and dry benzene (30 mL) were placed in a 100 mL two-necked round bottom flask fitted with a reflux condenser under N_2. The solution was protected from the light to avoid the formation of the closed photoisomer of diarylethene **14**. To this stirred solution, a solution of 7 9,9-Bis-decyl-9H-fluoren-2-ylamine (**17**) (0.6 mmol, 277 mg) in dry benzene (5 mL) was added dropwise at room temperature. After the addition was complete the solution turned yellow, without precipitates. The solution was stirred for 4 hours and then recrystallized $ZnBr_2$ (0.6 mmol, 135 mg) was added in one portion. While the resulting reaction mixture was heated (80 °C), a solution of hexamethyldisilazane (HMDS) (0.9 mmol, 145 mg, 190 μL) in dry benzene (2 mL) was added slowly in three equal portions over a period of 30 min, and the reaction mixture was then refluxed for 8 h. During the reflux period two additional portions of $ZnBr_2$ and HMDS were added at 4 h, and the reaction followed by TLC (hexane:ethyl acetate 90:10). Upon completion, the reaction mixture was cooled to room temperature and poured into 0.5 N HCl (15 mL). The aqueous phase was extracted with ethyl acetate (2 x 25 mL), and the combined organic extracts were washed successively with 30 mL of saturated $NaHCO_3$ and brine solution and dried over $MgSO_4$. The solution was concentrated under reduced pressure

and a light brown solid was recovered. (80 wt% yield, 379.3 mg). δ: 7.8 (d, 1H, ArH), 7.7 (d, 1H, ArH), 7.5 (m, 2H, ArH), 7.25 (m, 3H, ArH), 2.27 (d, 6H, CH_3), 2.3 (s, 3H, CH_3), 1.97 (d, 6H, CH_3), 1.95 (m, 4H, CH_2), 1.82 (s, 3H, CH_3), 1.60 (bm, 14H, CH_2), 1.4 (bm, 14H, CH_2), 0.85 (t, 6H, CH_3), 0.68 (s, 4H, CH_2).

CHAPTER 5. ENHANCEMENT OF NONLINEAR OPTICAL PROPERTIES OF DIARYLETHENES BY FÖRSTER RESONANCE ENERGY TRANSFER

RET from two-photon absorbing fluorene derivatives to the photochromic diarylethenes will be discussed in this chapter. Results from the investigation of RET in solution and in polymer films will be presented. The quenching of the steady-state fluorescence of donor molecules in the presence of the diarylethene acceptor was used to study the nature of resonance energy transfer. The Förster's distances and critical acceptor concentrations were determined for non-bound donor-acceptor pairs in homogeneous molecular ensembles.

5.1 Materials, Methods, and Instruments

Two-photon absorbing fluorene derivatives 2,7-bis[4-(9,9-didecylfluoren-2-yl)vinyl] phenyl benzothiazole (**19**) and poly(9,9-didecyl-2,7-diphenylaminofluorene) (**20**) (Figure 5.1) were synthesized and characterized as previously described [39a, 39b]. Spectroscopic grade hexane, THF, and ethyl acetate were used as solvents. Preparation of poly[methylmethacrylate-*co*-(diethyl vinyl benzyl phosphonate)] (PMMA-*co*-VBP) was described previously, consisting of a 1:3 molar ratio of diethyl vinylbenzylphosphonate to methylmethacrylate (MMA) [49]. All measurements were performed in spectroscopic grade hexane (Alfa Aesar). The steady state absorption spectra were obtained with an Agilent 8453 UV-visible spectrophotometer in 10 mm,

1 mm, 0.1 mm, and 0.01 mm path length quartz cuvettes, depending on the concentration of the corresponding solutions of donor (**D)** and acceptor (**A**) molecules. The steady-state fluorescence spectra were measured with a PTI Quantamaster spectrofluorimeter in 10 mm path length fluorometric quartz cuvettes under the right-angle observation geometry [42] and molecular concentrations, $C \leq 2 \cdot 10^{-6}$ M. For concentrated solutions, a 0.1 mm path length quartz cuvettes and zero-angle front-face excitation geometry was used [42]. The optical density of all the investigated solutions did not exceed 0.15 at the excitation wavelengths. Fluorescence quantum yields in solutions and polymer films were determined relative to 9,10-diphenylanthracene in cyclohexane [42]. The refractive index of a transparent PMMA-*co*-VBP polymer film (~ 40 μm) was determined on a Abbe refractometer (American Optical Corp.).

5. 2 Evidence of Förster's RET Mechanism: Calculation of Förster's Distances and Critical Concentrations in Solution and Polymer Films

Intermolecular RET from highly efficient two-photon absorbing fluorenes to a diarylethene was studied in order to develop more efficient 2PA photochromic materials for applications in 3D optical data storage and to provide a nondestructive readout method. As demonstrated by Castellano *et al.* [36b] the closed form of diarylethene **2** can be used as a photochromic energy transfer quencher of the emission of a fluorescent dye. Compared to previously reported diarylethene fluorescent switches (in which fluorescent dyes are covalently linked to the diarylethene) [36a], fluorescence modulation from non-covalently attached fluorescent dyes is a particularly intriguing approach due to the relative synthetic ease and versatility in materials selection. This alternative employs a mixture of 2PA dyes and photochromic molecules. The 2PA dye serves as a donor (**D**) and the photochromic compound

as an acceptor (**A**), combining efficient two-photon excitation with intermolecular RET. We investigated RET from two-photon absorbing fluorene derivatives to the open isomer of the photochromic diarylethene 3,4-bis-(2,4,5-trimethyl-thiophen-3-yl) furan-2,5-dione in hexane under one- and two-photon excitation [50]. Virgili *et al.* [51a] demonstrated efficient Förster transfer from poly (9,9-dioctylfluorene), PFO to the fluorescent red dye tetraphenylporphyrin (TPP) in films of PMMA. From the spectral overlap of the donor emission and acceptor absorption spectra, they calculated a Förster's distance (R_0), value of 48 Å. A Förster radius of 42 Å was determined by a femtosecond pump-probe spectroscopy method in a series of PFO/TTP blends with different TPP concentrations [51b]. For the success of this two-photon readout system (i.e., efficient readout of the two-photon up-converted fluorescence data modulated by cyclical transformations of the photochromic material), a 2PA dye needs to have (1) suitable two-photon up-converted fluorescence emission overlapping the absorption spectrum of the closed form of diarylethene **2**, (2) high fluorescence quantum yield at the selected readout excitation wavelength, (3) higher δ_{2PA} (at least one order of magnitude greater than that of the closed form of diarylethene **2**), and (4) high photostability to facilitate numerous readout cycles. Fluorene derivatives **19** and **20** (Figure 5.1) were introduced in order to provide a signal output used for read-out (two-photon up-converted fluorescence/RET). These fluorene derivatives were selected from a group of efficient two-photon absorbing (2PA) fluorescent probes synthesized in our laboratory [39], since they exhibit all the characteristics previously described.

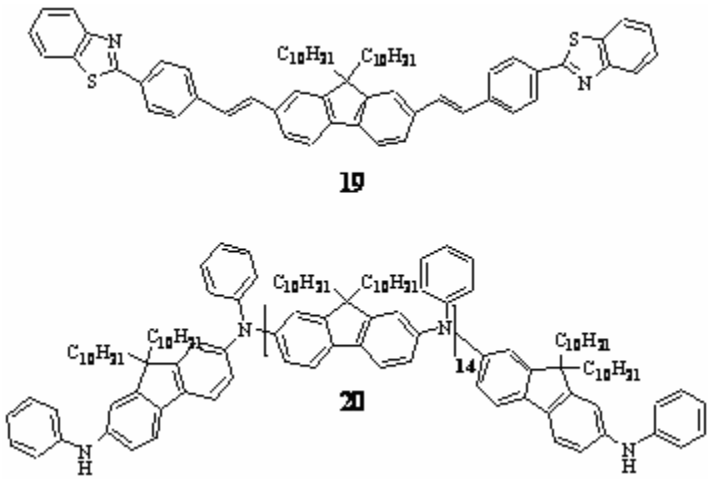

Figure 5.1. Molecular structures of fluorene derivatives **19** and **20**

Absorption and single-photon induced emission spectra of fluorenes **19** and **20** in THF and in polymer films of PMMA-*co*-VBP are shown in Figure 5.2. Fluorescence quantum yields (Φ_f) of **19** were 1.0 ± 0.05 in hexane and 0.98 ± 0.05 in THF [39b]. The Φ_f of **20** was near unity in hexane and cyclohexane [39a]. Fluorene derivative **19** belongs to the A-π-π-π-A molecular structure. The extended π-conjugation and the presence of acceptor groups facilitate photo-induced charge transfer along the conjugation path upon excitation, resulting in large optical nonlinearities [39]. The δ_{2PA} of fluorene **19** was 6000 GM at 600 nm and ≈1200 GM at 800 nm [39b]. Compound **20** belongs to the D-π-D type of 2PA chromophores, having high thermal and photo stability. The δ_{2PA} of fluorene **20** (containing 16 chromophore units) was 16500 GM at 660 nm and 2000 GM at 720 nm [39a]. Figure 5.3 shows the normalized absorption spectra of the open form and photostationary state of diarylethene **2** after irradiation at 254 nm, and the absorption and emission spectra of fluorene derivative **19** (λexc.= 400 nm).

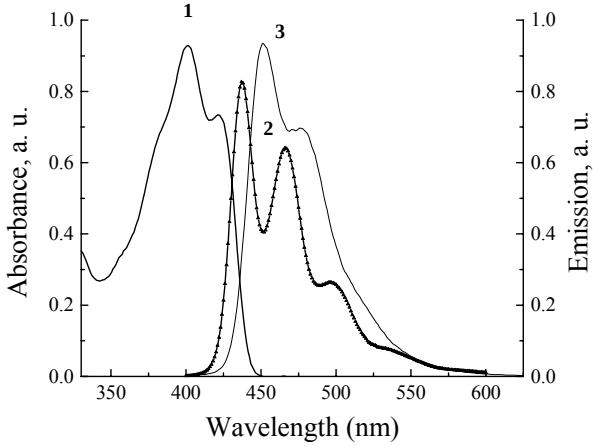

a

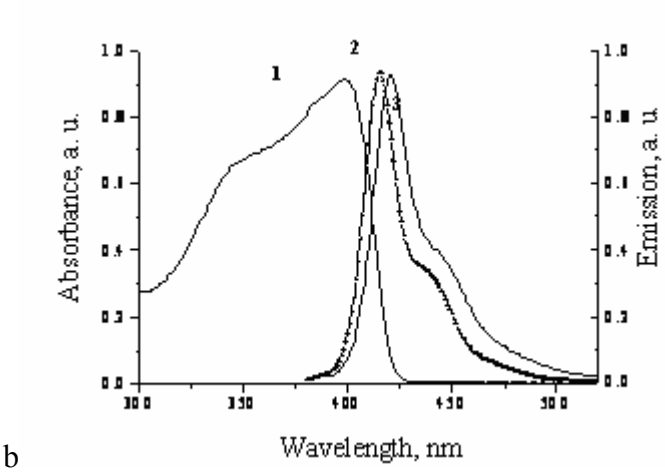

b

Figure 5.2. (1a) Absorption spectrum of fluorene derivative **19** in THF; (2a) emission spectra of fluorene derivative **19** in THF; (3a.) emission spectra of fluorene derivative **19** in polymer film; (1b) absorption spectrum of fluorene derivative **20** in THF; (2b.) emission spectra of fluorene derivative **20** in THF and (3b) emission spectra of fluorene derivative **20** in polymer film of PMMA-co-VBP.

As shown in Figure 5.3, there is good spectral overlap between the absorption spectrum of the closed form of diarylethene **2** and the emission spectrum of fluorene **19**. Experimental observation of the fluorescence quenching of the fluorene **19** donor molecules was performed in solutions with different concentrations of **A** in 0.1 mm cuvettes under zero-angle front-face excitation geometry. The absorption spectra of fluorene **19** in THF solutions with diarylethene **2**, along with the corresponding quenched fluorescence spectra are shown in Figure 5.4.

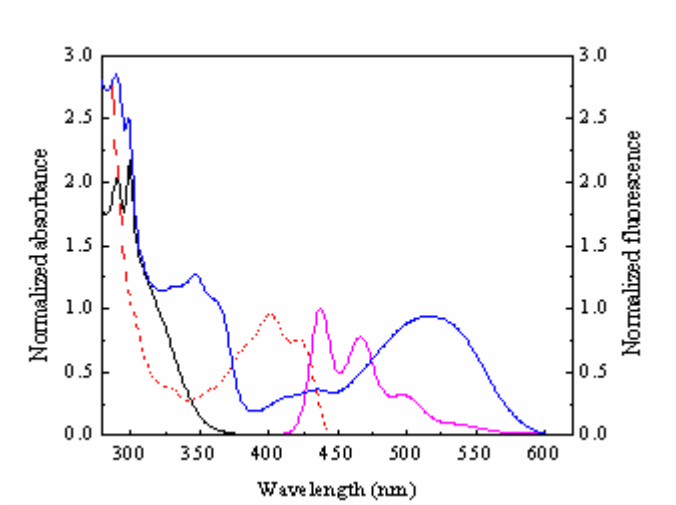

Figure 5.3. Normalized absorption spectra of open form (black) and photostationary state (blue) of diarylethene **1** (irradiating at 254 nm), and absorption (red) and emission spectra (pink) of fluorene derivative **19** ($\lambda_{exc.}$= 400 nm).

One-photon excitation was performed at λ_{exc} = 393 nm, where the optical density of the solutions was ≤ 0.10 in order to minimize reabsorption effects. Increasing concentrations of the closed isomer corresponded with decreasing emission of fluorene **19**.

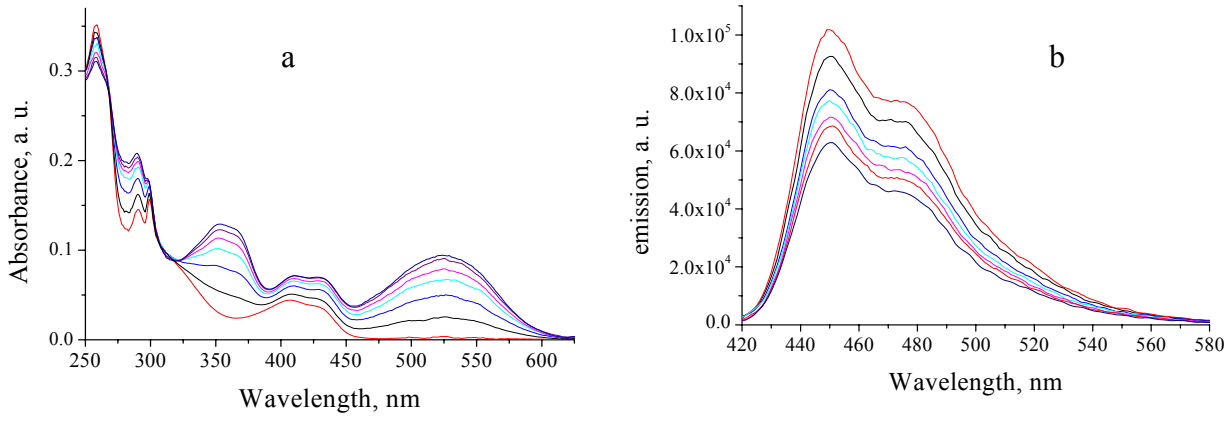

Figure 5.4. (a) Kinetic changes in the absorption spectra of 1 under irradiation at λexc = 254 nm in presence of fluorene **19** (temporal step between two adjacent spectra, Δt = 10 s). (b) Kinetic changes in the single-photon emission spectra of fluorene derivative **19** by the closed form of diarylethene derivative **2** in THF (λexc = 383 nm).

Experimental observation of the fluorescence quenching was also performed in polymer film of PMMA-*co*-VBP. Spectral changes of a film with 0.9 wt% of fluorene derivative **2** and

22 wt% of fluorene **19** during irradiation are shown in Figure 5.5. This figure demonstrates reversible fluorescence control with complete on-off of a polymer film doped with diarylethene **2** and fluorene **19**.

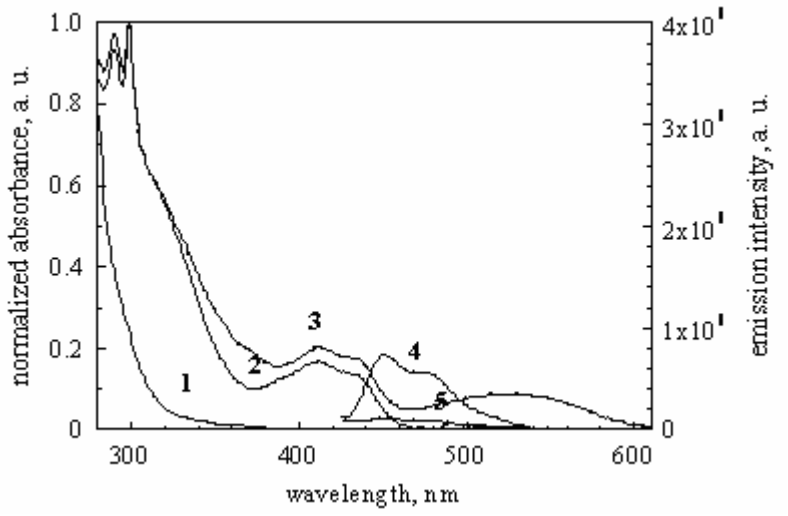

Figure 5.5. 1. Absorption spectrum of a film of PMMA-co-VBP; 2) absorption spectrum of a PMMA-co-VBP film containing diarylethene **1** (open form) and fluorene **19** 3) same film as 2 after irradiation at 254 (long absorption band corresponds to the closed form of diarylethene **1**) 4) emission of fluorene **19** before irradiation of the film 5) emission of fluorene **19** after irradiation of the film containing.

Based on the spectral data, and taking into account that $\varepsilon_A(\lambda^{\max}) \approx 9.9 \times 10^3$ $M^{-1} \cdot cm^{-1}$ for the closed form of diarylethene **2** in THF, the efficiency of RET can be estimated. Under the Förster's RET mechanism, $k_T(r)$ (the rate of energy transfer from **D** to **A)**, is proportional to $(R_0/r)^6$, and can be expressed as [42]:

$$k_T(r) = \frac{1}{\tau_D}\left(\frac{R_0}{r}\right)^6 = \frac{\Phi_{FL} \cdot k^2}{\tau_D r^6} \cdot \left(\frac{9000\ln(10)}{128\pi^5 N_A n^4}\right) \cdot J \qquad (1)$$

where R_0 is the Förster distance, r is the distance between **D** and **A** molecules, τ_D and Φ_{FL} are the lifetime and fluorescence quantum yield of **D** in the absence of **A**, respectively; k is the orientation factor; N_A is Avogadro's number; n is the refractive index of the medium; J is the

overlap integral expressed the degree of spectral overlap between the emission of **D** and absorption of **A** [42]:

$$J = \frac{\int_0^\infty F_D(\lambda) \cdot \varepsilon_A(\lambda) \cdot \lambda^4 d\lambda}{\int_0^\infty F_D(\lambda) \cdot d\lambda} \qquad (2)$$

$F_D(\lambda)$ is the corrected fluorescence intensity of **D**; $\varepsilon_A(\lambda)$ is the extinction coefficient of **A** ($M^{-1} \cdot cm^{-1}$) at wavelength, λ (cm). From equation 1 the Förster distance R_0 (at which the transfer rate $k_T(r)$ is equal to the decay rate of the donor in the absence of acceptor ($1/\tau_D$)) can be expressed as [42]:

$$R_0 = \left[\frac{9000 \ln(10) k^2 \Phi_{FL}}{128 \pi^5 N_A n^4} \cdot J \right]^{\frac{1}{6}} \qquad (3)$$

$A_0 \approx 447 / R_0^3$ is the so-called critical concentration of **A** in M. The fluorescence quantum yields, Φ_{FL}, calculated overlap integrals, J, Förster radius R_0 and critical concentrations A_0 for fluorenes **19** and **20** in THF and in polymer films are presented in Table 1 (n^{20}_D of PMMA-*co*-VBP film was 1.44±0.01).

From this data, fluorene **19** is characterized by the highest potential efficiency of Förster's RET, whereas fluorene **20** is not expected to be as efficient in energy transfer to diarylethene **2** due to its lower value of *J*.

Table 5.1. Quantum yields, Φ_{FL}, calculated overlapping integrals, J, Förster radius, R_0, and critical concentrations, A_0, for fluorenes **19** and **20** in THF and in polymer films of PMMA-co-VBP

Fluorene	**19 (THF)**	**19 (film)***	**20 (THF)**	**20 (film)***
Φ_{FL} x10^2	98 ± 5	97 ± 5	98 ± 5	96 ± 5
J x10^{15}, $M^{-1}\cdot cm^3$	29.5	33.8	12.4	15.3
R_0 , Å	40.3±2.3	40.5±2.3	34.9±2.0	35.5±2.0
A_0 x10^3, M	6.8±0.4	6.7±0.4	10.5±0.6	10.0±0.6

*30 μm polymer films

CHAPTER 6. DEMONSTRATION OF NOVEL RET-BASED TWO-PHOTON 3D OPTICAL DATA STORAGE *VIA* FLUORESCENCE MODULATION OF AN EFFICIENT FLUORENE DYE BY A PHOTOCHROMIC DIARYLETHENE

Results from the preliminary studies described in Chapters 3 and 5 are the basis for subsequent studies in solid thin films described in this chapter. The principle of the device was demonstrated by recording and reading out data by single- and two-photon excitation in polymeric films, in single and multilayer (3D) configurations. For the solid film studies, PMMA-*co*-VBP was used as the host polymer [49]. This polymer was chosen due to its excellent solubility in acetonitrile and its ability to solubilize diarylethenes and fluorene derivatives at high concentrations without aggregation.

6.1 Single-Photon Recording/Single-Photon Readout

For single-photon recording, diarylethene **2** and fluorene derivatives **19** or **20** were dispersed into PMMA-*co*-VBP to make the photochromic polymeric storage medium (Figure 6.1). Solutions containing approx. 0.01 M of the open form of diarylethene **1** (approx. 22 wt% of diarylethene **2**) and 2 wt% fluorene derivatives **19** or **20** (relative to the polymer) were irradiated in a Rayonet photoreactor at 254 nm (~3mW/cm^2), until the photostationary state of diarylethene **2** was reached (determined by monitoring the UV-visible absorption spectrum).

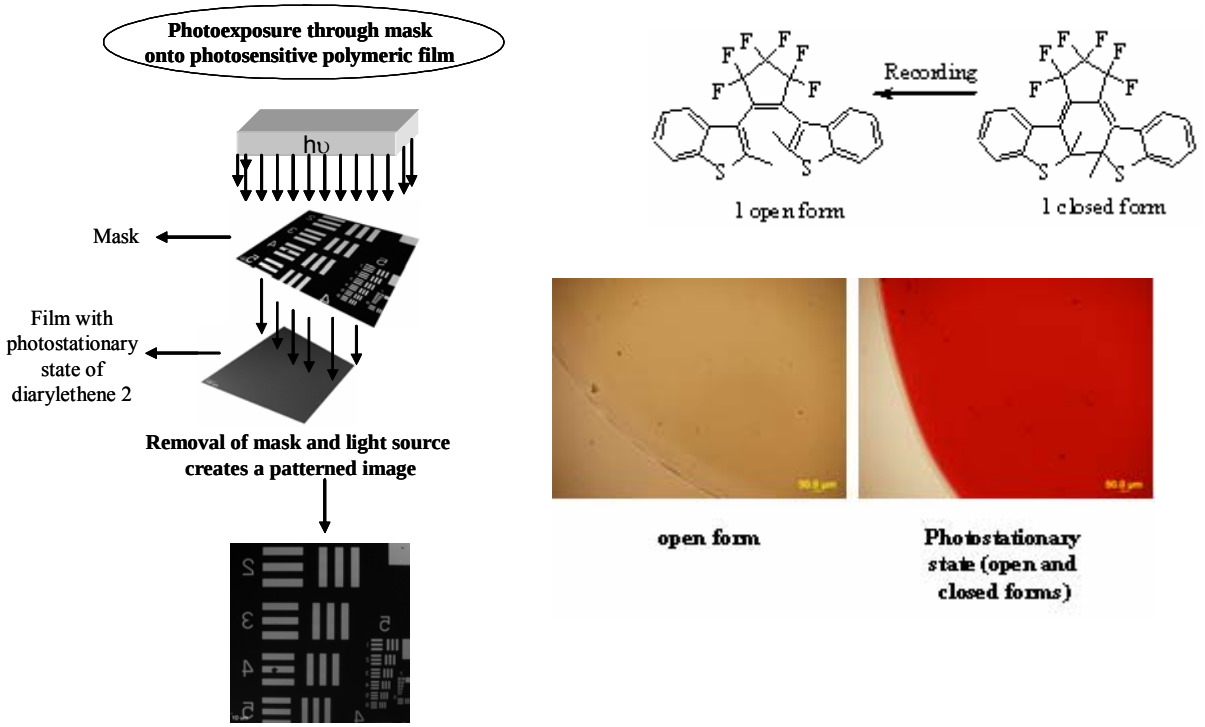

Figure 6.1. Schematic representation of single-photon data recording onto photosensitive polymeric films containing the photostationary state (open and closed forms) of diarylethene **2**. Transmission image of a polymer film containing the open and photostationary state for diarylethene **2**.

Red solutions were obtained before coating. Films of ca. 40 μm were coated on glass slides using the photostationary state mixture (Figure 6.1). Films were placed on the stage of an inverted microscope (Olympus IX81) and irradiated through the condenser of the same microscope (N.A.= 0.55). A bandpass filter (IF550, Olympus) with peak transmission at 520 nm and full width at half-maximum equal to 65 nm was placed in front of the light source (halogen lamp from the Olympus IX81 microscope U-LH100-3). A number of different masks, including Air Force resolution targets, TEM and home made masks (Figures 6.2, 6.3 and 6.4), were used.

Data was recorded by focusing the excitation light (~10 mW/cm^2) through one mask and then exposing the photochromic film, subsequently changing the ratio of the closed-to-open forms in the irradiated areas, and, therefore, changing the refractive index. After mask removal, confocal fluorescence microscopy (using a filter cube with λ_{ex}: 377/50nm, a Dichroic mirror:

409nm and a longpass filter λ_{em}: 460/50 nm) or standard Differential Interference Contrast (DIC) microscopy was used to readout the recorded data, where a 10x (Olympus UplanFLN 10x, N.A.=0.3) or a 20x (Olympus LUCplanFLN 20x, N.A.=0.45) objective lens was used. The optimal exposure time for this storage medium under single-photon excitation was estimated by identifying the intensity profile and calculating the contrast (signal-to-background ratio). For 40 μm thick films a contrast of 5.7 was achieved after 20 s exposure, while a contrast of 3.6 was obtained after 10 s exposure. Improvement of the recorded signal-to-noise ratios minimized the potential hazard of overexposing films and compromising of resolution.

Figures 6.2(a) and 6.2(b) show typical DIC images (using the 10x objective) obtained before and after single-photon recording. To determine the smallest readout pattern achieved in this absorbance-based single-photon readout method, intensity profiles across one specific line were obtained. Figures 6.2(f) and 6.2(g) show the intensity profiles of the data mask (the Air Force resolution target) and our recorded data, respectively. The size of the patterns (bar width) marked by the red circles in Figures 6.2(c) and 6.2(d) correspond to 7.8 μm. When using the 20x objective to read-out the same recorded data in the right-hand-side patterns in Fig 6.2(d), we found that the smallest readout pattern achieved in this system was ~3.5 μm (as shown in Figure 6.2(e) and 6.2(h)). TEM grids (400-mesh nickel square and 100-mesh hexagonal grids from Polysciences, Inc.) were also used as masks (Figures 6.3 (a) and (e)). Figures 6.3(c) and 6.3(g) show the intensity profiles of the data mask (TEM grids) and Figures 6.3(d) and 6.3(h) show the intensity profiles of the recorded data. The line width of the hexagonal pattern in the original projected TEM mask (Figure 6.3 (a)) corresponds to 10.0 μm. The line width after recording corresponds to 8.0 μm (Figure 6.3 (b)).

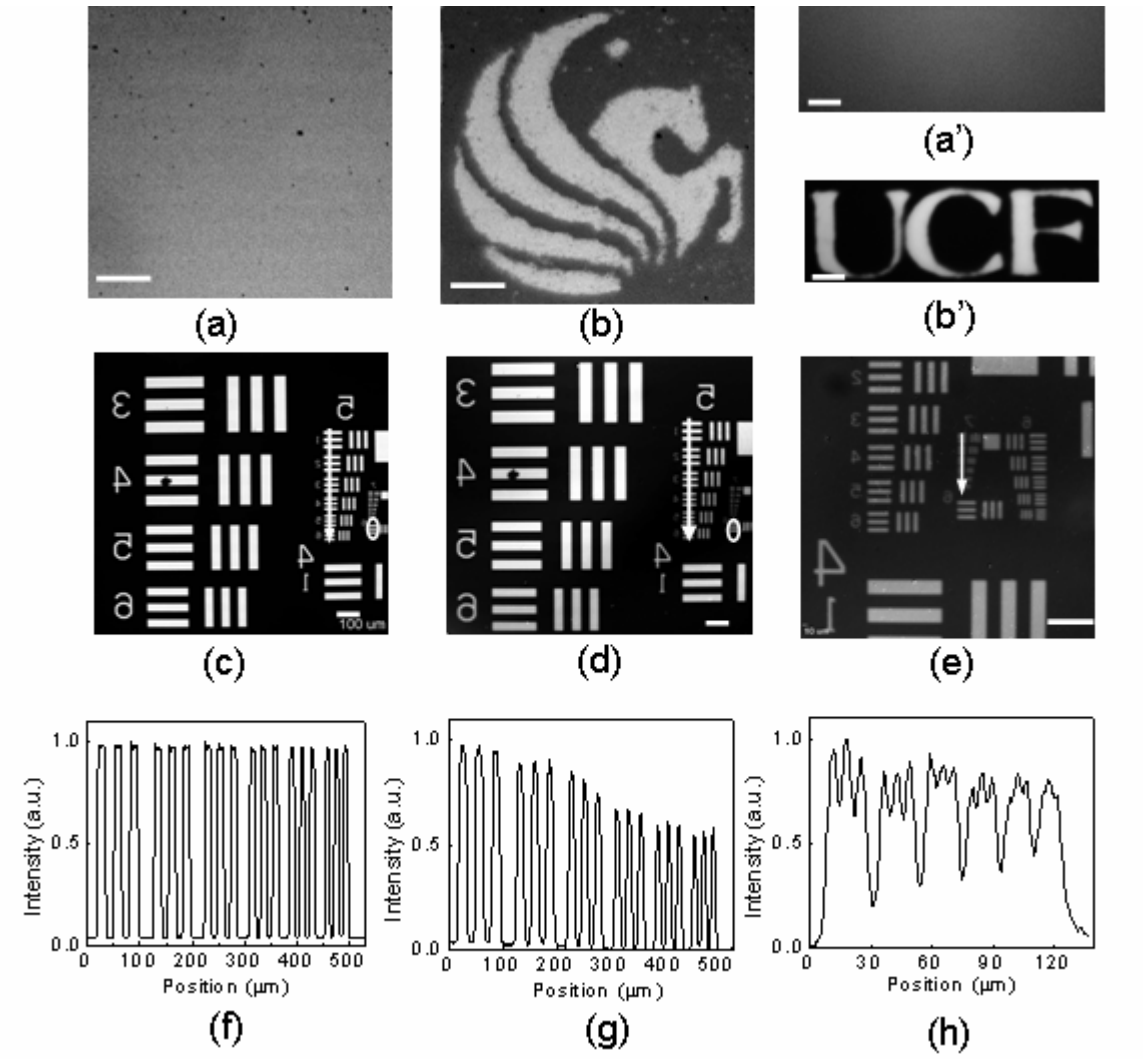

Figure 6.2. DIC images of storage medium before (a and a') and after (b and b') single-photon data recording; (c) Air Force resolution mask (data mask), (d) readout data using 10x objective; (e) readout data using 20x objective; (f), (g) and (h) are the intensity profiles (whose direction is shown by the arrows) of the corresponding patterns in (c), (d) and (e), respectively. The scale bars in (a)-(e) correspond to 100 μm.

As shown in Figures 6.3(c) and 6.3(d), the intensity profiles for the original mask and the recorded pattern were nearly the same. The line width of the square pattern in the original projected TEM mask (Figure 6.3 (g)) was 5.5 μm. The line width after recording was 4.5 μm (Figure 6.3 (h)).

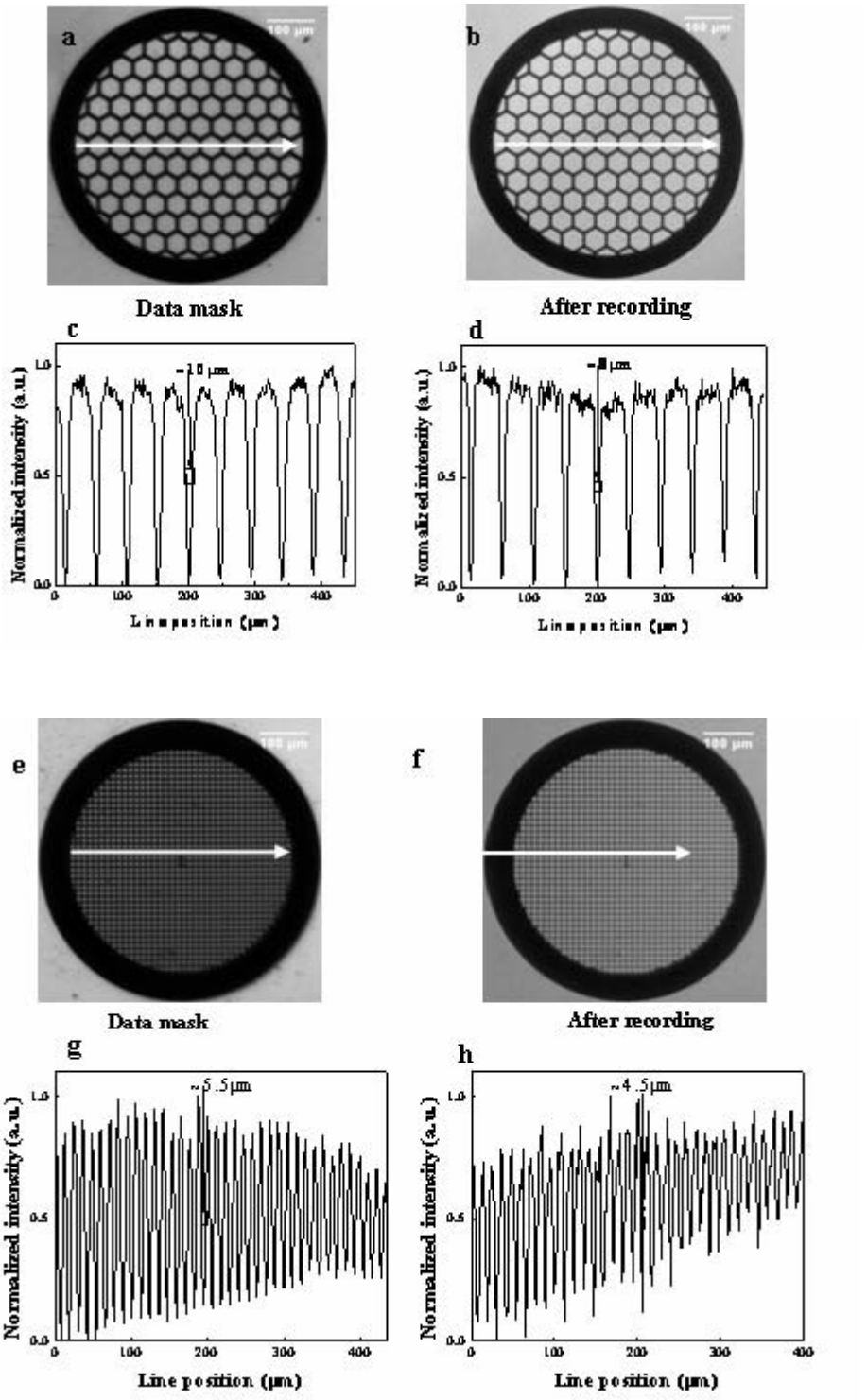

Figure 6.3. (a, e) DIC images of the data mask (TEM grids), (b, f) DIC readout images of data patterns inside the photochromic medium recorded by the single-photon method. Curves (c) and (d) are the line profiles (whose direction is shown by the arrows) of the corresponding patterns in (a) and (b), respectively. Curves (g) and (h) are the line profiles of the corresponding patterns in (e) and (f), respectively.

It is worth mentioning that fluorescent readout by **single-photon** excitation of the fluorenes **19** or **20** (Figure 6.4) did not provide a non-destructive readout method, since there is considerable absorption of the closed form of the diarylethene at the excitation wavelength used in the fluorescence read-out (377nm). In contrast, due to the differences in nonlinear absorption of the components of the system at the excitation wavelength, a virtually non-destructive read-out method by **two-photon** excitation was demonstrated (Section 6.2.1).

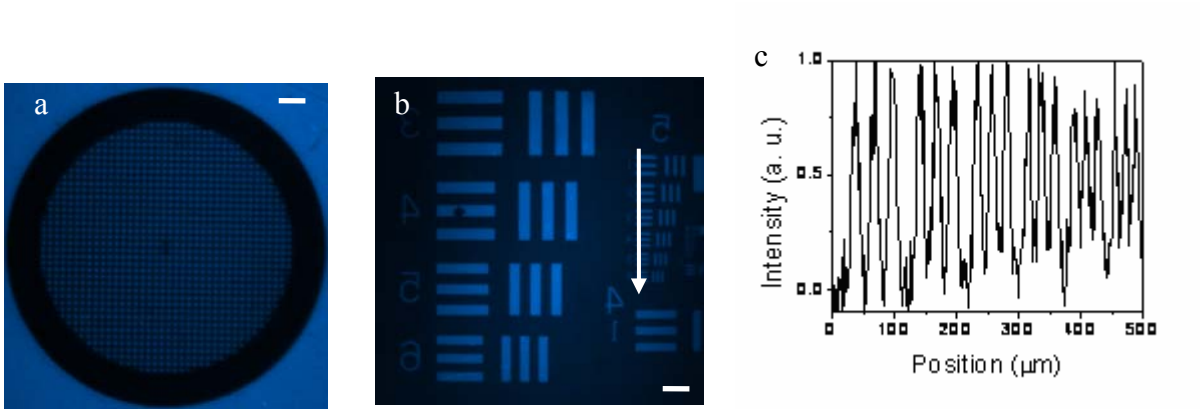

Figure 6.4. Fluorescence readout of storage medium after single-photon data recording of a TEM mask (a) and air force resolution target (b) (using 10x objective); (c) is the intensity profile (whose direction is shown by the arrows) of the corresponding pattern in (b). The scale bars correspond to 100 μm.

Recording of data can also be accomplished by using the open form of diarylethene **2** (as shown in Figures 6.5 and 6.6) and the same recording procedure as previously described (using a short pass filter at 420 nm instead of the IF550 bandpass filter).

Figure 6.6A shows typical DIC images (using the 10x objective), obtained before and after single-photon recording. Photosensitive films containing only the open form isomer (6.6a) or the photostationary state (6.6a') were tested. A home-made mask (6.6b) was projected onto the films. In the exposed areas in 6.6c, photoisomerization from the open to the closed form occurred, showing the recorded data as a dark pattern over a bright background.

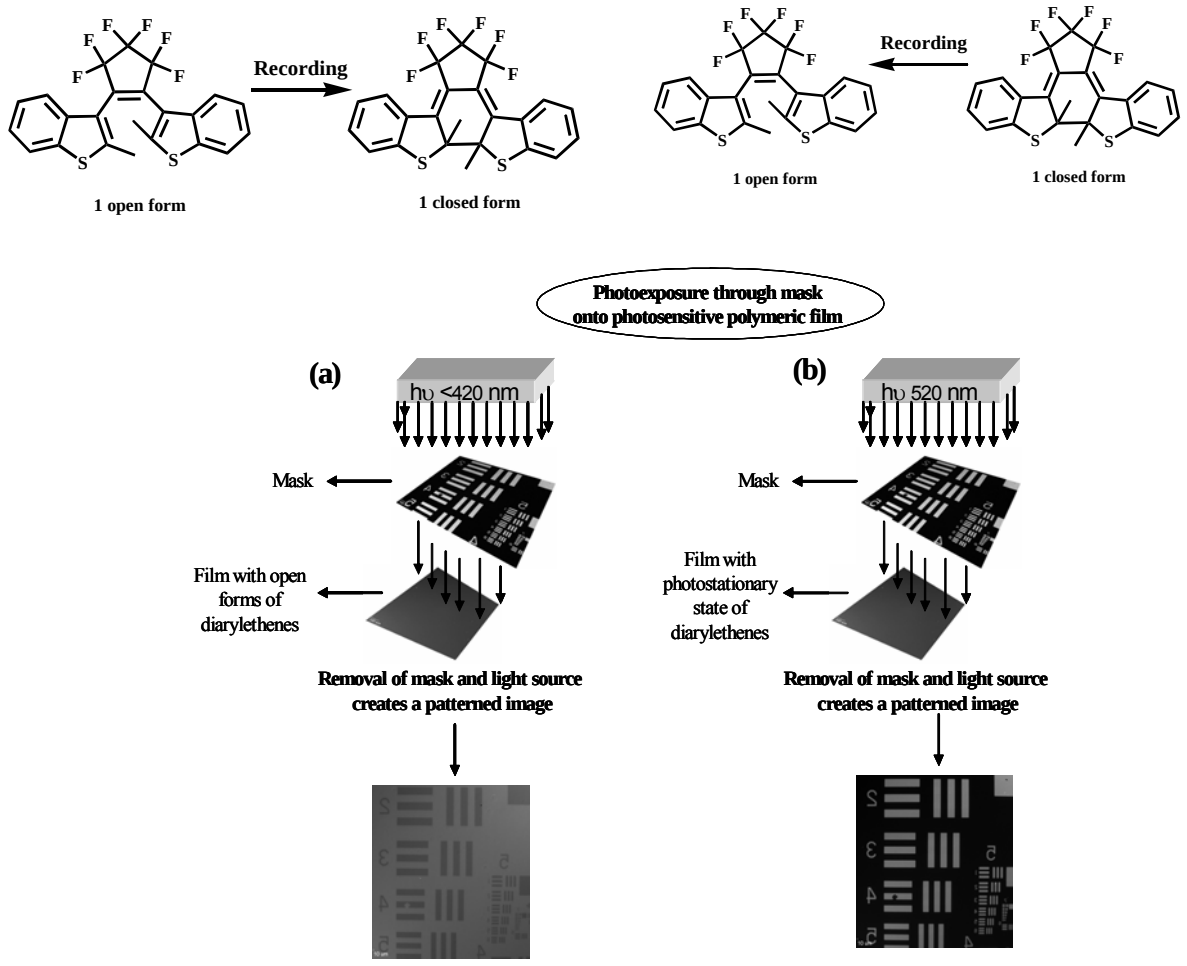

Figure 6.5. Schematic representation of single-photon data recording onto photosensitive polymeric films containing the open form (a) and the photostationary state (open and closed forms, b) of diarylethene **2**.

On the contrary, in the exposed areas in Figure 6.6c', photoisomerization from the closed to the open form occurred, showing the recorded data as a bright pattern over a dark background. Contrast and resolution of these recording methods were compared by using photosensitive films with the same thickness and same concentration of diarylethene **2** and fluorene **19,** and an Air Force resolution target (Figure 6.6B).

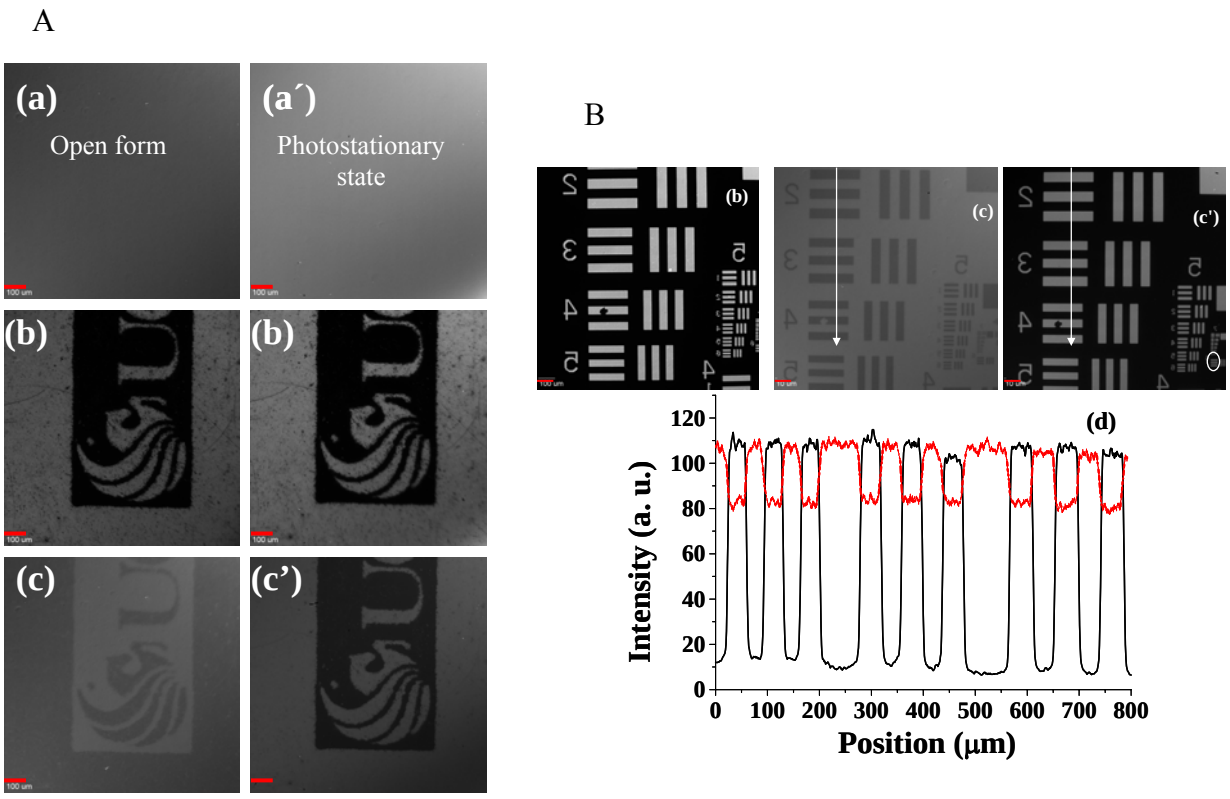

Figure 6.6. DIC images of the original photosensitive films containing (a) open form and (a') photostationary state of diarylethene **2** before recording. DIC images of a home-made and air force resolution mask (b). Readout (DIC images) of data patterns inside photochromic medium recorded by single-photon excitation (c and c') containing the open form and (c) and photostationary state (c') of diarylethene **2**. d. Intensity profiles of the recorded patterns in 2c (red) and 2c' (black)

Figure 6.6Bc and 6.6Bc' show images obtained after single-photon recording. Intensity profiles across one specific line were obtained. Figure 6.6B (d) shows the comparison of the intensity profiles. Intensity profiles were normalized for the different intensities of the filters used for excitation. In the case of 6.6B(c) a contrast (signal-to-noise ratio) of 1.3 was calculated. In 6.6B (c'), a much better contrast of 8.5 was obtained. The size of the patterns (bar width) marked by the white circle in Figure 6.6B (c') corresponds to 7.8 μm.

6.1.2 Rewritable data storage by single-photon recording/single-photon readout

Since the introduction of diarylethenes, the capability of having a rewritable memory device using photochromic diarylethenes has been reported [52]. The ability to write, erase, and rewrite information by single-photon excitation into the same region of a PMMA-*co*-VBP film containing diarylethene **2** was demonstrated in Figure 6.7. Figure 6.7a shows a DIC image (20x) of the photosensitive film containing the open form isomer of diarylethene **2** before exposure. The marked (circled) artifact is use to indicate that the images are in the same area of the film. An Air Force resolution mask (6.7b) was projected onto the film.

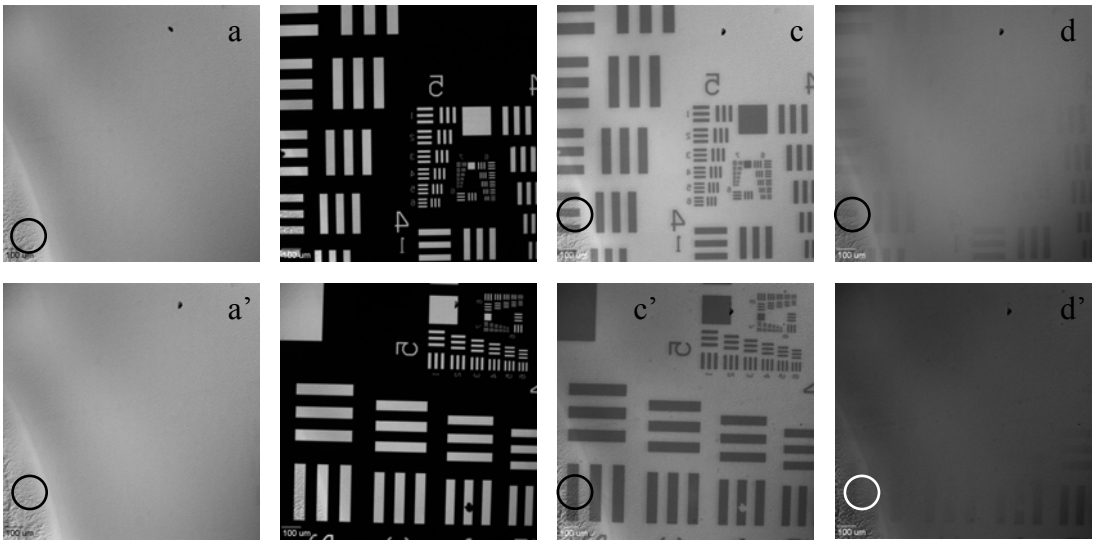

Figure 6.7. Demonstration of writing, erasing, and rewriting in the same area of a PMMA-*co*-VBP /photochromic film using single-photon excitation. The marked artifact indicates that the images are in the same area. DIC images of (a) and (a') the films before recording, (b) and (b') masks, (c) and (c') data recorded in the first and second cycles, respectively, (d) and (d') data erased ($\lambda_{exc.}$:525 nm, 20ms) after the first and second cycles, respectively.

Data was recorded by focusing the excitation light ($\lambda_{exc.}$: 325 nm, 240mW/cm^2.s) through the mask and then exposing the photochromic film (6.7c). This data was partially erased (6.7d) after 20ms of excitation at 525 nm by using the Hg lamp from the Olympus IX81 microscope and a filter cube (Tritc $\lambda_{exc.}$: 525/40 nm), and it was totally erased after 60 ms exposure (6.7a'). A

different pattern (6.7b') was subsequently rewritten in the same area of the film (6.7c') and erased (6.7d') for the second time. The same procedure was repeated 20 times (Figure 6.8) with no apparent damage of the polymer film, demonstrating rewritable optical memory.

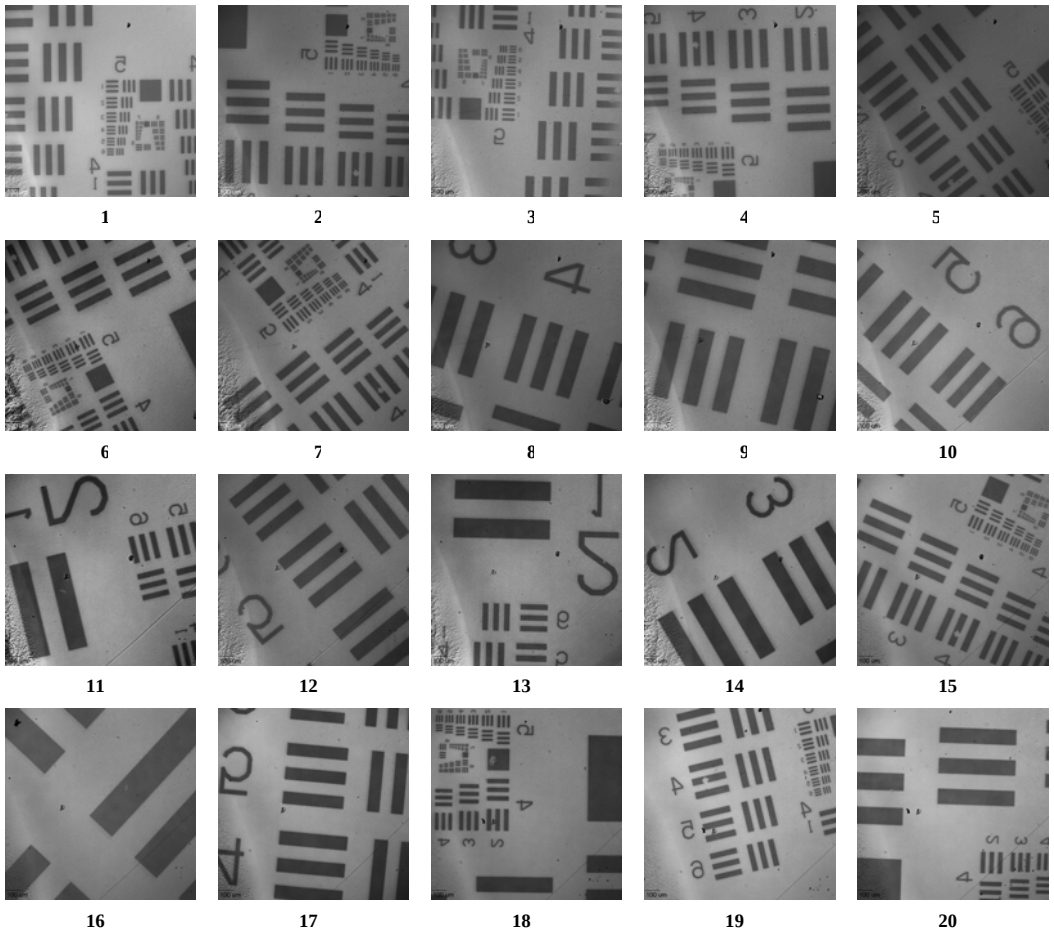

Figure 6.8. Demonstration of 20 writing, erasing and rewriting cycles in the same area of the PMMA-*co*-VBP/ containing photochromic film via single-photon excitation.

Writing, erasing and rewriting capability on a polymer film containing the photostationary state of diarylethene **2** was also demonstrated (Figure 6.9).

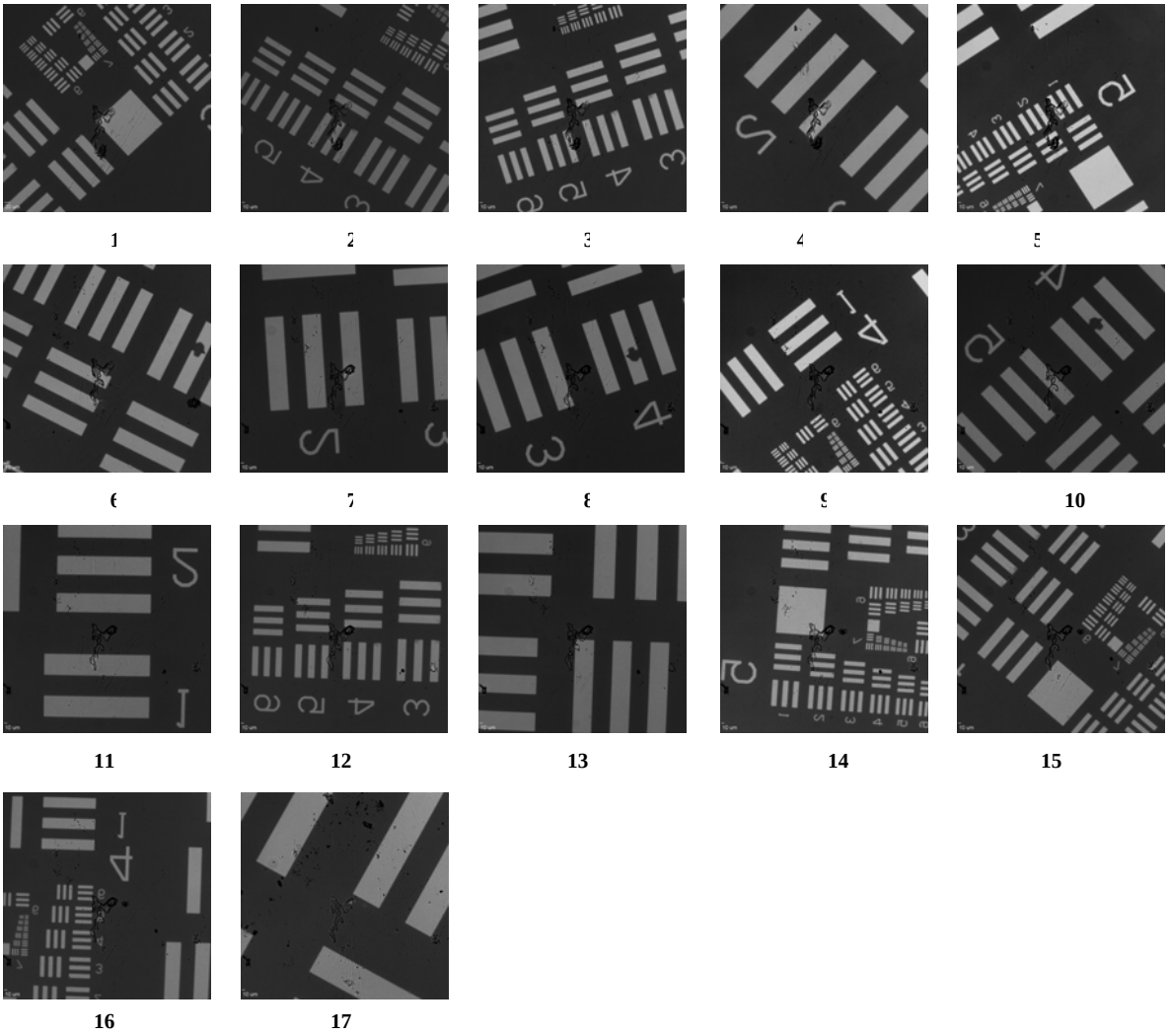

Figure 6.9. Demonstration of 17 writing, erasing and rewriting cycles in the same area of a PMMA-*co*-VBP/containing photochromic film using single-photon excitation. The artifact in the center of the image indicates that the recording cycles were performed in the same area of the film.

6.2 Single-Photon Recording/Two-Photon Readout

Using a modified Olympus Fluoview FV300 two-photon microscope equipped with a tunable femtosecond laser, two-photon readout was convincingly demonstrated (Figure 6.10). In particular, reading of the memory (data) was achieved by recording the two-photon up-converted fluorescence of fluorene **19** at 800 nm as a function of position (for fluorene **20** the femtosecond laser was tuned at 720 nm). At 800 nm, fluorene **19** has a δ_{2PA} of 1185 GM, while the δ_{2PA} of the closed form of diarylethene **2** was ~120 GM from picosecond Z-scan experiment (one order of magnitude lower than that of fluorene **19**). So when a weak 720 nm or 800 nm femtosecond laser beam (<8 mW) was utilized for the readout process, strong two-photon fluorescence from **19** was obtained. However, this incident intensity is too weak to cause the closed form of diarylethene **19** to undergo significant photochemical reaction (which is related to data erasing). For future practical application of this two-photon readout system, the relatively expensive femtosecond Ti:sapphire laser could be replaced with cheaper nanosecond laser diodes (λ = 785 nm), if appropriate output laser intensity and materials sensitivity can be achieved in order to drive the photoisomerization reaction. To further confirm that fluorene **19** underwent 2PA under these conditions, the total integrated up-converted fluorescence intensity was measured as a function of the incident intensity (pump power). Theoretically, fluorescence from a 2PA process should exhibit a quadratic dependence on incident intensity. Figure 6.10(c) suggests that fluorene **19** underwent two-photon absorption as evidenced by the slope of the plot of fluorescence emission intensity vs. several pump powers. Figure 6.11 shows two-photon readout of the data recorded by single-photon excitation shown in Figure 6.3.

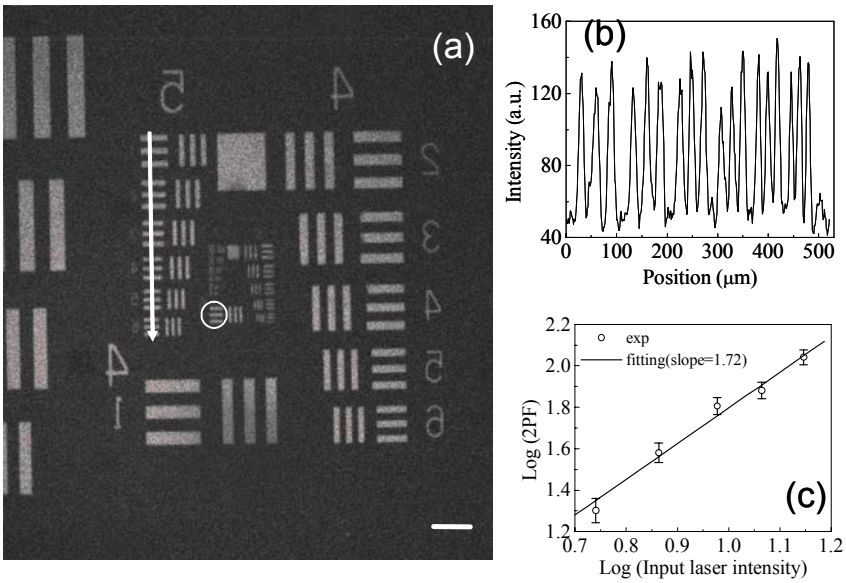

Figure 6.10. (a) Two-photon readout of data recorded by single-photon excitation. The scale bar corresponds to 100 μm), (b) intensity profile (the direction is shown by the arrows) of group 5, and (c) input intensity dependent up-converted fluorescence of fluorene **19**.

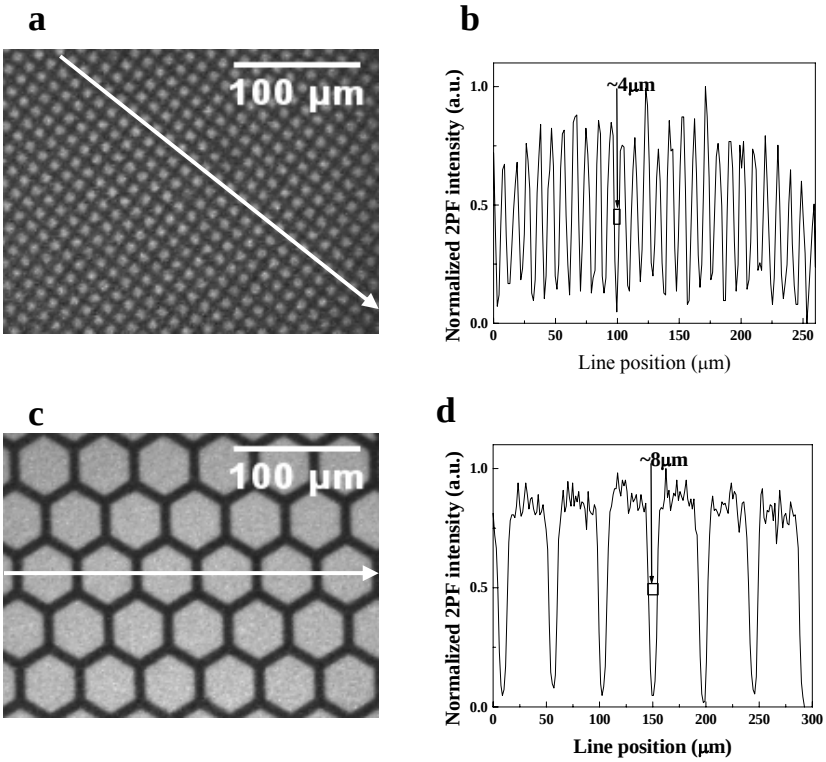

Figure 6.11. Two-photon readout of data recorded by single-photon excitation shown in Figure 6.3. (a) patternfrom a 400 mesh TEM mask (b) intensity profile (direction is shown by the arrows) of the recorded data in (a);(c) pattern from a 100 mesh TEM mask; (d) intensity profile (direction is shown by the arrows) of the recorded data in (c).

6.2.1 Non-destructive two-photon readout

Photochromic reactions are accompanied by rearrangement of chemical bonds. During the rearrangement, undesirable side reactions take place to some extent. This of course limits the number of cycles of photochromic reactions. Fatigue resistance is defined as the number of photochromic cycles at which the absorbance change of the open-ring isomer (or the closed-ring isomer) decreases to 80% of the first cycle. The best diarylethene derivatives can be cycled 10,000 times with only 20% decrease of the initial absorbance [8]. In Figure 6.12, the non-destructive capability of the two-photon up-converted fluorescence readout method proposed in this dissertation is demonstrated. Particularly noteworthy is that 10,000 read-out cycles were accomplished (Figure 6.12b) with no more than 20% decrease in the contrast and fluorescence intensity of the original two-photon image (Figure 6.12a) as demonstrated by the comparison of the corresponding intensity profiles (Figure 6.12c), fulfilling the requirements of "non-destructive readout".

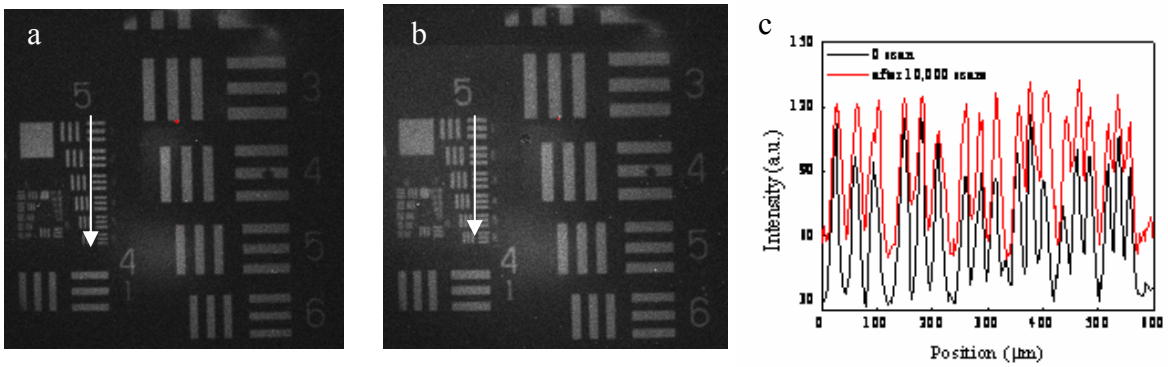

Figure 6.12. Demonstration of the non-destructive capability of the two-photon upconverted fluorescence readout method based on fluorene derivative a) initial two-photon fluorescence readout of data patterns recording by single-photon excitation b) two-photon fluorescence readout after 10,000 readout cycles c) Comparison of the intensity profiles in a) and b)

6.2.2 Multilayer two-photon readout

In Figure 6.13, the ability to read multiple layers of information by the two-photon read-out method was demonstrated. A multilayer assembly was constructed by stacking two storage layers (recorded with different data using single-photon excitation) with data sides (films) against each other. The assembly was translated in the axial (or z) direction by a computer-controlled step motor connected to the focusing knob of the microscope. 3D data from this memory stack was read by successively imaging 38 XY data planes along the axial direction (5 μm distance between each image).

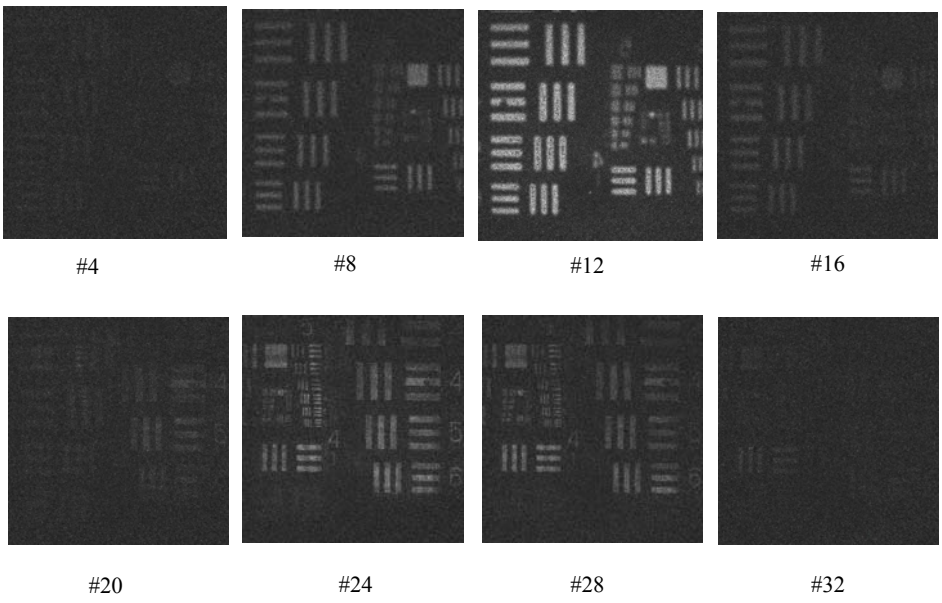

Figure 6.13. Two-photon readout of 38 consecutive layers. The layer intervals were 5μm.

Since the δ_{2PA} of the closed form of diarylethene **2** is very small, transformation of the closed form to the open form under two-photon excitation (two-photon recording) requires high excitation intensity. A multilayer assembly was constructed by stacking two storage layers (shown in Figure 6.13). The assembly was translated in the axial (or z) direction. 3D data from this memory stack was read by successively imaging 31 XY data planes along the axial direction

(5 μm distance between each image). A 3D image was reconstructed from the real original two-photon fluorescence imaging planes using 3D constructor ver. 5.1 (MediaCybernetics Inc.). An *xy* planar scan of each film (hexagonal grid image on the bottom and square grid image on the top) within the multilayer clearly shows the photo-patterned image (Figure 6.14). Important to note is that there is no cross-talk laterally (with a layer of recorded information) or radially (between data layers).

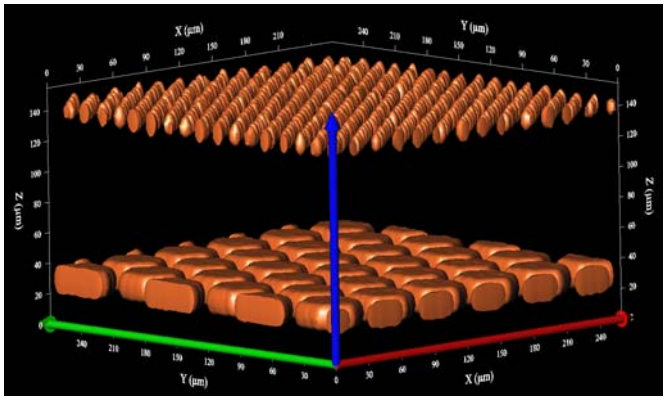

Figure 6.14. Two-photon fluorescent images of the photosensitive films constructed in a multilayer configuration.

6.3 Two-Photon Recording/Two-Photon Readout

Figure 6.15 shows a schematic representation of two-photon data recording and readout onto photosensitive polymeric films containing diarylethene **2** and fluorene **19**. For demonstrating the two-photon recording ability in this photochromic system, the same equipment used in data readout was employed, except that the incident power was adjusted to a considerably higher value at the focus (90 mW). A rectangular pattern (consisting of 445 x 345 bits) was recorded in the storage medium, by repeated scanning of the laser beam across the rectangular area for 5 min (1.2 s/scan, Figure 6.16).

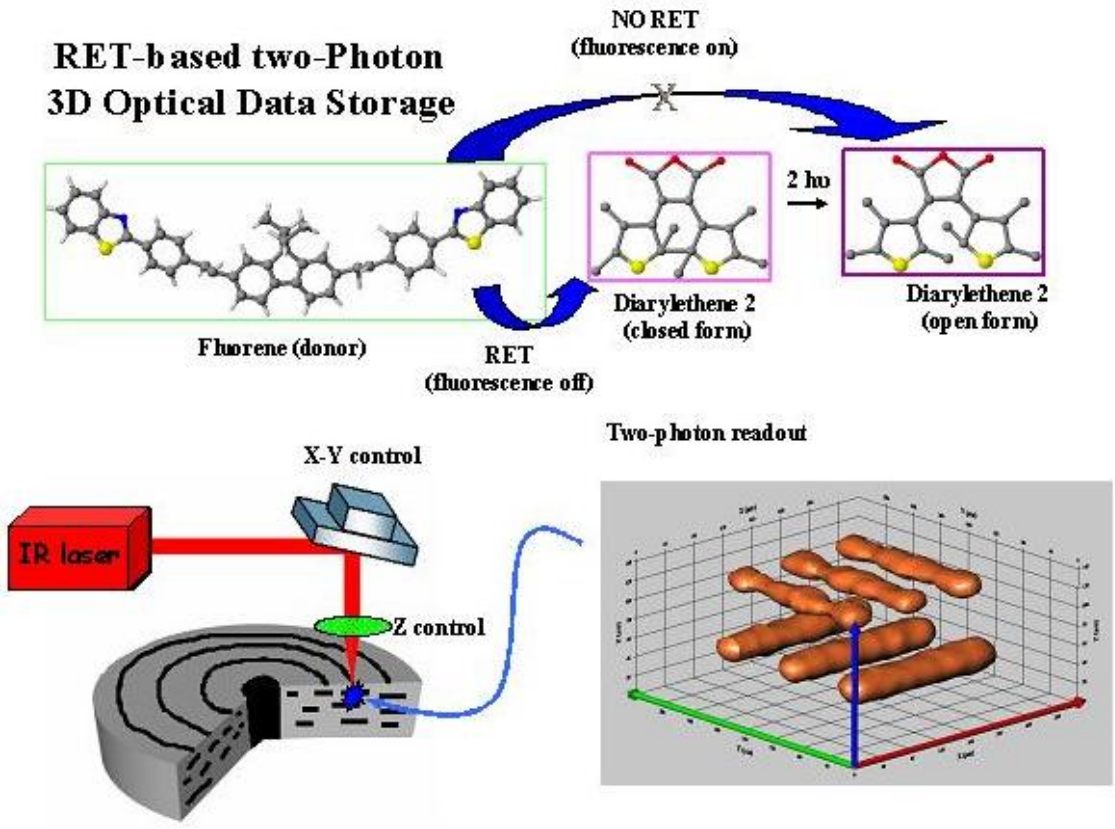

Figure 6.15. Schematic representation of two-photon data recording and readout onto photosensitive polymeric films containing diarylethene **2** and fluorene **19**

As the exposure time for each bit was estimated to be ~7.8 μs/scan and 250 scans were used, the total exposure time of each bit was estimated to be about 2 ms. After the two-photon recording process, data was read by the same two-photon fluorescence microscopy method (described above) using a low incident average power of 7 mW (Figure 6.16(b)). Furthermore, the quadratic relationship between fluorescence emission intensity and incident power provides strong evidence that the data readout in Figure 6.16(b) is, indeed, a result of two-photon induced fluorescence (Figure 6.16(d)), further confirming that the closed form of diarylethene **2** can transform to open form by two-photon excitation when excited by near-IR laser irradiation with

high incident intensity for data recording but essentially remains unchanged upon two-photon readout of the 2PA dye.

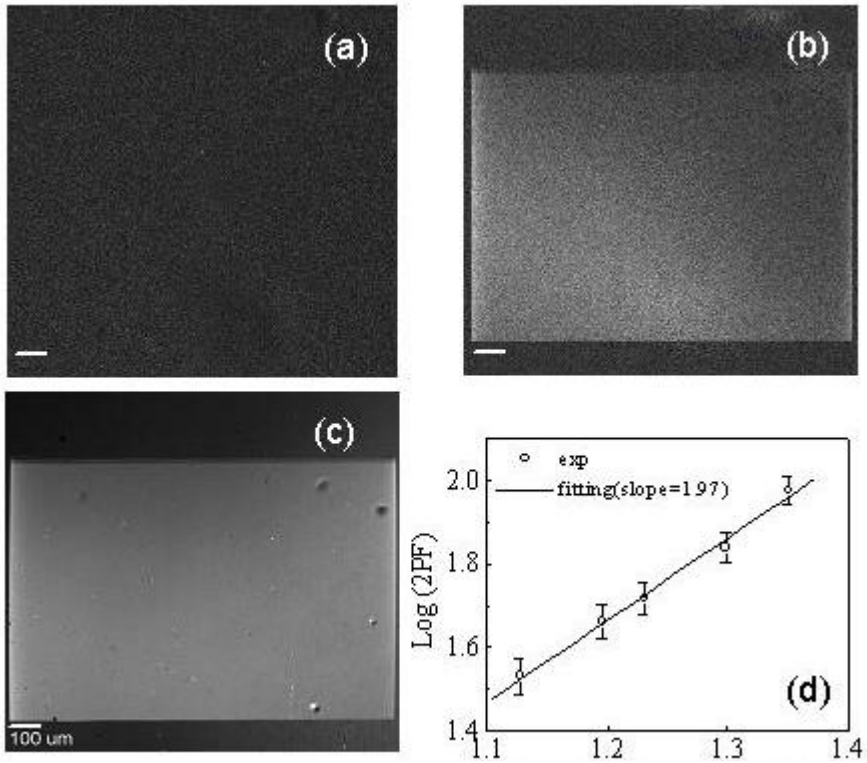

Figure 6.16 Two-photon fluorescence image of storage medium before (a) and after (b) two-photon recording, (c) DIC readout of the storage data after two-photon recording, and (d) input intensity dependent up-converted fluorescence of fluorene **19**.

It is interesting to learn that, when the incident power of the two-photon recording process was reduced to 45 mW, the total exposure time for each bit increased to ~8 ms (4 times greater than that under 90 mW of average power excitation) to generate data with comparable contrast as that under 90 mW of average power excitation. This finding is consistent with the quadratic dependence of two-photon absorption on the incident light power. Thus, it can be estimated that, if the incident average power was further reduced to 7 mW, the exposure time for each bit would increase to ~330 ms. On the other hand, this estimation means that if a rectangular area (stored data, consisting of 512 x 512 bits) were readout under 7mW incident

average power with a scan speed of 1.2 s/scan (which is the typical speed used in the two-photon readout), the exposure time for each bit was estimated to be ~4.6 μs/scan. Up to 7.2×10^4 readout cycles (scans) are, in principle, required before the total exposure time of each bit reaches 330 ms, which is related to significant erasure of the data points. In fact, we demonstrated that, under the previous experimental conditions, up to 10,000 readout cycles resulted in only a negligibly small decrease in the contrast and fluorescence intensity of the original image (see section 6.2.1), consistent with the results reported above. In contrast to other writing/reading systems, in which the read and write wavelengths are well separated, our system can be recorded and read-out using the same wavelength (simply by changing the intensities, and taking advantage of RET for both data writing and data read-out).

6.3.1. Bit oriented memory: two-photon recording and readout as a function of recording time

In Figure 6.17 we further demonstrate the two-photon bit-by-bit recording ability in this photochromic system. A 20x microscope objective (NA=0.50) was used to focus the femtosecond laser (λ = 800 nm, average power = 12.6 mW) into the film, where the exposure time (from 1 s to 10 s, see Fig. 6.17) was manually controlled and the distance between two bits (15 μm) was controlled by moving the film position with a manual X-Y linear stage (Model 406, Newport Corp.). Exposure times less than 1s were not attempted by this manual method. The data bits were readout by the same two-photon fluorescence microscopy method using a low incident intensity of 4 mW and a 20x objective (Figure 6.17 (a) & (b)). 3D data from these data bits was readout by successively imaging 45 XY data planes along the axial direction (1 μm distance between each image). The 3D image shown in Fig. 6.17(e) was also reconstructed from

the real, original two-photon fluorescence imaging planes using 3D constructor ver. 5.1 (MediaCybernetics Inc.), and clearly indicates that the volume of the data bits (voxels) can be controlled by the exposure time.

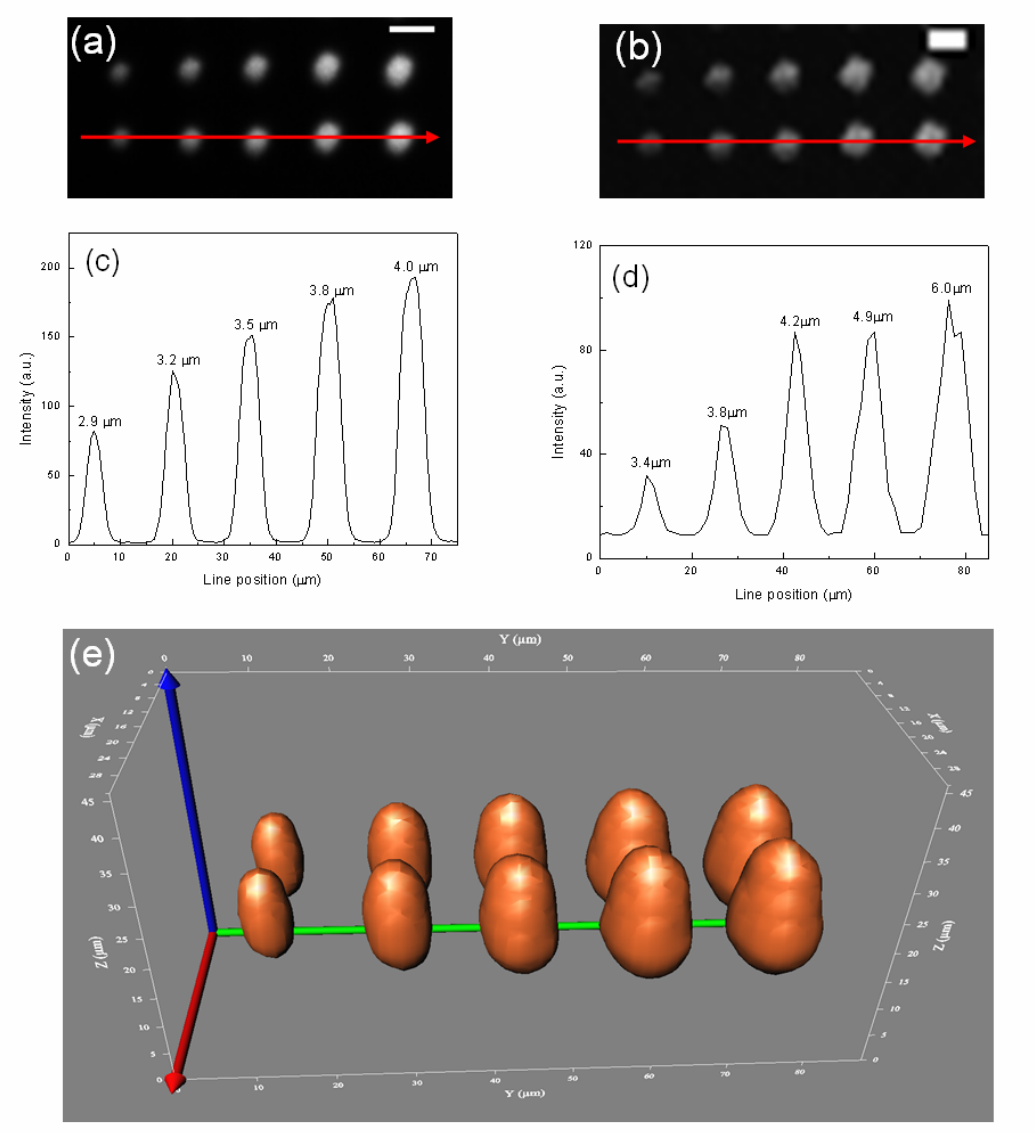

Figure 6.17 (a) Single-photon and (b) two-photon read-out of data bits recorded by two-photon excitation (recording: obj. 20x/NA = 0.5, λ = 800 nm, P = 12.6 mW, t = 1, 3, 5, 7, 10 s (from left to right); readout: λ = 800nm, average power = 4 mW. The scale bar corresponds to 10 µm. The corresponding intensity profiles (the direction is shown by the arrows, (c) represents image (a) and (d) represents image (b), and (e) 3D image representing 45 consecutive layers (1 µm layer interval).

6.3.2. Bit oriented memory: two-photon recording and readout as a function of recording intensity

In Figure 6.18 we demonstrate the two-photon bit-by-bit recording ability in this photochromic system as a function of laser intensity, while maintaining a constant exposure time. A 20x microscope objective (NA=0.50) was used to focus the femtosecond laser (λ = 800 nm) into the film, where the exposure time (7 s) was manually controlled and the distance between two bits (15 μm) was controlled by moving the film position with a manual XY linear stage (Model 406, Newport Corp.). Several recording average powers (P) (P = 4, 6, 8, and 10 mW) were tested. After recording, the data bits were readout by the same two-photon fluorescence microscopy method using a low incident average power of 4 mW and a 20x objective and by DIC (Figure 6.18). Figure 6.18 (c) and (d) show the corresponding intensity profiles of the recorded bits (the direction is shown by the arrows), read out by DIC (a) and by two-photon fluorescence (b), respectively. 3D data from these data bits was readout by successively imaging 45 XY data planes along the axial direction (1 μm distance between each image). The 3D image shown in Fig. 6.19 was reconstructed from the real original two-photon fluorescence imaging planes using 3D constructor ver. 5.1 (MediaCybernetics Inc.) and clearly indicates that the volume of data bits can be controlled by the exposure time.

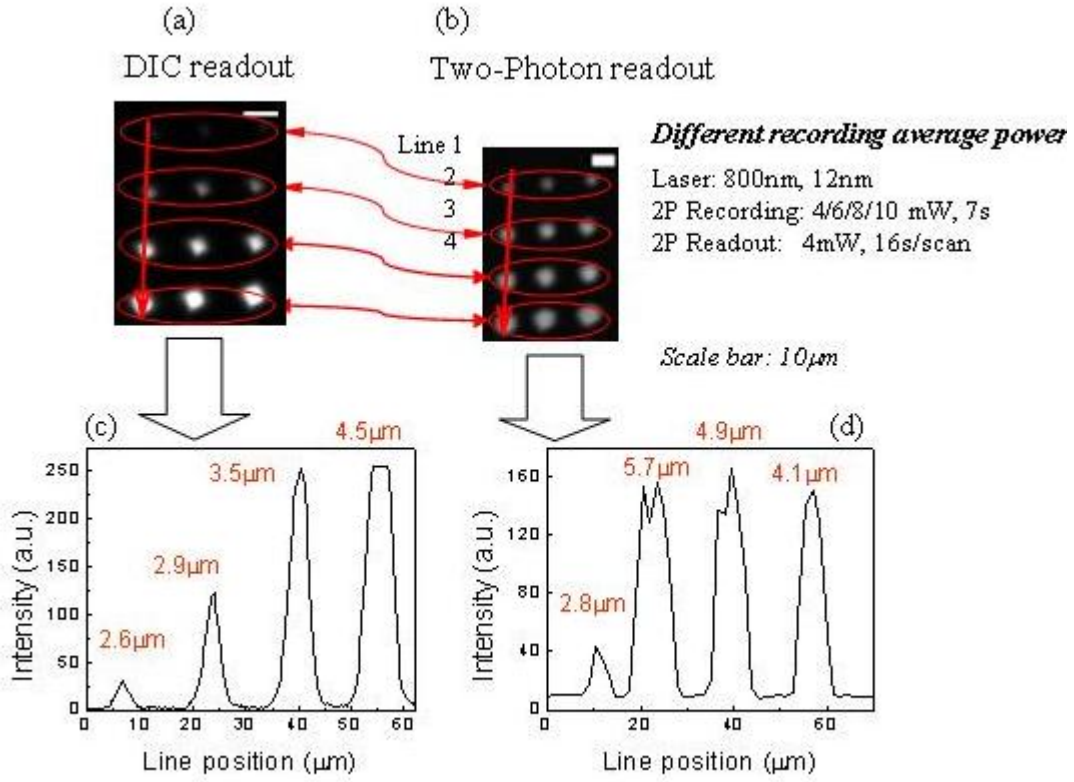

Figure 6.18 (a) Single-photon (DIC) and (b) two-photon read-out of data bits recorded by two-photon excitation (recording: obj. 20x/NA = 0.5, λ = 800 nm, P = 4, 6, 8, and 10 mW, t = 7 s (from top to bottom); readout: λ =800nm, P = 4 mW. The scale bar corresponds to 10 μm. (c) and (d) show the corresponding intensity profiles of the recorded bits (the direction is shown by the arrows), readed out by DIC (a) and by two-photon fluorescence (b), respectively. (c) represents image (a) and (d) represents image (b)

These results demonstrate the multiple advantages of this two-photon 3D optical data storage system, not the least of which is that our approach does not require complex, multistep synthesis to prepare a modified photochromic compound. Also, since no covalent attachment of the fluorene is required, the electronic distribution and conformation of the photochrome is not perturbed, and desirable photochromic properties are not lost. Finally, the diarylethene isomers (open or closed) are not directly used to read-out the stored information, so the read-out method is non-destructive, as demonstrated in section 6.2.1.

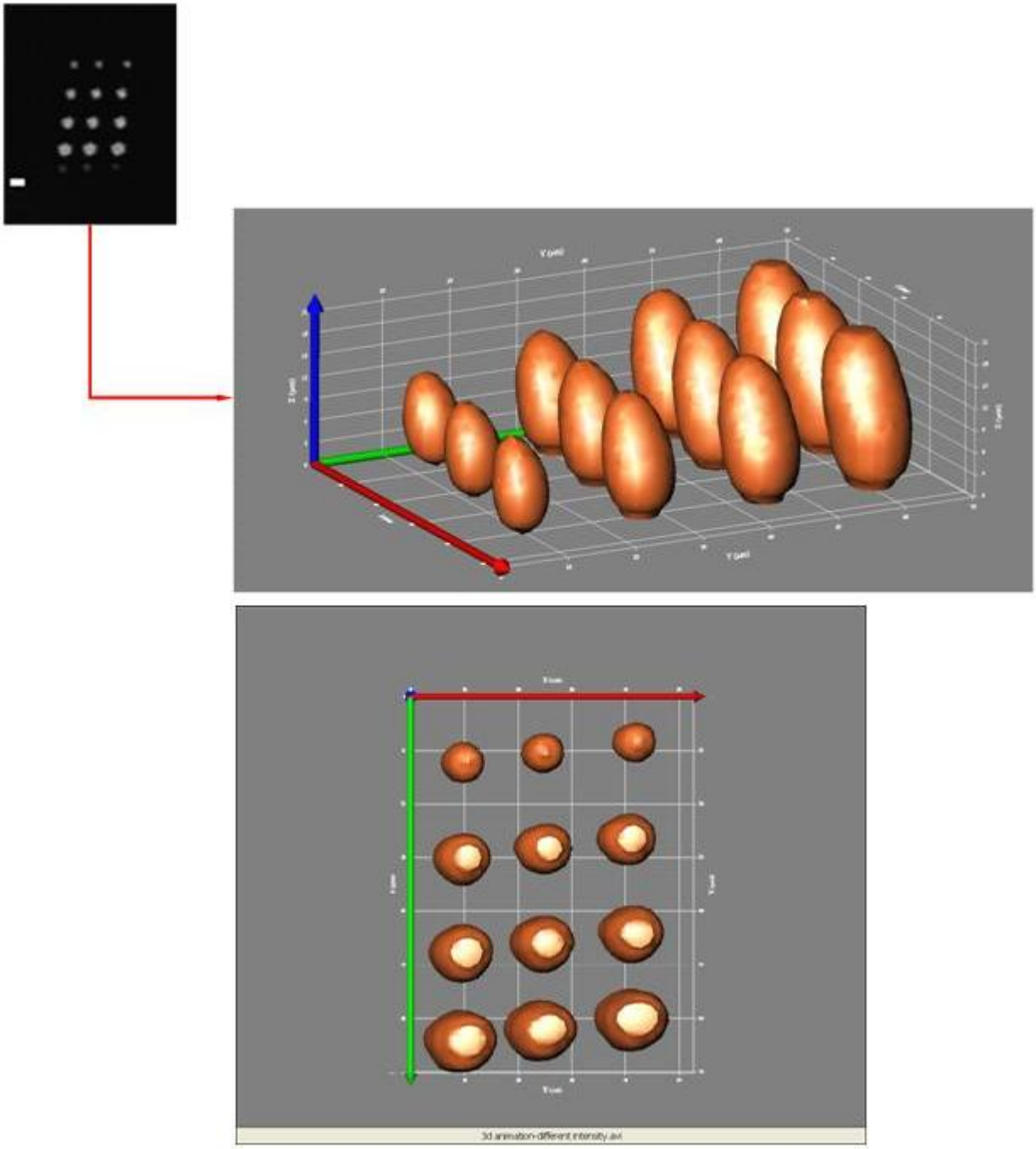

Figure 6.19 3D image reconstructed from the real original two-photon fluorescence imaging planes using 3D constructor ver. 5.1 (MediaCybernetics Inc.) indicating that the volume of data bits can be controlled by the excitation intensity.

CHAPTER 7. PHOTOPHYSICAL STUDIES OF NEW FLUORENE DERIVATIVES FOR APPLICATIONS IN RET-BASED TWO-PHOTON 3D OPTICAL DATA STORAGE: PHOTOSTABILITY

The fluorene derivatives presented in the previous chapter were shown to undergo efficient 2PA after fs irradiation. As a result of intensive investigation in this research group, new promising fluorene derivatives have been synthesized, showing strong molecular polarizability for sufficiently strong nonlinear absorption upon excitation [39]. In particular, fluorene derivatives **21** and **22** (Figure 7.1) showed relatively large two-photon absorption cross-sections (the values of δ_{2PA} for **21** and **22** were 270 ± 50 GM and 460 ± 80 GM, respectively at 840 nm) and high fluorescence quantum yields (~0.9 – 1.0), making these compounds quite promising for application in 3D fluorescence imaging and optical data storage. However, if the compounds cannot withstand the intense irradiation conditions required for nonlinear excitation, their optical properties will be rendered useless for long-term applications. Hence, the photostability of such fluorene derivatives is a key parameter to establish, and facilitate their full utility in critical applications in, for instance, RET-based two-photon 3D optical data storage. The following discussion will concentrate on photostability studies in solution of fluorene derivatives **21** and **22** (Figure 7.1).

Photodecomposition (the irreversible light-induced destruction of a material) is one of the main limitations of many organic dyes for their application in nonlinear optics and photonics. Hence, the photochemical stability of organic dyes, such as fluorene derivatives, under one- and

two-photon excitation is critical for a number of emerging nonlinear optical applications. Photodecomposition of simple fluorene derivatives was investigated early on with regards to problems of environmental contamination [53].

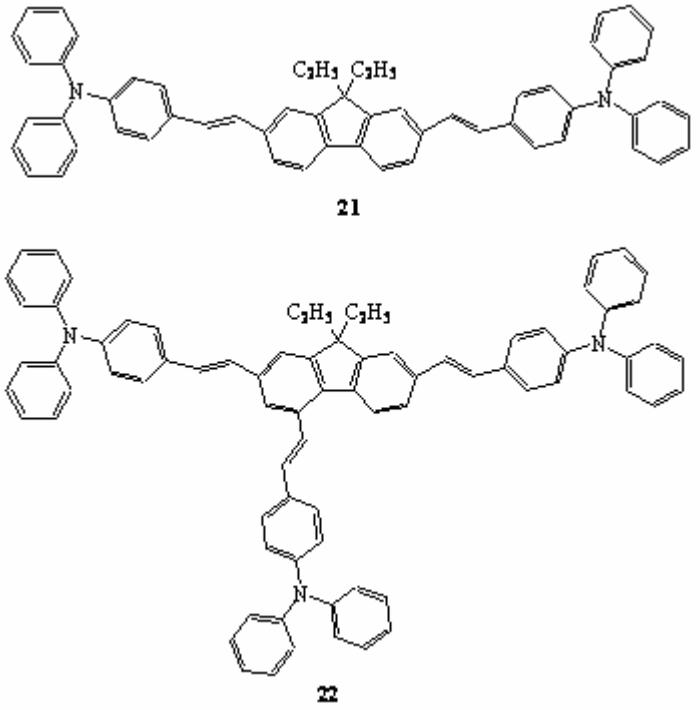

Figure 7.1 Molecular structures of linear and branched fluorene derivatives **21** and **22**.

Photolytic degradation of certain fluorene derivatives under UV irradiation and the dependence of photolysis kinetics on molecular weight and type of substituents were shown [54]. The effect of solvent and substituents on the photooxidation of a few fluorene derivatives and the photochemical behavior of fluorene at a silica gel/air interface have been reported [55]. A theoretical study of the photo-oxidation of the 2PA chromophore AF50 [56a] and formation of its possible photoproducts was also reported [56b].

Photochemical decomposition under two-photon excitation may well be different from the reactions induced by low intensity irradiation [41a]. Even in the case when the same excited state of the molecule is populated under one- and two-photon excitation, additional photochemical processes, such as photoionization and bond fission [41b], are possible for the latter type of excitation due to high irradiation intensities. There is evidence, that in many dye systems, the photobleaching rates by two-photon excitation are significantly enhanced with respect to one-photon excitation at comparable photon-emission yields [41c]. Until now, relatively little is known about two-photon photodecomposition of fluorene derivatives possessing high nonlinear absorptivity. Preliminary investigation of photochemical processes of select fluorene derivatives under two-photon excitation were investigated in our lab [44], and an increase in the photodecomposition quantum yield was observed for (7-benzothiazol-2-yl-9,9-didecylfluoren-2-yl)diphenylamine in CH_2Cl_2 under femtosecond two-photon excitation. The primary goal of this work is the investigation of the photochemical stability of new linear and branched fluorene derivatives (Figure 7.1) that possess large 2PA cross-sections (maximum values ~ 2000 - 4000 GM) [57].

In addition, a cursory examination of several photoproducts of **21** and **22** was undertaken to provide some speculative, but informative, insight into the photodecomposition processes. Potential photobleaching pathways were investigated by working at different dye concentration (to determine the dependence of photobleaching on molecular concentration) and oxygen concentration. Oxygen, a strong triplet quencher, can minimize photobleaching via the triplet state, but on the other hand, reactive singlet oxygen (O_2 ($^1\Delta_g$)) can be generated by triplet-triplet annihilation between O_2 ($^3\Sigma_g^-$) and the dye molecule, both in their triplet states. Since some fluorene derivatives synthesized in our laboratory have the ability to generate singlet oxygen O_2

($^1\Delta_g$), under single and two-photon excitation with high quantum yields (Φ_Δ=0.35 to 0.75) [58] there is great interest in determining the effect of oxygen concentration on the photostability of these fluorenes derivatives. Photostability or lack thereof, is often considered the Achilles Heel of organic photochromic materials, and the studies conducted herein are critical to determine the robustness and limitations of potentially useful nonlinear absorbing dyes.

7.1 Materials, Methods, and Instrumentation

Photochemical properties of the fluorene derivatives 4,4'-[[9,9-bis(ethyl)-9H-fluorene-2,7-diyl]di-2,1-ethenediyl]bis(N,N-diphenyl)benzeneamine (**21**, reference 39e) and 4,4',4''-[[9,9-bis(ethyl)-9H-fluorene-2,4,7-triyl]tri-2,1-ethenediyl]tris(N,N-diphenyl)benzene amine (**22,** reference 39e) were studied in air saturated and deoxygenated spectroscopic grade poly(tetrahydrofuran) (pTHF) (MW 250) at room temperature [39e]. Deoxygenated solutions were obtained by bubbling Ar through the solutions for 30 min or repeated freeze-pump-thaw cycles (both procedures yielded identical results). The absorption spectra were recorded using an Agilent 8453 UV-visible spectrophotometer in 10 mm path length quartz cuvettes for concentrations, C, $\leq 2 \times 10^{-5}$ M. The fluorescence, excitation, and excitation anisotropy spectra of **21** and **22** were obtained using a PTI Quantamaster spectrofluorimeter in 10 mm fluorometric quartz cuvettes for dilute solutions ($C \leq 10^{-6}$ M). Two-photon absorption cross-sections, δ_{2PA}, of **21** and **22** in pTHF were determined by an open aperture Z-scan method [46] and an up-converted fluorescence technique (relative to fluorescein in water) [45], using a femtosecond laser system (Clark-MXR, CPA2010, Ti:Sapphire amplified system followed by an optical parametric generator/amplifier (TOPAS 4/800, Light Conversion) with pulse duration, $\tau_P \approx 140$ fs

(FWHM), repetition rate, f = 1 kHz, tuning range 560 - 2100 nm, and maximum average power, $P_0 \approx 25$ mW).

The quantum yields of the photochemical reactions (photodecomposition) of **21** and **22** in pTHF under one-photon (Φ_{1PA}) and two-photon (Φ_{2PA}) excitation were determined by absorption and fluorescence methods, described in detail in Refs. 44 and 59. These methods are based on measurements of the temporal changes in the steady-state absorption and fluorescence spectra during irradiation, respectively. The absorption method was described in section 3.2. The values of Φ_{1PA} were obtained also by employing a fluorescence method with the corresponding equation [58b]:

$$\Phi_{1PA} = [1 - F(t_{ir}) / F(0)] / \{\int_{\lambda} \int_{0}^{tir} I_0(\lambda)\, \sigma(\lambda)\, [F(t) / F(0)] d\lambda dt\}, \qquad (2)$$

where F(0) and $F(t_{ir})$ are the initial and final fluorescence intensity expressed in relative arbitrary units (typically, in counts/s) and $\sigma(\lambda)$ is the one-photon absorption cross-section (cm^2). The experimental setup for one-photon excitation is shown in Figure 7.2a. The entire volume of the fluorene solution was irradiated simultaneously with the UV-lamp, LOCTITE 97034 (average irradiance, $I_0 \approx 130$ mW/cm^2), in the spectral range 400 - 440 nm (using glass UV-visible filters). In the case of the absorption method, 2 mL of pTHF solutions of **21** and **22** were placed into quartz cuvettes (10 x 10 x 35 mm) and temporal changes in the absorption spectra were measured spectrophotometrically. Whereas a microcuvette (1 x 1 x 10 mm) was used in the fluorescence method, and the changes in the fluorescence spectra during irradiation were measured with the spectrofluorimeter.

The quantum yields of the photodecomposition processes under two-photon excitation, Φ_{2PA}, were determined with the experimental setup presented in Figure 7.2b. The values of Φ_{2PA} were obtained by the fluorescence method [44, 58b], using the PTI spectrofluorimeter and femtosecond laser system described above. Calculations of Φ_{2PA} were performed from the initial slope of the dependencies F(t) [44, 58b] using a Gaussian spatial and temporal beam profile approximation.

Photochemical products of **21** and **22** formed in pTHF (after one-photon excitation) were analyzed by HPLC and mass spectrometry (MS) techniques.

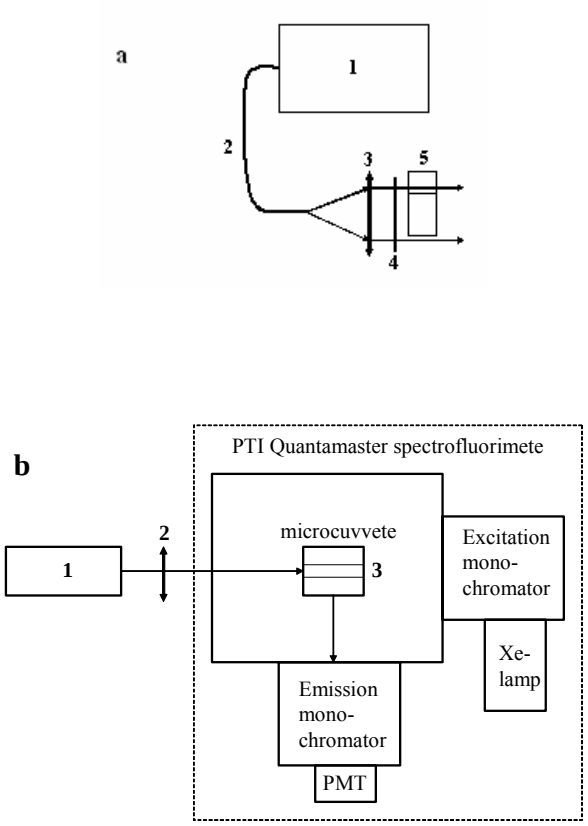

Figure 7.2 Schematic diagrams of the experimental setup. (a) One-photon excitation: 1 – UV-lamp (LOCTITE 97034); 2 – liquid waveguide; 3 – lens (5 cm); 4 – glass UV-visible filters; 5 – 10 x 10 x 35 mm quartz cuvette. (b) Two-photon excitation: 1 – femtosecond laser system (CPA2010); 2 – lens (30 cm); 3 – 1 x 1 x 10 mm quartz microcuvette.

A Waters HPLC instrument equipped with a binary pump (1525), an in-line degasser, a PDA detector (2996), and a manual injector (7725I) was used for HPLC method development. The best chromatographic separation was achieved by using a silica gel analytical column (4.6 x 150 mm, particle size 5 μ, pore size 100 Å), with a 97:3 hexane:ethyl acetate mobile phase in isocratic flow mode. The flow rate was 1.0 mL/min, the injection volume was 50 μL, the column temperature was 30 ^{o}C, and the run time was 16 min. Atmospheric pressure chemical ionization mass spectrometry (APCI-MS) was performed with a Thermo-Finnigan LCQ Duo LC-MS instrument equipped with an UV detector (UV6000 PDA), and APCI source (Thermo-Finnigan), and an ion-trap. Samples were analyzed using APCI ionization and monitored in the positive ionization mode (nitrogen was used as a nebulizer gas and as a dryer gas).The vaporizer and capillary temperatures were 450 and 200 °C, respectively. The corona discharge voltage (4.5 kV), sheath gas flow (48 a.u.), auxiliary gas flow (3 a.u.), discharge current (10 μA), capillary voltage (38 V), and the SID fragmentor voltage (6V) were determined by tuning the mass analyzer by infusing a solution of **21** and **22** at 10 μL/min and monitoring the mass-to-charge ratios in the region of 100 to 1500 u. The injection volume was 100 μL. Data was acquired with Xcaliber v1.2 software.

7.2 Spectral Properties

The absorption, fluorescence, and excitation anisotropy spectra of **21** and **22** in pTHF are shown in Figure 7.3. The shapes of the fluorescence spectra were independent of the excitation wavelength over the entire spectral range of the measurements. The changes in the excitation anisotropy spectra (curves 3) revealed the spectral position of different electronic transitions in

the absorption spectrum. Linear fluorene **21** (Figure 7.1) exhibited a fairly constant value of anisotropy in the long wavelength absorption band, corresponding to one electronic transition in this spectral range (370 nm – 470 nm).

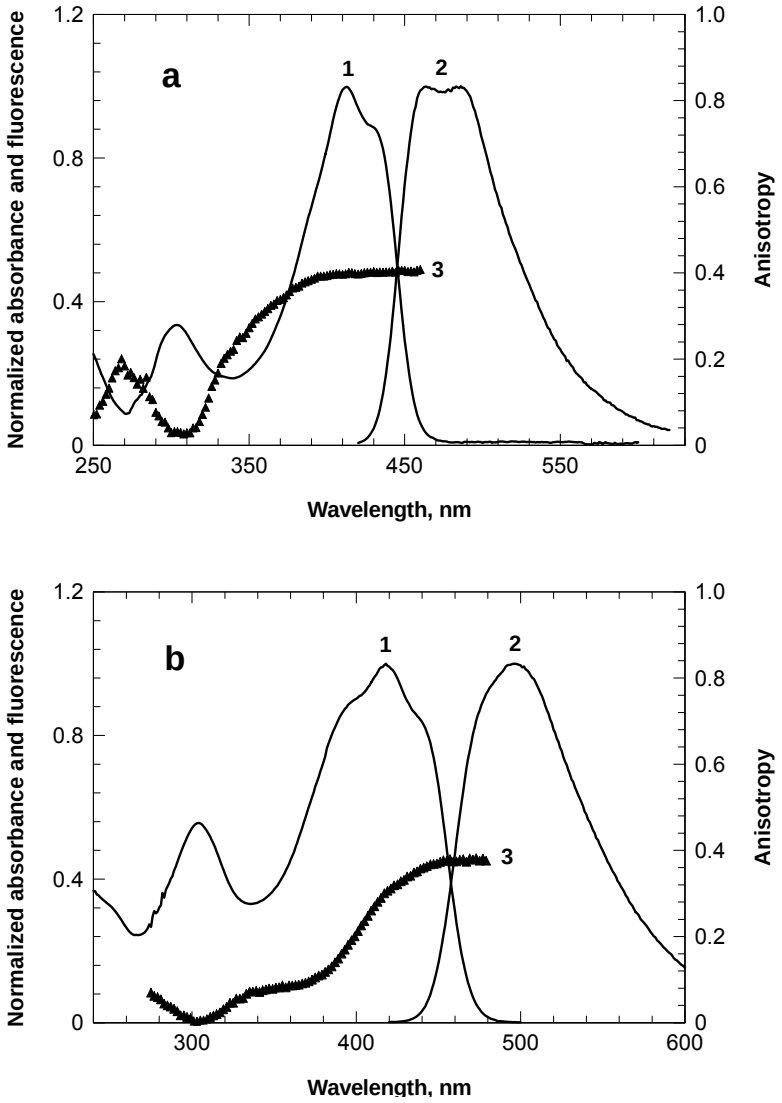

Figure 7.3 Absorption (1), corrected fluorescence (2), and excitation anisotropy (3) spectra of **21** (a) and **22** (b) in pTHF. Excitation anisotropy spectra (3) were observed at the emission wavelengths 500 nm (a) and 510 nm (b), respectively.

In contrast, a decrease in the anisotropy of branched compound **22** revealed at least two different electronic transitions in the main absorption band (360 nm – 480 nm). A comprehensive analysis of the electronic structure of **21** and **22** including quantum-chemical calculations was recently reported [60]. Extinction coefficients of **21** and **22** for the determination of one-photon photodecomposition quantum yields were obtained in p-THF, and nearly equal to each other $\varepsilon(\lambda_{max}) \approx 10^5$ M^{-1} cm^{-1} (λ_{max} is the wavelength of the corresponding maximum). Two-photon absorption cross-sections, δ_{2PA}, were determined in pTHF at the excitation wavelength, λ_{exc} = 840 nm, by two different methods (open aperture z-scan [46] and up-converted fluorescence techniques [45] with femtosecond excitation).

The values of δ_{2PA} for **21** and **22** were 270 ± 50 GM and 460 ± 80 GM, respectively at 840 nm. Both methods gave similar results for the δ_{2PA}. High fluorescence quantum yields of **21** and **22** (~0.9 – 1.0), in combination with relatively large δ_{2PA}, make these compounds quite promising for application in 3D fluorescence imaging and optical data storage.

7.3 One-Photon Photochemical Stability

The quantum yields of the photochemical (photodecomposition) reactions of **21** and **22** in pTHF, Φ, were determined by the absorption and fluorescence methods described above. Kinetic changes in the absorption and fluorescence spectra under UV irradiation are presented in Figures 7.4 and 7.5. The initial slopes of the temporal dependences of the optical density, D(t), and fluorescence intensity, F(t), were used for the quantum yield calculations. The values of Φ obtained by the two different methods are listed in Table 7.1. Both methods afforded nearly the

same photochemical stability results. Taking into account the large differences in the concentrations for absorption (C ≈ 2 x 10^{-5} M) and fluorescence methods (C ≈ 10^{-6} M), one can assume first order photoreaction of **21** and **22** in pTHF (i.e. photodecomposition is independent of concentration). Deoxygenation of pTHF increased the photostability of **21** and **22** under UV irradiation by at least an order of magnitude (Table 7.1), indicating the important role of the molecular oxygen in the photobleaching (photodecomposition) processes.

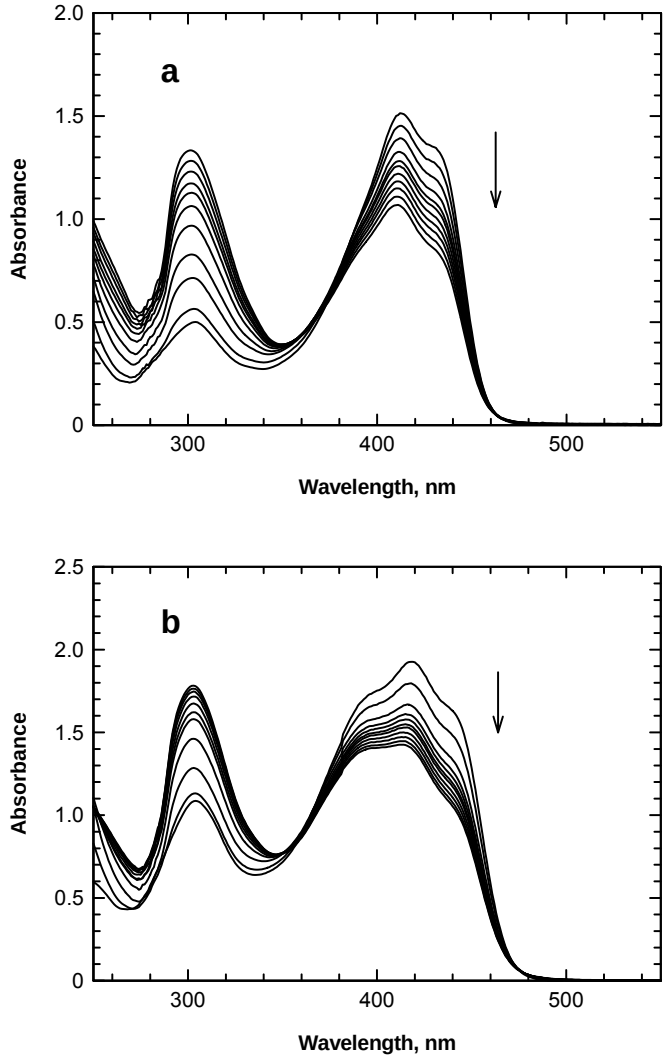

Figure 7.4 Kinetic changes in the absorption spectra of **21** (a) and **22** (b) in pTHF upon irradiation at λ_{exc} ≈ 420 nm. The temporal interval between adjacent spectra was 10^3 s. Excitation irradiance, I_0 ≈ 130 mW/cm^2.

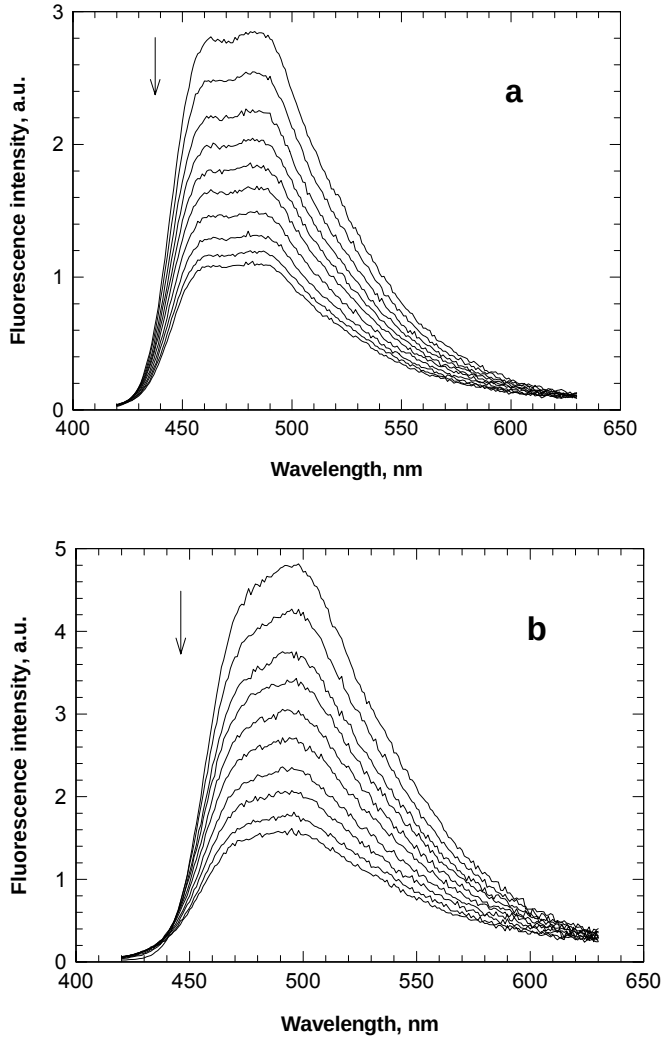

Figure 7.5 Kinetic changes in the fluorescence spectra of **21** (a) and **22** (b) in pTHF upon irradiation at $\lambda_{exc} \approx 840$ nm. The temporal interval between adjacent spectra was 360 s. Excitation irradiance, $I_0 \approx 130$ mW/cm^2.

Table 7.1. Quantum yields of the photoreactions of **21** and **22**, Φ_{1PA} and Φ_{2PA}, in air-saturated and deoxygenated pTHF under one- and two-photon excitation at 420 and 840 nm, respectively.

Compound, solvent condition	Absorption method Φ_{1PA} x 10^6, [C] (M)	Fluorescence method Φ_{1PA} x 10^6, [C] (M)	Fluorescence method Φ_{2PA} x 10^6, [C] (M)
21 air-saturated	2.0 ± 0.2 [1.8 x 10^{-5}]	1.9 ± 0.2 [1 x 10^{-6}]	1.9 ± 0.5 [1.8 x 10^{-5}, 1 x 10^{-6}]
21 deoxygenated	0.12 ± 0.02 [1.8 x 10^{-5}]	-	-
22 air-saturated	2.1 ± 0.2 [1.9 x 10^{-5}]	2.0 ± 0.2[1 x 10^{-6}]	1.5 ± 0.4 [1.9 x 10^{-5}, 1 x 10^{-6}]
22 deoxygenated	0.2 ± 0.05 [1.9 x 10^{-5}]	-	-

C is the concentration of solution in M.

To our knowledge, the values of $\Phi \sim 10^{-7}$ (in deoxygenated solutions) are among the highest level of UV photochemical stabilities reported for large conjugated organic compounds (for example, the yields of photobleaching of typical coumarin dyes in aqueous solution are on the order of 10^{-3} to 10^{-4}, and for Rhodamine 6G is 7.5×10^{-6}) [61] and, therefore, compounds **21** and **22** possess high photostability, critical for practical applications as optical and photonic materials.

7.4 Two-Photon Photochemical Stability

The two-photon induced quantum yield Φ_{2PA} of the photodecomposition of **19** and **20** (Table 7.1) were determined by the fluorescence method from the initial slopes of the temporal dependences of the two-photon induced up-converted fluorescence, F(t), shown in Figure 7.5. The same values of Φ_{2PA} were obtained for two different concentrations, supporting first order photoreactions. The excitation wavelength, λ_{exc} = 840 nm, energetically corresponds to the linear UV-lamp irradiation at $\lambda_{exc} \approx 420$ nm, and it was possible to assume excitation to the same excited electronic state of **21** and **22** occurred during photoexcitation. The corresponding one- and two-photon photodecomposition quantum yields, Φ_{1PA} and Φ_{2PA}, are shown in Table 7.1. From this comparison, **21** and **22** had nearly the same photodecomposition quantum yields ~ (1.5 – 2) x 10^{-6} under one- and two-photon excitation, suggesting similar mechanisms of photodecomposition of **21** and **22** in pTHF under both types of excitation. High two-photon photostability of both **21** and **22** is a promising feature of these compounds for a number of nonlinear optical applications.

7.5 Cursory Photoproduct Analysis of 21

In order to understand the type of photodecomposition processes incurred by **21** and **22**, separation and characterization of photoreaction mixtures was undertaken. Normal phase HPLC proved to be very useful in the separation of photoproducts of **21** and **22**. Photodecomposition of **21** in pTHF under UV irradiation resulted in 6 main photoproducts **21**Ph1 - **21**Ph6, with retention times of: **21**Ph1 at 2.1 min, **21**Ph2 at 2.4 min, **21**Ph3 at 3.9 min, **21**Ph4 at 6.9 min, **21**Ph5 at 7.5 min, **21**Ph6 at 9.0 min. The retention time of unreacted **21** was 4.3 min. Peak purity test for the peaks of **21**Ph1 and **21**Ph2 showed that they did not consist of a single compound, and, therefore, were excluded from analysis. The signal-to-noise ratio of **21**Ph4 was less than 3 and was also excluded from analysis. The absorption spectra of **21**Ph3, **21**Ph5 and **21**Ph6 (extracted from the PDA detector) are shown in Figure 7.6. The spectral shapes of the absorption bands of **21**Ph5 and **21**Ph6 are similar to the structurally related compound 2,7-diphenylamino-9,9-didecylfluorene [59a], showing a short wavelength maximum at ≈ 300 nm.

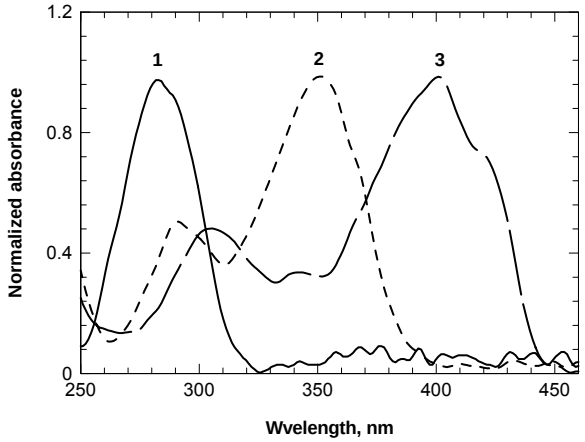

Figure 7.6 Absorption spectra of the photoproducts of **21**: (1) **21**Ph3 (λ_{max} ≈ 283 nm), (2) **21**Ph5 ((λ_{max} ≈ 351 nm), and (3) **21**Ph6 ((λ_{max} ≈ 403 nm).

In order to understand the mechanism of photodegradation and determine the chemical structures of possible photoproducts, the APCI mass spectra of **21**, and the most abundant photoproducts (**21**Ph5 and **21**Ph6) were obtained. Mass spectra of other photoproducts (**21**Ph3 and **21**Ph4) could not be detected accurately, since the amount of these photoproducts formed was too low. Negative ionization mode did not provide useful information. In contrast, positive ionization mode yielded reproducible mass spectral data. Fragment ions and the molecular ion for **21**Ph5 are given in Table 7.2. Based on the analysis of the APCI mass spectra and Ref. 62, some possible structures of fragment ions of **21**Ph6 are proposed in Figure 7.7. Since aromatic amines are generally photostable [62], photochemical reactions were expected to involve other functional groups in the molecule, particularlly the C=C double bonds.

Table 7.2 Fragment ions in the APCI mass spectra of photoproducts **21**Ph2, **21**Ph6, **22**Ph1, **22**Ph2, **22**Ph3 and **22**Ph4

Photo product	Fragment ions	Photo product	Fragment ions	Photo product	Fragment ions
21Ph2	167.22 244.28 $[M+H]^+$ 245.32 274.16 294.27 465.70 738.81	**22**Ph1	223.14 251.15 301.17 329.14 $[M+H]^+$ 391.19 405.24	**22**Ph3	167.24 $[M+H]^+$ 244.30 245.25 274.24 327.13 437.23 767.43
21Ph6	166.15 256.40 272.24 279.36 399.24 475.37 $[M+H]^+$ 476.36 505.36 719.44	**22**Ph2	231.23 298.29 383.14 $[M+H]^+$ 439.16 495.18	**22**Ph4	231.20 274.22 $[M+H]^+$ 275.19 579.24 705.40 789.37 790.38 791.32

$[M+H]^+$ indicates the molecular ion

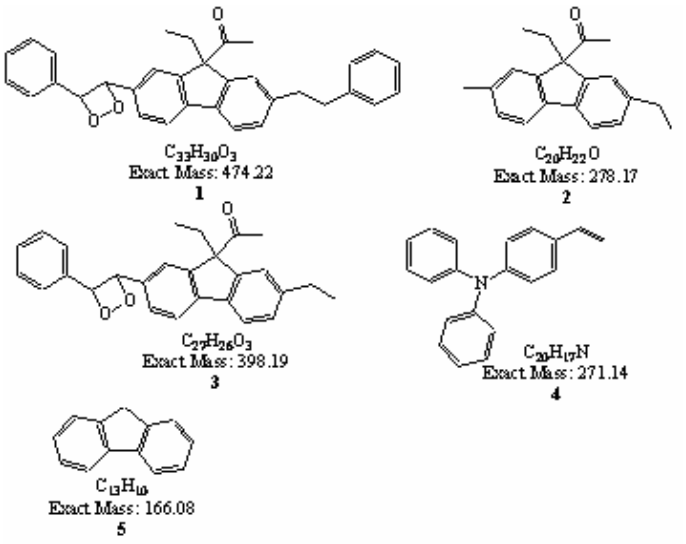

Figure 7.7 Proposed structures of the fragment ions at m/z 166.15, 272.24, 279.36, 399.24 and 475.37 in the full scan APCI mass spectrum of **21**Ph6.

Some of the proposed fragments can be explained by the [2+2] cycloaddition reaction of oxygen with the double bond of **21**, and by hydrogen abstraction from the alkyl chain with radical formation, subsequent oxidation, and cleavage to produce fragments 1, 2, and 3, suggesting that oxygen is involved in the mechanism of photodegradation.

7.6 Cursory Photoproduct Analysis of 22

Photobleaching of **22** under UV irradiation resulted in 4 main photoproducts (**22**Ph1 - **22**Ph4). The absorption spectra of **22**Ph1 – **22**Ph4 of **22** are shown in Figure 7.8. The profiles of the absorption bands of **22**Ph3 and **22**Ph4 were similar to the structurally related compound 2,7-diphenylamino-9,9-didecylfluorene (with shorter conjugated length) [59a] and also to the parent compounds **21** and **22**, respectively. Insight into possible reaction pathways may be generated by the APCI mass spectra of **22**, and **22**Ph1 – **22**Ph4, presented in Figure 7.9 and Table 7.2. Due to the high photostability of **22**, the analysis of photoproducts by HPLC-MS proved difficult, due

to the low amount of material available, even after very long irradiation times and high concentrations. As previously mentioned, aromatic amines are generally photostable [62], and photochemical reactions were expected to involve other functional groups in the molecule, such as C=C double bonds. Based on these assumptions and analysis of Ref. 62, the structures of some possible fragment ions of **22**Ph1 and **22**Ph3 can be proposed (Figure 7.9). Molecular oxygen also can participate in the photoreactions resulting in the formation of possible structures (Figure 7.9).

In order to determine the role of singlet oxygen ($^1O_2$) in the photodecomposition mechanism of **21** and **22**, $^1O_2$ was generated by sensitization with a well known singlet oxygen sensitizer (methylene blue, singlet oxygen quantum yield Φ_Δ: 0.49) and the photodecomposition products of **22** were compared to the previously detected ones. Mostly **22** and methylene blue were recovered, and no evidence of the presence of previously detected photodecomposition products was found. Results from this experiment suggest that ground state oxygen, rather than excited state oxygen is involved.

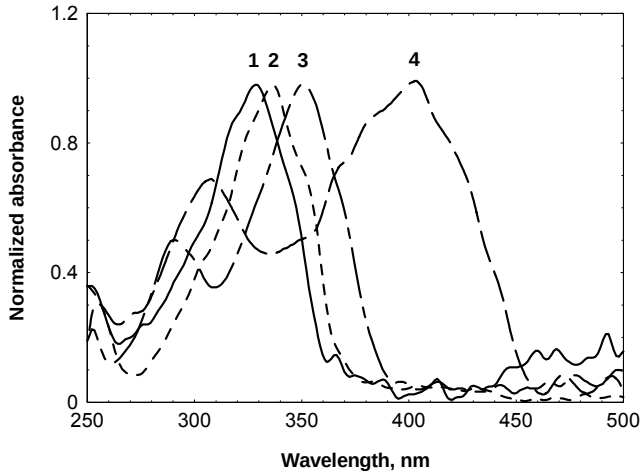

Figure 7.8. Absorption spectra of the photoproducts of **22**: (1) **22**Ph1 ($\lambda_{max} \approx 329$ nm), (2) **22**Ph2 ($\lambda_{max} \approx 336$ nm), (3) **22**Ph3 ($\lambda_{max} \approx 351$ nm), (4) **22**Ph4 ($\lambda_{max} \approx 403$ nm)

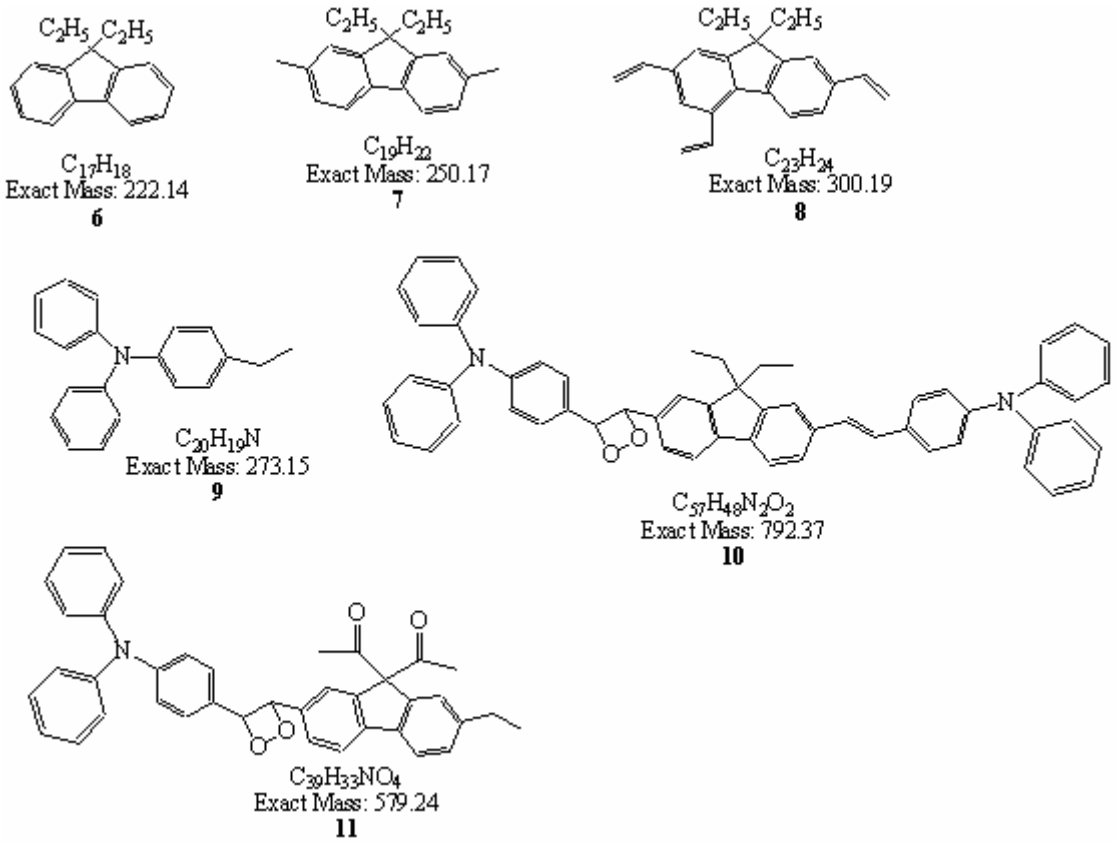

Figure 7.9 Proposed structures of the fragment ions at m/z 223.14, 251.15, and 301.17 in the full scan APCI mass spectrum of **22**Ph1, at m/z 274.0 in the full scan APCI mass spectrum of **22**Ph3 and **22**Ph4, and at m/z 791.32 and 579.24 in the full scan APCI mass spectrum of **22**Ph4.

Photochemical stability of two promising fluorene derivatives was investigated using both the absorption and fluorescence methods under one- and two-photon excitation in air-saturated and deoxygenated pTHF. The quantum yields of the photochemical reactions exhibited no concentration dependence, in accordance with the first-order photodecomposition processes. The values of quantum yields were in the range $\Phi \approx (1.9 - 2.1) \times 10^{-6}$ and $\Phi_{2PA} \approx (1.5 - 1.9) \times 10^{-6}$ for one- and two-photon excitation, respectively. Close values of Φ and Φ_{2PA} provide strong support for similar photobleaching processes of **21** and **22** for both types of excitation. In deoxygenated pTHF, the photostability of **21** and **22** increased by at least an order of magnitude relative to that in air-saturated solutions, revealing an important role of molecular oxygen in the

photoreactions. Several photochemical products of **21** and **22** were resolved by HPLC and investigated by APCI-MS spectroscopy. Analysis of the mass spectra provides insight into the possible reaction pathways and confirmed participation of the molecular oxygen in photobleaching processes. Results from experiments with a known $^1O_2$ photosensitizer shown no difference in photoreactivity, suggesting than ground state oxygen rather than excited state oxygen is involved.

Fluorene derivatives **21** and **22** with large two-photon absorption cross-sections, high fluorescence quantum yields, and one- and two-photon photochemical stability, can be used for various linear and nonlinear optical applications, especially for 3D fluorescence imaging and optical data storage, topics to be reported on separately in the future.

CHAPTER 8. CONCLUSIONS AND FUTURE WORK

8.1 Synopsis

This research focused on the development of a novel two-photon 3D optical storage system based on the modulation of the fluorescence emission of a fluorene derivative by a photochromic diarylethene, useful for recordable and rewritable data storage and the underlying science upon which to base the system. A complete photophysical characterization of two commercial diarylethenes under one- and two-photon excitation in solution was pursued. Results from this studies demonstrated relatively low two-photon absorption cross-sections (δ_{2PA}) of their open and closed photoisomers. A synthetic methodology to increase δ_{2PA} by incorporating efficient two-photon fluorene derivatives into the structure of diarylethenes was developed. This allowed the isolation of one derivative that, unfortunately, did not retain the original photochromism of the parent diarylethene. Efforts directed towards the increase of the two-photon efficiency of diarylethenes by combining RET from fluorene derivatives proved fruitful. Salient features of the studies described in this dissertation are presented as the following:

Photochemical studies of diarylethenes 1 and 2 under one- and two-photon excitation: The steady-state spectral properties of **1** in hexane, revealed a relatively complex long wavelength absorption band of the **O**-form. The broad **O**-form absorption spectrum

corresponded to three strongly overlapped electronic transitions with different orientations of their transition dipoles.

The photochromic cyclization and cycloreversion reaction quantum yields, $\Phi_{O\rightarrow C}$ and $\Phi_{C\rightarrow O}$, were determined over a broad spectral range and the optimal writing wavelengths were found for different irradiation doses. The photochemical stability of **1** was investigated in hexane, and corresponding photodecomposition quantum yields, Φ_{Ph}, were determined for different λ_{exc}. The highest photostability under one-photon excitation, $\Phi_{Ph} \approx (1.5–2)\times10^{-5}$, was obtained at $\lambda_{exc} \approx 390$ and ≈ 440 nm, useful information to enable optimization of the writing processes. The 2PA spectrum of the O-form of **1** was obtained with the maximum cross section $\approx$ 80GM at 674 nm. This corresponded to the transition with the corresponding λ_{max} of 337 nm. The two-photon induced cyclization reaction of **1** was demonstrated under picosecond excitation at λ_{exc} = 810 nm. The 2PA photocyclization quantum yield, $\Phi_{O\rightarrow C}$ 2PA $\approx 0.22\pm0.05$, was in good agreement with the corresponding value of $\Phi_{O\rightarrow C} \approx 0.23\pm0.02$ under one-photon excitation, compelling evidence that both one- and two-photon induced cyclization reaction of **1** occurs by similar means.

To ascertain the optimized experimental conditions for subsequent two-photon recording and readout, two-photon absorption cross-sections (δ_{2PA}) of the open and closed forms of diarylethene **2** were determined. The δ_{2PA} of the open form at 520 nm (corresponding to 260 nm of one-photon excitation) was 85 GM. The δ_{2PA} of the closed form of diarylethene **2** at 680, 750, and 800 nm were 150, 145, and 120 GM, respectively.

Synthesis of diarylethene-containing fluorene derivatives: the synthesis of diarylethenes **15** and **16** containing fluorene moieties (shown in Figure 4.5) was attempted in

order to increase the two-photon absorption cross-sections of the open and closed isomers of the parent diarylethene. However, the synthesis of these derivatives proved to be unsuccessfull under the synthetic conditions attempted. The synthesis of diarylethene **18** containing an unsubstituted fluorene moiety (shown in Figure 4.5) proved to be successful. Spectroscopic studies demonstrated that diarylethene derivative **18** loses its photochromic activity, since UV excitation of the open form did not generate the expected absorption spectrum of the closed photoisomer.

Increase of the nonlinear optical properties of diarylethenes by RET from fluorene derivatives: Efficient two-photon fluorene derivatives that exhibited good spectral overlap between their emission spectra and the absorption spectrum of the closed form of diarylethene **2** were selected for RET studies. Experimental observation of the fluorescence quenching of the fluorene molecules was performed in solution and in polymer films. The values of Förster's distance, R_0, for nonbonding donor - acceptor pairs were determined to be 40.3 ± 2.3 Å for fluorene **19** and 34.9 ± 2.0 Å for fluorene **20**, indicative of a RET mechanism. Critical acceptor concentrations, A_0, for mixtures of diarylethene **2** with fluorenes **19** and **20** in THF were determined to be 6.8 ± 0.4 M and 10.5 ± 0.6 M, respectively. These results demonstrated that the RET mechanism between the components in this system has potential for development of new two-photon based photochromic 3D-optical data storage devices.

Demonstration of novel RET-based two-photon 3D optical data storage: a novel two-photon 3D optical storage system was demonstrated based on the modulation of the fluorescence emission of a highly efficient two-photon absorbing fluorescent dye and a photochromic diarylethene. In this two-photon 3D optical data storage system, multiple

synthetic steps in order to attach a fluorescent dye to the photochromic diarylethene are not required. Since no covalent attachment of the fluorene is required, the electronic distribution and conformation of the photochrome is not perturbed, and the desirable photochromic properties are not lost. The diarylethene isomers (open or closed) are not directly used to read-out the stored information. Instead, the fluorescence quenching of the fluorene derivative by the closed form of the diarylethene provides a convenient mechanism for switching the fluorescence on and off. It was demonstrated that this read-out method is virtually non-destructive.

Photostability of novel fluorene derivatives with potential applications in RET-based 3D optical data storage:

Photochemical stability of two promising fluorene derivatives (**21** and **22**) was investigated under one- and two-photon excitation. Close values of Φ and Φ_{2PA} provide strong support for similar photobleaching processes of **21** and **22** for both types of excitation. An important role of molecular oxygen in the photoreactions was revelead. Results from experiments with a known $^1O_2$ photosensitizer suggesting than ground state oxygen rather than excited state oxygen is involved.

8.2 Future work

Key issues for commercial applications of this two-photon 3D optical memory system are the demonstration of 3D two-photon recording and read-out, the increase in storage capacity, and the use of a laser source with a decreased physical footprint and cost. The demonstration of two-photon recording and read out in several layers and mechanisms to increase the storage density

are already under investigation. Significant updates in our experimental set-up are underway, such as the implementation of an automatic XYZ stage, an automatic shutter for maximum control of the exposure times, and a beam expander. Objectives with higher numerical aperture will be tested in order to decrease the bit size, thereby increasing the storage density. The new automatic stage and automatic shutter will give greater 3D recording capability. As previously mentioned, key issues for commercial applications are the physical footprint of the laser source, overall electrical to optical power conversion efficiency, lifetime of the laser devices and cost. Currently under investigation is the feasibility of recording in this medium by a high-power mode-locked external cavity semiconductor laser using inverse bow-tie semiconductor optical amplifiers (SOA's), developed by Dr. Peter Delfyett. SOA's possess appropriate operating characteristics that can satisfy commercial requirements, such a small physical footprint compared to the conventional laser sources and a very long lifetime. An average output power of 700 mW has been demonstrated in continuous-wave (CW) operation while 400 mW of average power is obtained in both passive and hybrid mode-locked operation. These results show the promise of novel SOA devices for use as gain elements in external cavity semiconductor lasers. The generated output pulse characteristic from mode-locked operation is sufficient, in principle, for use in novel 3D optical data storage. Collaborative efforts currently underway will demonstrate the ability of this high-power mode-locked external cavity semiconductor to record in the proposed media.

APPENDIX A: STRUCTURES, ^{1}H SPECTRA OF FLUORENE DERIVATIVES AND ^{13}C SPECTRUM OF DIARYLETHENE 18

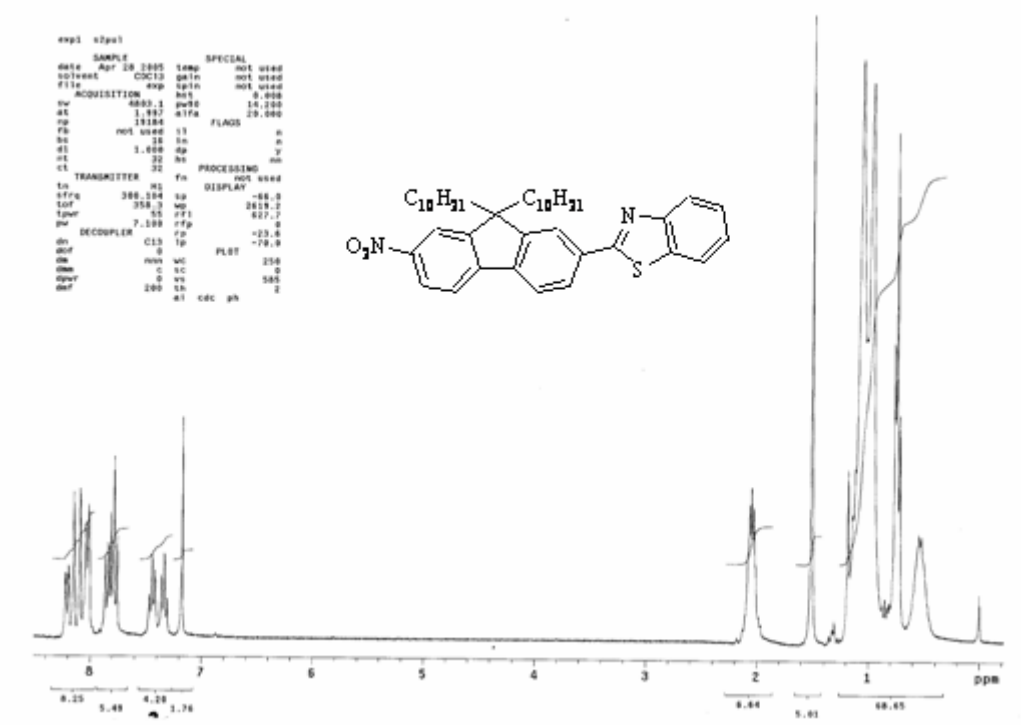

Figure A. 1. ^{1}H NMR spectrum of 2-(9,9-didecyl-7-nitrofluoren-2-yl)benzothiazole (**6**)) in $CDCl_3$ (in section 4.2.5)

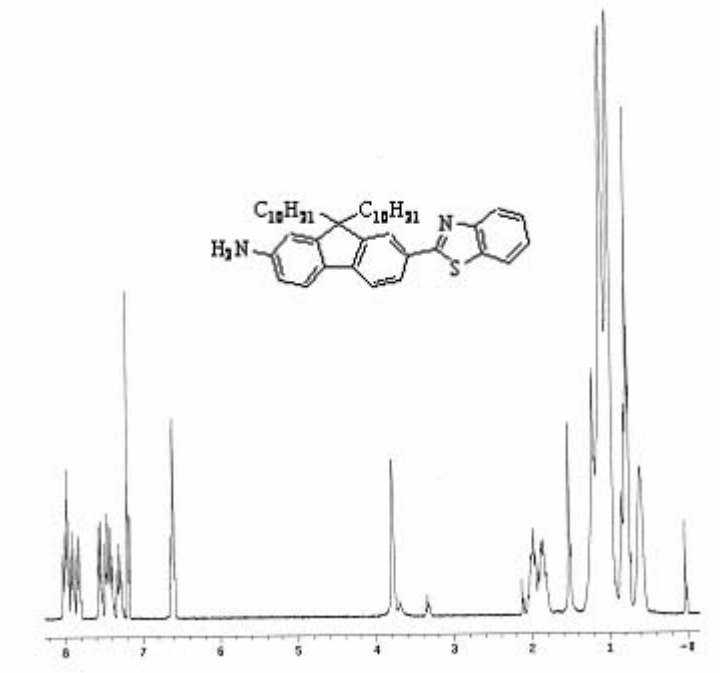

Figure A.2. ^{1}H NMR spectrum of 7-benzothiazol-2-yl-9,9-didecyl-fluoren-2-ylamine (**7**)) in $CDCl_3$ (in section 4.2.6)

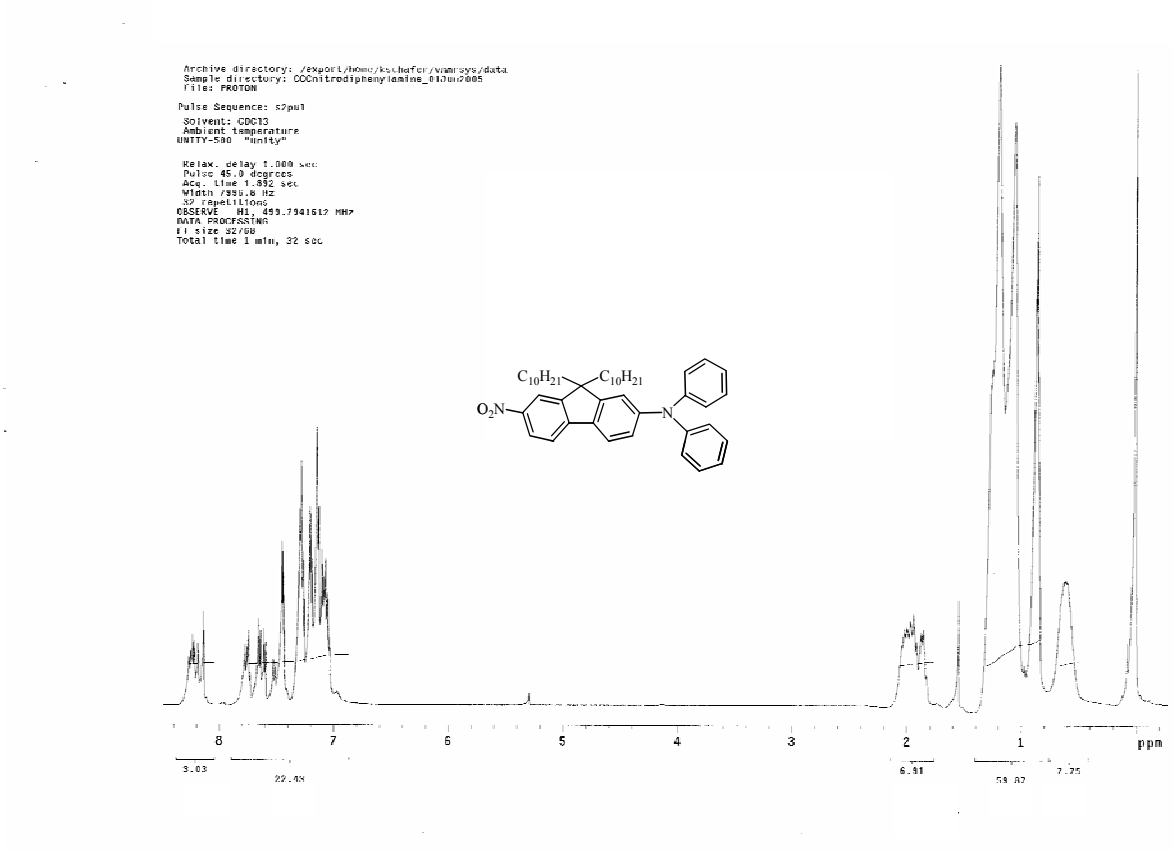

Figure A.3. ^{1}H NMR spectrum of 2-(9,9-didecyl-7-nitrofluoren-2-yl)diphenylamine (9)) in $CDCl_3$ in section 4.2.7)

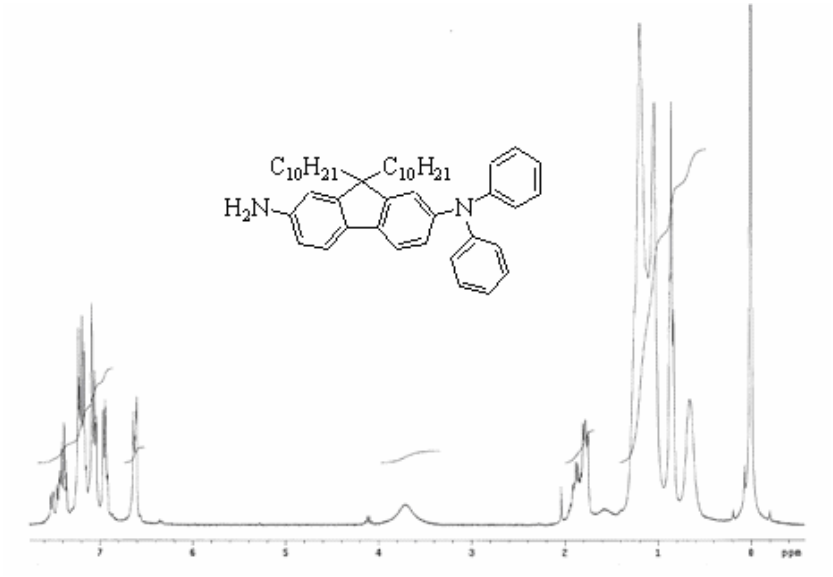

Figure A.4. ^{1}H NMR spectrum of 9,9-didecyl-N,N-diphenyl-fluorene-2,7-diamine (10)) in $CDCl_3$ (in section 4.2.8)

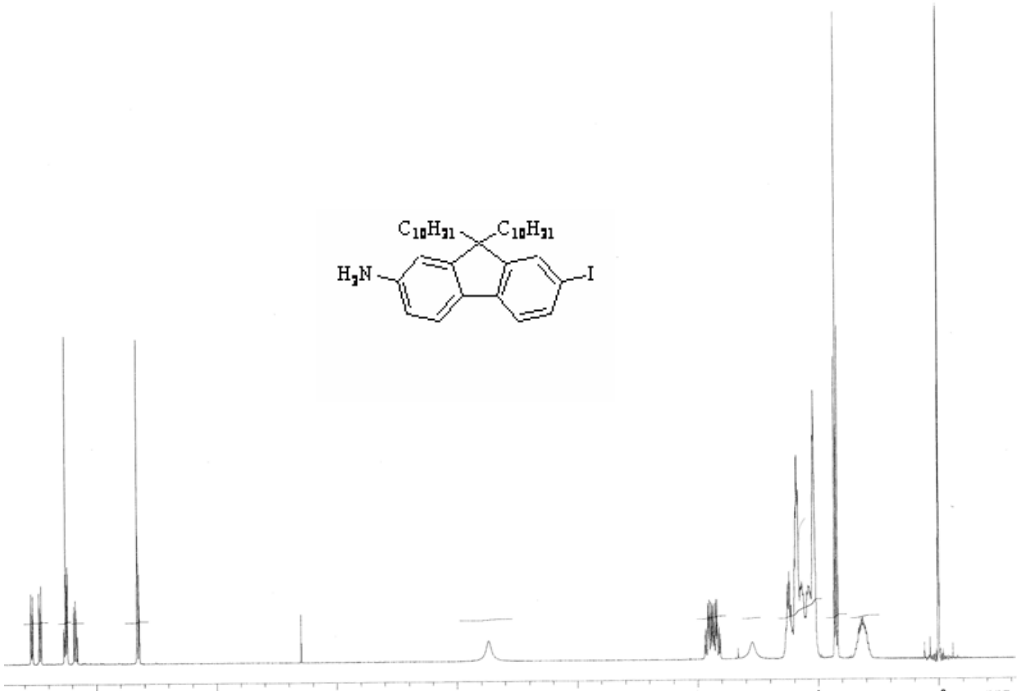

Figure A.5. ^{1}H NMR spectrum of 2-amino-7-iodo-fluorene (**11**) in $CDCl_3$ (in section 4.2.9)

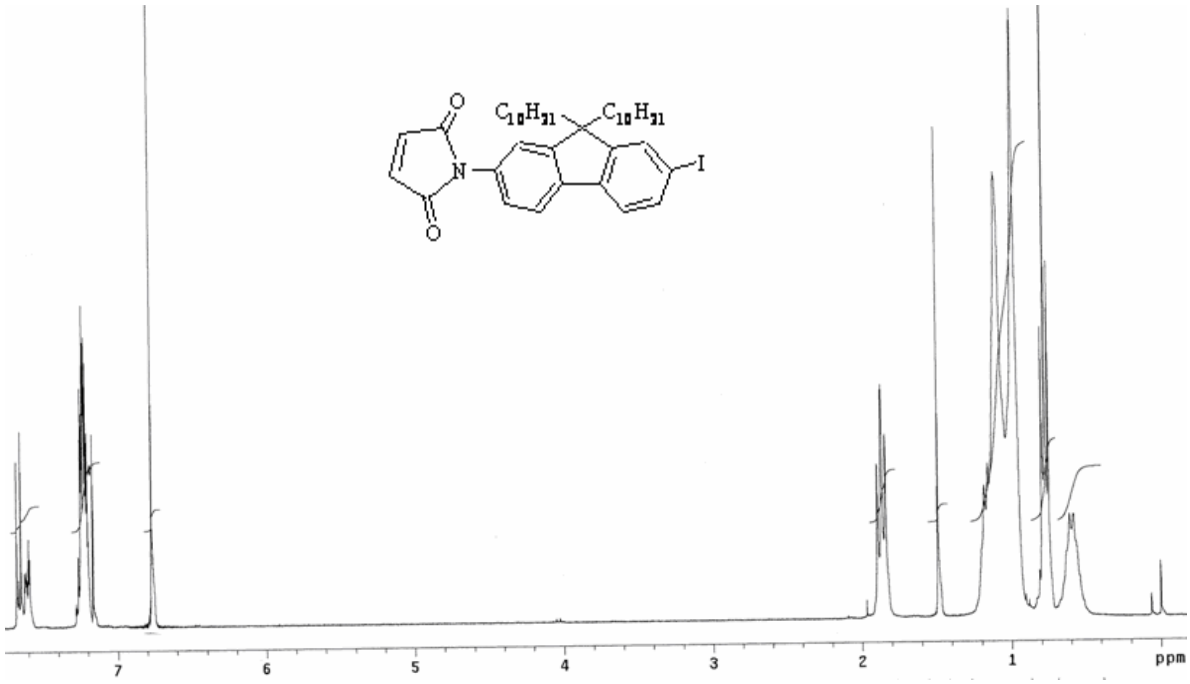

Figure A.6. ^{1}H NMR spectrum of 1-(9,9-bis-didecyl-7-iodo-9H-fluoren-2-yl)-pyrrole-2,5-dione (**13**)) in $CDCl_3$

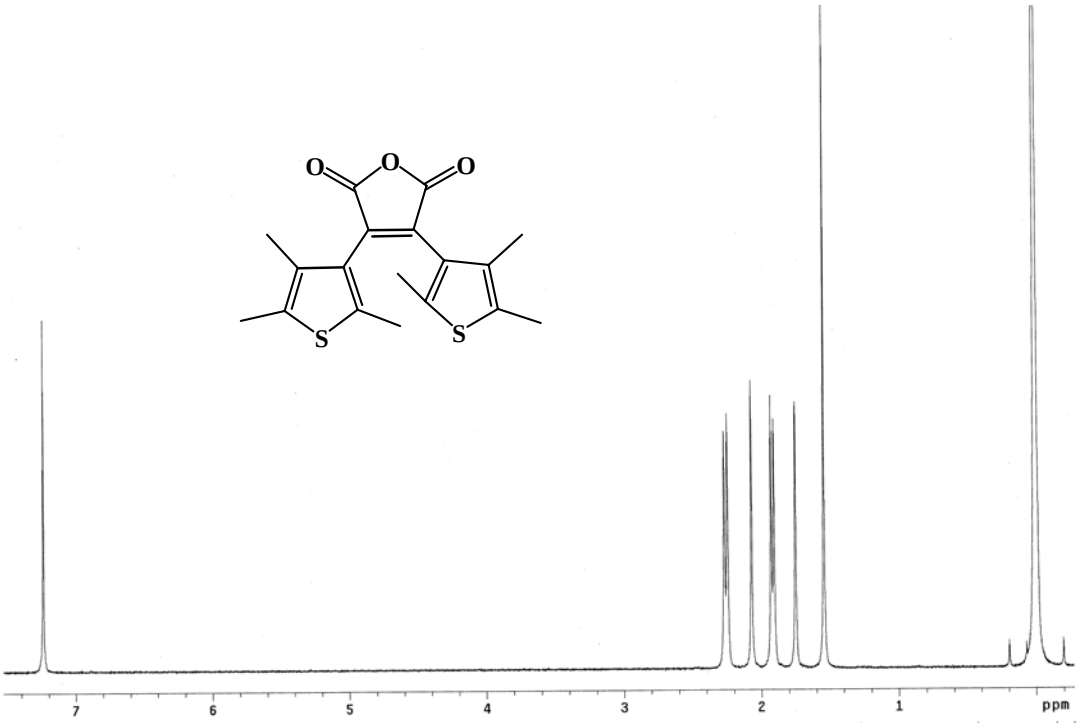

Figure A.7. ^{1}H NMR spectrum of diarylethene **14** in $CDCl_3$

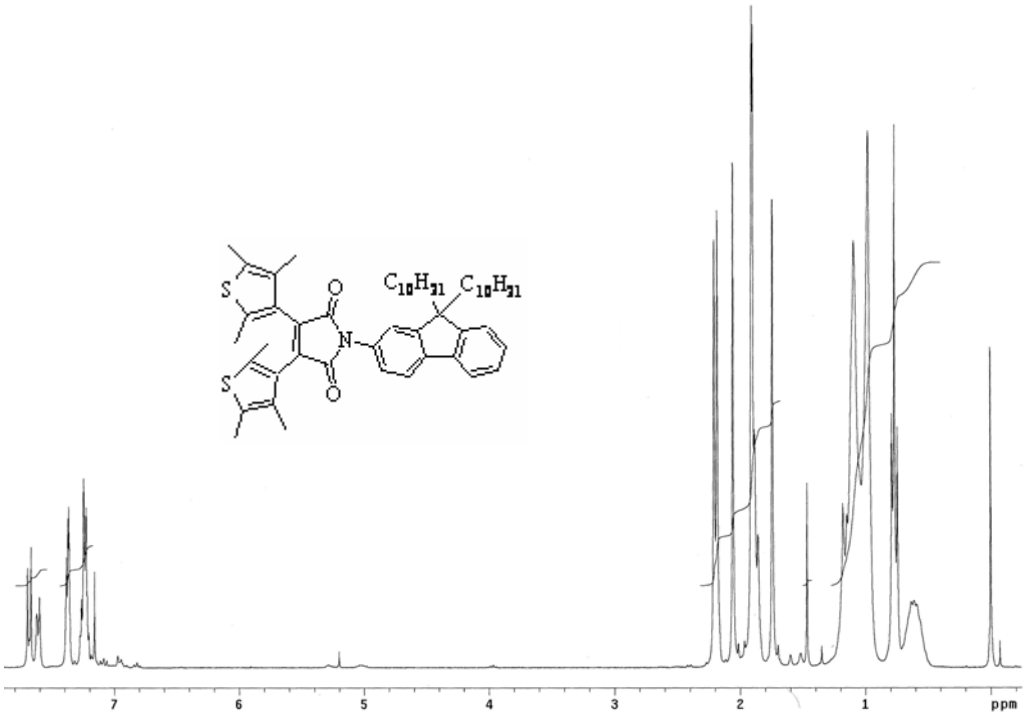

Figure A.8. ^{1}H NMR spectrum of diarylethene of 1-(9,9-Bis-decyl-9H-fluoren-2-yl)-3,4-bis-(2,4,5-trimethyl-thiophen-3-yl)-pyrrole-2,5-dione (**18**) in $CDCl_3$ (in section 4.2.11)

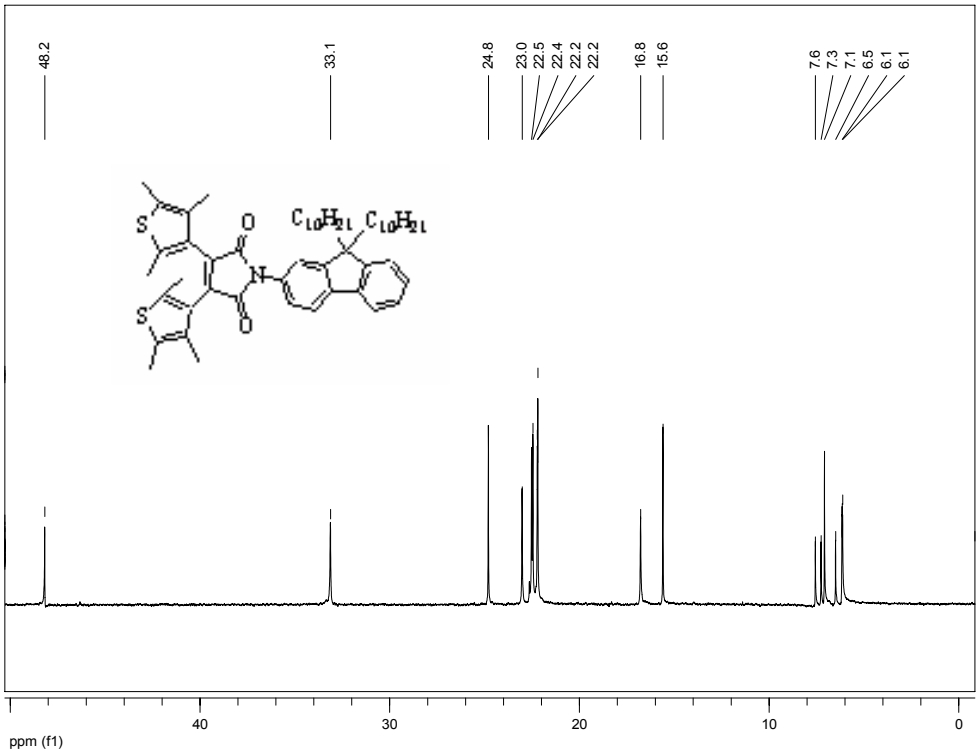

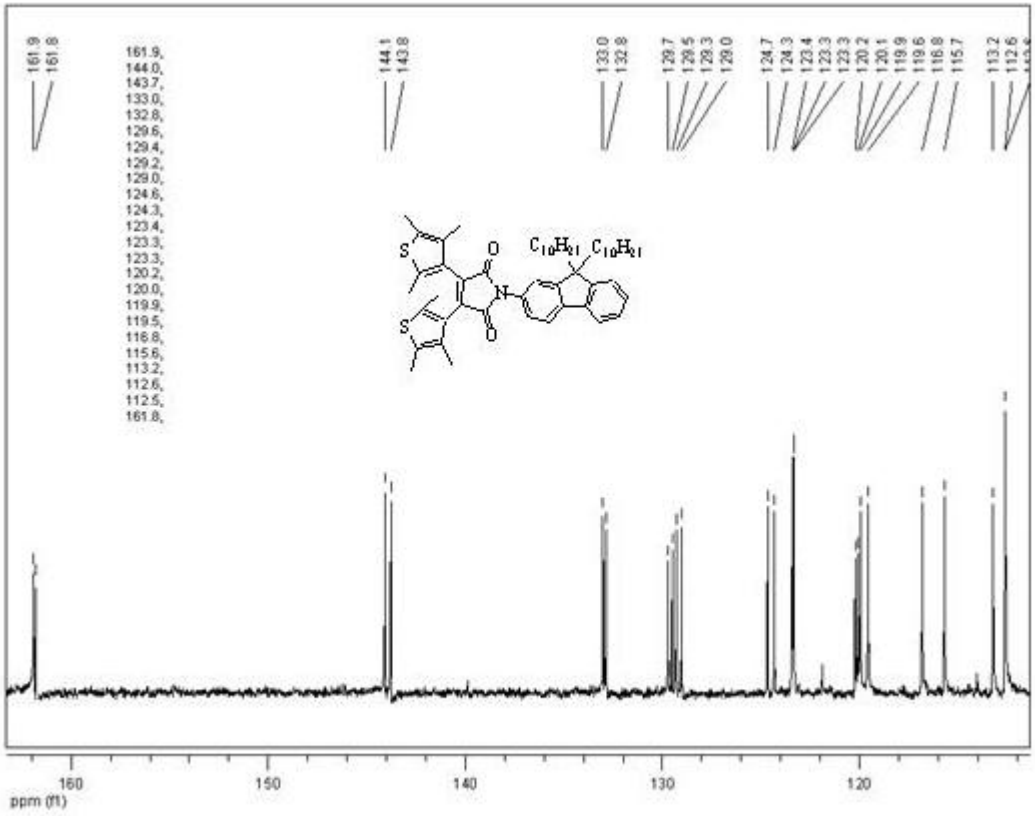

Figure A.9. ^{13}C NMR spectrum (aliphatic and aromatic regions) of diarylethene of 1-(9,9-Bis-decyl-9H-fluoren-2-yl)-3,4-bis-(2,4,5-trimethyl-thiophen-3-yl)-pyrrole-2,5-dione (**18**) in $CDCl_3$ (in section 4.2.11)

APPENDIX B: PUBLICATIONS TO DATE FROM THESIS WORK

1. C. C. Corredor, K. D. Belfield, M. V. Bondar, O. V. Przhonska, S. Yao "One- and two-photon photochemical stability of linear and branched fluorene derivatives" *J. Photochem. Photobiol. A* **2006,** *184 (1-2)*, 105-112.

2. C. C. Corredor, K. D. Belfield, M. V. Bondar, O. V. Przhonska, F. E. Hernandez, O. D. Kachkovsky "One- and two-photon photochromism of 3,4-bis-(2,4,5-trimethyl-thiophen-3-yl)furan-2,5-dione" *J. Photochem. Photobiol. A* **2006**, *184(1-2)*, 177-183.

3. C. C. Corredor, Z-L. Huang, K. D. Belfield "Two-photon 3-D optical data storage in a photochromic diarylethene polymer composite" *Polym. Preprints.* **2006**, *47(2)*, 1058-1059.

4. C. C. Corredor, Z-L. Huang, K. D. Belfield "Two-photon RET-based 3D optical data storage in a composite polymer containing a photochromic diarylethene and a fluorene dye." *Proc. SPIE* **2006**, 6330, 63300A.

5. C. C. Corredor, Z-L. Huang, K. D. Belfield "Two-Photon 3D Optical Data Storage via Fluorescence Modulation of an Efficient Fluorene Dye by a Photochromic Diarylethene" *Adv. Mater.* **2006**, 18, *21*, 2910-2914.

6. K. D. Belfield, M. V. Bondar, C. C. Corredor, F. E. Hernandez, O. V. Przhonska, S. Yao. "Two-photon photochromism of a diarylethene derivative enhanced by Förster's resonance energy transfer from two-photon absorbing fluorenes" *ChemPhysChem*, **2006**, *7*, 1-7.

7. C. C. Corredor, Z.-L. Huang, K. D. Belfield, A. R. Morales, M. V. Bondar "Bichromophoric RET-based Two-Photon Photochromic Optical Data Storage" *Adv. Func. Mat.* Submitted.

LIST OF REFERENCES

[1] a) H. Mustroph, M. Stollenwerk, V. Bressau, "Current developments in optical data storage with organic dyes" *Angew. Chem. Int. Ed.* **2006**, *45*, 2016. b) B. Tieke, M. Dekker, N. Pfeffer, R. Van Woudenberg, G-F. Zhou, I. P. D. Ubbens, "High data-rate phase-change media for the digital video recording system" *Jpn. J. Appl. Phys.* **2000**, *39*, 76.

[2] M. Abramowitz, K. R. Spring, H. E. Keller, M. W. Davidson. "Basic principles of microscope objectives". *BioTech.* **2002**, *33*, 772.

[3] M. Laurenzis, M. Foerst, P. P. H. Bolivar, H. Kurz, "Influence of hot carrier diffusion on the density limitation of optical data storage". *Jap. J. App. Phys*. **2004**, *43*, 4700.

[4] D. A. Parthenopoulos, P. M. Rentzepis "Three-dimensional optical storage memory" *Science* **1989**, *245*, 843.

[5] J. H. Strickler, W. W. Webb,"Three-dimensional optical data storage in refractive media by two-photon point excitation" *Opt. Lett*. **1991**, *16*, 1780.

[6] Y. Kawata, H. Ishitobi, S. Kawata, "Use of two-photon absorption in a photorefractive crystal for three-dimensional optical memory" *Opt. Lett.* **1998**, *23*, 756.

[7] a) M. M. Wang, S. C. Esener, F. B. McCormick, I. Çokgör**,** A. S. Dvornikov, P. M. Rentzepis "Experimental characterization of a two-photon memory" *Opt. Lett.* **1997**, *22*, 558. b) A. S. Dvornikov, Y. C. Liang, P. M. Rentzepis "Ultra-high-density non-destructive readout rewritable molecular memory" *Res. Chem. Interm.* **2004**, *30*, 545. c) A. S. Dvornikov, Y. Liang, C. S. Cruse, P. M. Rentzepis "Spectroscopy and Kinetics of a Molecular Memory with Nondestructive Readout for Use in 2D and 3D Storage Systems". *J. Phys. Chem. B* **2004**, *108*, 8652.

[8] a) M. Irie "Diarylethenes for memories and Switches" *Chem. Rev*. **2000**, 100, 1685. b) H. Tian, S. Yang "Recent progresses on diarylethene based photochromic switches" *Chem. Soc. Rev*. **2004**, *33*, 85.

[9] a) J. C. Owrutsky, H. H. Nelson, A. P. Baronavski, O.-K. Kim, G. M. Tsivgoulis, S. L. Gilat, J.-M. Lehn, "Optical properties and dynamics of a photochromic bisthienylethene in solution and in a polymer film" *Chem. Phys. Lett.* **1998**, *293*, 555. b) G.M. Tsivgoulis, J.-M. Lehn "Photonic Molecular Devices: Reversibly Photoswitchable Fluorophores for Nondestructive Readout for Optical Memory" *Angew. Chem. Int. Ed.* **1995**, *34*, 1119.

[10] a) S. Kawata, Y. Kawata, "Three-Dimensional Optical Data Storage Using Photochromic Materials" *Chem. Rev.* **2000**, *100*, 1777. b) T. B. Norsten, N. R. Branda, **"**Axially Coordinated Porphyrinic Photochromes for Non-destructive Information Processing" *Adv. Mat.* **2001**, *13*, 347. c) H. Hu, J. Pei, D. Xu, G. Qi, H. Hu, F. Zhang, X. Liu, "Multi-level optical storage in photochromic diarylethene optical disc" *Opt. Mat.* **2006**, *28*, 904.

[11] M. Göppert-Mayer "Elementary actions with two quantum leaps" *Ann. Phys.* **1931**, *9*, 273.

[12] W. Kaiser, C. G. B. Garret "Two-photon excitation in CaF_2:Eu^{2+}", *Phys. Rev. Lett.* **1961**, *7*, 229.

[13] a) G. S. He, J. D. Bhawalkar, C. F. Zhao, P. N. Prasad, "Optical limiting effect in a two-photon absorption dye doped solid matrix" *Appl. Phys. Lett.* **1995**, *67*, 2433. b) J. E. Ehrlich, X. L. Wu, I.-Y. S. Lee, Z.-Y. Hu, H. Röckel, S. R. Marder, J. W. Perry "Two-photon absorption and broadband optical limiting with bis-donor stilbenes" *Opt. Lett.* **1997**, *22*, 1843.

[14] a) W. Denk, J. H. Strickler. W. W. Webb "Two-photon laser scanning fluorescence microscopy" *Science* **1990**, *248*, 73. b) R. H. Kohler, J. Cao, W. R. Zipfel, W. W. Webb, M. R. Hanson "Exchange of protein molecules through connections between higher plant plastids". *Science* **1997**, *276*, 2039.

[15] a) S. Kawata, H.-B. Sun, T. Tanaka, K. Takada "Finer features for functional microdevices" *Nature* **2001**, *412*, 697. b) W. H. Zhou, S. M. Kuebler, K. L. Braun, T. Yu, J. K. Cammack, C. K. Ober, J. W. Perry, S. R. Marder "An efficient two-photon-generated photoacid applied to positive-tone 3D microfabrication" *Science* **2002**, *296*, 1106.

[16] a) P. K. Frederiksen; M. Jorgensen, P. R. Ogilby "Two-photon photosensitized production of singlet oxygen" *J. Am. Chem. Soc.* **2001**, 123, 1215. b) W. R. Dichtel, J. M Serin, C. Edder, J-M Frechet, M. Matuszewski, L-S Tan, T. Y. Ohulchanskyy, P. N. Prasad, "Singlet Oxygen Generation via Two-Photon Excited RET" *J. Am. Chem. Soc.* **2004**, *126*, 5380.

[17] a) J. D. Bhawalkar, G. S. He, P. N. Prasad, "Nonlinear multiphoton processes in organic and polymeric materials". *Rep. Prog. Phys.* **1996**, *59*, 1041. b) J. E. Ehrlich, S. P. Ananthavel, S. Barlow, K. Mansour, K. Mohanalingam,; S. R. Marder, J. W. Perry, M. Rumi, S. Thayumanavan, "Nonlinear optical absorption properties of bis-diarylaminobiphenyl chromophores". *Mol. Cryst. Liq. Cryst. Sci. Tech. B* **2001**, *27*, 121. c) M. Albota, D. Beljonne, J-L Bredas, J. E. Ehrlich, J-Y Fu, A. A. Heikal, S. E. Hess, T. Kogej, M. D. Levin, S. R. Marder, D. McCord-Maughon, J. W. Perry, H. Rockel, M. Rumi, G. Subramaniam, W. W. Webb, X-L Wu, C. Xu, "Design of organic molecules with large two-photon absorption cross sections". *Science*, **1998**, 281, 1653.

[18] a) A. T. Yeates, **"**Nonlinear Optical Transmission and Multiphoton Processes in Organics III". *Proc. SPIE.* **2005,** 5934. b) P. Cronstrand, Y Luo, H. Aagren, "Multi- photon absorption of molecules" *Adv. Quant. Chem.* **2005**, *50*, 1. c) E. W. Van Stryland L. L. Chase, "Two - photon absorption. Inorganic materials". *CRC Handb. Laser Sci. Technol.* **1994,** *2*, 299.

[19] J. H. Strickler, W. W. Webb "Two-photon excitation in laser scanning fluorescence microscopy" *Proc. SPIE* **1991**, *1398*, 107.

[20] a) S. Kawata, T. A. Tanaka, Y. Hashimoto, Y. Kawata, "Three-dimensional confocal optical memory using photorefractive materials" *Proc. SPIE* **1993**, *2042*, 314. b) H. Ueki, Y. Kawata, S. Kawata, "Three-dimensional optical bit-memory recording and reading with a photorefractive crystal: Analysis and experiment" *Appl. Opt.* **1996**, *35*, 2457.

[21] a) A. Toriumi, J. M. Herrmann, S. Kawata "Nondestructive readout of a three-dimensional photochromic optical memory with a near-infrared differential phase-contrast microscope". *Opt. Lett.* **1997**, *22*, 555 b) A. Toriumi, S. Kawata, M. Gu "Reflection confocal microscope readout system for three-dimensionalphotochromic optical data storage" *Opt. Lett.* **1998**, *23*, 1924.

[22] a) D. Day, M. Gu, A. Smallridge, "Use of two-photon excitation for erasable-rewritable three-dimensional bit optical data storage in a photorefractive polymer". *Opt. Lett.* **1999**, *24*, 948. b) D. Day, M. Gu, A. Smallridge, "Rewritable 3D bit optical data storage in a PMMA-based photorefractive polymer". *Adv. Mater.* **2001**, *13*, 1005. c) D. Day, M. Gu, A. Smallridge, "Review of optical data storage". *Top. Appl. Phys.* **2003**, *86*, 1.

[23] H. E. Pudavar, M. Joshi, P. Prasad, B. Reinhardt "High-density three-dimensional optical data storage in a stacked compact disk format with two-photon writing and single photon readout" *Appl. Phys. Lett.* **1999**, *74*, 1338.

[24] a) K. D. Belfield, K. J. Schafer "A New Photosensitive Polymeric Material for WORM Optical Data Storage Using Multichannel Two-Photon Fluorescence Readout" *Chem. Mater.* **2002**, *14*, 3656. b) K. D. Belfield "Photosensitive polymeric material for WORM optical data storage with two-photon fluorescent readout" U.S. patent 7001708 2006, 33 pp. c) K. D. Belfield, Y. Liu, F. E. Hernandez "Two-photon photochromism in a fulgide-containing polymer for holographic recording" *Polym. Preprints* **2002**, *43*, 612.

[25] S. Kobatake, M. Irie "Photochromism" *Ann. Rep. Prog. Chem. C.* **2003**, *99*, 277.

[26] a) E. Fischer, Y. Hirshberg "Formation of colored forms of spirans by low-temperature irradiation" *J. Chem Soc.* **1952**, 4522. b) Y. Hirshberg, "Reversible formation and eradication of colors by irradiation at low temperatures. A photochemical memory model" *J. Am. Chem. Soc.* **1956**, *78*, 2304.

[27] a) G. Berkovic, V. Krongauz, V. Weiss, "Spiropyrans and spirooxazines for memories and switches" *Chem. Rev.* **2000**, *100*, 1741. b) Y. Liang, A. S. Dvornikov, P. M. Rentzepis, "Synthesis and Properties of Photochromic Fluorescing 2-Indolyl Fulgide and Fulgimide Copolymers" *Macromolecules* **2002,** *35*, 9377. c) F. Wei, H. Kun, W. Mei-Xiang "Photophysical characteristics of polyaniline with photochromic azobenzene side groups" *Chinese Phys.* **2005,** *14*, 306.

[28] a) N. Tamai, H. Miyasaka, "Ultrafast dynamics of photochromic systems" *Chem. Rev.* **2000**, *100*, 1875. b) M. Irie, M. Mohri "Thermally irreversible photochromic systems. Reversible photocyclization of diarylethene derivatives" *J. Org. Chem.* **1988**, *53*, 803. c) H.-G. Cho, B.-S. Cheong "Theoretical Investigation of 2,3-bis(2,4,5-trimethyl-3-thienyl)maleic anhydride: A Thermally Irreversible Photochromic System" *Bull. Korean Chem. Soc.* **1998**, *19*, 308. d) K. Higashiguchi, K. Matsuda, S. Kobatake, T. Yamada, T. Kawai, M. Irie "Fatigue Mechanism of Photochromic 1,2-Bis(2,5-dimethyl-3-thienyl)perfluorocyclopentene" *Bull. Chem. Soc. Jpn.* **2000**, *73*, 2389.

[29] a) H. Miyasaka, S. Araki, A. Tabata, T. Nobuto, N. Mataga, M. Irie "Picosecond laser photolysis studies on photochromic reactions of 1,2-bis(2,4,5-trimethyl-3-thienyl)maleic anhydride in solutions" *Chem. Phys. Lett.* **1994**, *230,* 249. b) H. Miyasaka, T. Nobuto, M. Murakami, A. Itaya, N. Tamai, M. Irie "Solvent Viscosity Effects on Photochromic Reactions of a Diarylethene Derivative As Revealed by Picosecond Laser Spectroscopy" *J. Phys. Chem. A* **2002**, *106*, 8096.

[30] a) M. Irie, K. Sayo "Solvent Effects in the Photochromic Reactions of Diarylethenes Derivatives" *J. Phys. Chem.* **1992**, *96*, 7671. b) K. Kasatani, T. Fujiwaki "Photochromic cyclization reaction efficiency and fluorescence of dithienylethenes in polymer films and organic solvents" *ITE Lett. Batteries, New Technol. Med.* **2001**, *2*, 215. c) K. Kasatani, S. Kambe, M. Irie "Photochromic reaction and fluorescence of dithienylethenes in the solid state" *J. Photochem. Photobiol. A: Chem.* **1999**, *122*, 11.

[31] a) K. Uchida, E. Tsuchida, Y. Aoi, S. Nakamura, M. Irie "Substitution effect on the coloration quantum yield of a photochromic bisbenzothienylethene" *Chem. Lett.* **1999**, *1*, 63. b) S. Kobatake, M. Yamada, T. Yamada, M. Irie "Photochromism of 1,2-bis(2-methyl-6-nitro-1-benzothiophen-3-yl)-perfluorocyclopentene in a single-crystalline phase: dichroism of the closed-ring form isomer" *J. Am. Chem. Soc.* **1999**, *121*, 8450. c) T. Yamaguchi, M. Irie "Photochromism of bis(2-alkyl-1-benzothiophen-3-yl) perfluorocyclopentene derivatives" *J. Photochem. Photobiol. A* **2006**, *178*, 162. d) Y.-C. Jeong, S. I. Yang, K-H Ahn, E. Kim "Highly fluorescent photochromic diarylethene in the closed-ring form" *Chem. Comm.* **2005**, *19*, 2503.

[32] a) Y. Atassi, J. Chauvin, J. A. Delaire, J.-F. Delouis, I. Fanton-Maltey, K. Nakatani "Photoinduced manipulations of photochromes in polymers: Anisotropy, modulation of the NLO properties and creation of surface gratings" *Pure Appl. Chem.* **1998**, *70*, 2157. b) J. A. Delaire, I. Fanton-Maltey, J. Chauvin, K. Nakatani, M. Irie "Nonlinear optical properties of diarylethenes" *Mol. Cryst. Liq. Cryst. Sci. Tech. A***. 2000**, *345*, 233.

[33] Z. Sekkat, H. Ishitobi, S. Kawata "Two-photon isomerization and orientation of photoisomers in thin films of polymer" *Opt. Comm.* **2003**, *222*, 269.

[34] a) S. Saita, T. Yamaguchi, T. Kawai, M. Irie "Two-Photon Photochromism of Diarylethene Dimer Derivatives" *ChemPhysChem.* **2005**, *6*, 2300. b) M. Shigeiwa, S. Maeda, H. Gorohmaru, S. Imamura, M. Irie "Development of Photochromic Two-Photon Absorption Dyes" *Mol. Cryst. Liq. Cryst.* **2005**, *430,* 173.

[35] a) Y. C. Liang, A. S. Dvornikov, P. M. Rentzepis "Nonvolatile read-out molecular memory" *Proc. Nat. Acad. Sci.* **2003**, *100*, 8109. b) J. Ern, A. T. Bens, H.-D. Martin, S. Mukamel, S. Tretiak, K. Tsyganenko, K. Kuldova, H. P. Trommsdorff, C. Kryschi "Reaction Dynamics of a Photochromic Fluorescing Dithienylethene" *J. Phys. Chem. A* **2001***, 105*, 1741. c) M. Irie, T. Fukaminato, T. Sasaki, N. Tamai, T. Kawai "A digital fluorescent molecular photoswitch" *Nature* **2002**, *420*, 759. d) H. Tian, S. Wang "Photochromic bisthienylethene as multi-function switches" *Chem. Commun.* 2007 DOI: 10.1039/b610004j

[36] a) L. Giordano, T. M. Jovin, M. Irie, E. A. Jares-Erijman "Diheteroarylethenes as Thermally Stable Photoswitchable Acceptors in Photochromic Fluorescence Resonance Energy Transfer (pcFRET)" *J. Am. Chem. Soc.* **2002**, *124*, 7481. b) D. V. Kozlov, F. N. Castellano "Photochemically Reversible Luminescence Lifetime Switching in Metal-Organic Systems" *J. Phys. Chem. A* **2004**, *108*, 10619.

[37] a) R. Gvishi, Z. Kotler, G. Berkovic, P. Krief, M. Sigalov, L. Shapiro, D. Huppert, V. Khodorkovsky, V. Lokshin, A. Samat "Resonance energy transfer in a novel two-component system: two-photon fluorophore and a photo-chromic acceptor molecule" *Proc. SPIE* **2005**, *5724,* 13. b) D. W. Brousmiche, J. M. Serin, J. M. J. Frechet, G. S. He, T-C Lin, S. J. Chung, P. N. Prasad "Fluorescence Resonance Energy Transfer in a Novel Two-Photon Absorbing System" *J. Am. Chem. Soc.* **2003**, *125*, 1448. c) D. W. Brousmiche, J. M. Serin, J.-M. Frechet, G. S. He, T-C Lin, S-J Chung, P. N. Prasad, R. Kannan, L.-S. Tan "Fluorescence Resonance Energy Transfer in Novel Multiphoton Absorbing Dendritic Structures" *J. Phys. Chem. B* **2004**, *108*, 8592.

[38] a) I. Wang, P. L. Baldeck, C. Martineau, G. Lemercier, J.-C. Mulatier, C. Andraud, "Photoinitiators for polymerization at 532 nm and 1064 nm by two-photon absorption; evaluation of their initiation efficiency using microlasers" *Nonlin. Opt., Quant. Opt.* **2004**, *32*, 161. b) Y. Morel, A. Irimia, P. Najechalski, Y. Kervella, O. Stephan, P. L. Baldeck, C. Andraud "Two-photon absorption and optical power limiting of bifluorene molecule" *J. Chem. Phys.* **2001**, *114*, 5391. c) K. D. Belfield, K. J. Schafer, Y. Liu, J. Liu, X. Ren, E. W. Van Stryland "Multiphoton-absorbing organic materials for microfabrication, emerging optical applications and non-destructive three-dimensional imaging" *J. Phys. Org. Chem.* **2000**, *13*, 837.

[39] a) K. D. Belfield, A. R. Morales, J. M. Hales, D. J. Hagan, E. W. Van Stryland, V. M. Chapela, J. Percino "Linear and Two-Photon Photophysical Properties of a Series of Symmetrical Diphenylaminofluorenes" *Chem. Mater.* **2004**, *16*, 2267. b) K. D. Belfield, A. R. Morales, B-S. Kang, J. M. Hales, D. J. Hagan, E. W. Van Stryland, V. M. Chapela, J. Percino "Synthesis, Characterization, and Optical Properties of New Two-Photon-Absorbing Fluorene Derivatives" *Chem. Mat.* **2004**, *16*, 4634. c) S. Yao, K. J. Schafer-Hales, I. Cohanoschi, F. E. Hernandez, K. D. Belfield "A water-soluble diaminostilbene derivative as a two-photon fluorescent probe" *Synlett* **2006**, *12*, 1863. d) A. R. Morales, K. D. Belfield, J. M. Hales, E. W. Van Stryland, D. J. Hagan "Synthesis of Two-Photon Absorbing Unsymmetrical Fluorenyl-Based Chromophores" *Chem. Mat.* **2006**, *18*, 4972. e) S. Yao, K. D. Belfield, "Synthesis of Two-Photon Absorbing Unsymmetrical Branched Chromophores through Direct Tris(bromomethylation) of Fluorene" *J. Org. Chem.* **2005**, 70, 5126. f) K. D. Belfield, S. Yao, A. R. Morales, J. M. Hales, D. J. Hagan, E. W. Van Stryland, V. M. Chapela, J. Percino "Synthesis and characterization of novel rigid two-photon absorbing polymers" *Polym. Adv. Tech.* **2005**, *16*, 150. g) J. M. Hales "Chemical structure-nonlinear optical property relationships for a series of two-photon absorbing fluorene molecules" Ph. D. Dissertation, University of Central Florida Orlando, Fla., 2004.

[40] a) C. L. Droumaguet, O. Mongin, M. H. V. Werts, M. Blanchard-Desce, "Towards ''smart'' multiphoton fluorophores: strongly solvatochromic probes for two-photon sensing of micropolarity" *Chem. Commun.* **2005**, *22*, 2802. b) S. I. Kato, T. Matsumoto, M. Shigeiwa, H. Gorohmaru, S. Maeda, T. Ishi-I, S. Mataka "Novel 2,1,3-benzothiadiazole-based red-fluorescent dyes with enhanced two-photon absorption cross-sections" *Chem. Eur. J.* **2006**, *12*, 2303.

[41] a) F.-J. Kao, Y.-M. Wang, J.-C. Chen, P.-C. Cheng, R.-W. Chen, B.-L. Lin "Photobleaching under single photon and multi-photon excitation: chloroplasts in protoplasts from *Arabidopsis thaliana*" *Opt. Commun.* **2002**, *201*, 85. b) P. D. Wood, L. J. Johnston "Photoionization and Photosensitized Electron-Transfer Reactions of Psoralens and Coumarins" *J. Phys. Chem. A* **1998**, *102*, 5585. c) P. S. Ditrich, P. Schwille, *Appl. Phys. B* "Photobleaching and stabilization of. fluorophores used for single-molecule analysis with one- and two-photon excitation" **2001**, *73*, 829.

[42] J. R. Lakowicz, Principles of Fluorescence Spectroscopy, Kluwer Academic/Plenum, New York, 1999.

[43] K. Kasatani, T. Fujiwaki "Photochromic cyclization reaction efficiency and fluorescence of dithienylethenes in polymer films and organic solvents" *ITE Lett. Batteries, New Technol. Med.* **2001**, *2*, 215.

[44] K. D. Belfield, M. V. Bondar, O. V. Przhonska, K. J. Schafer "Photochemical properties of (7-benzothiazol-2-yl-9,9-didecylfluoren-2-yl)diphenylamine under one- and two-photon excitation" *J. Photochem. Photobiol. A.* **2004**, *162*, 569.

[45] C. Xu, W. W. Webb "Measurement of two-photon excitation cross sections of molecular fluorophores with data from 690 to 1050 nm" *J. Opt. Soc. Am. B* **1996**, *13*, 481.

[46] M. Sheik-Bahae, A. A. Said, T. Wei, D. J. Hagan, E. W. Van Stryland "Sensitive measurement of optical nonlinearities using a single beam" *IEEE J. Quant. Electr.* **1990**, *26*, 760.

[47] K. D. Belfield, K. J. Schafer, W. Mourad, B. A. Reinhardt "Synthesis of new two-photon absorbing fluorene derivatives via Cu-mediated Ullmann condensations" *J. Org. Chem.* **2000**, *65*, 4475.

[48] a) M. M. Krayushkin, V. N. Yarovenko, S. L. Semenov, I. V. Zavarzin, A. Y. Martynkin, B. M. Uzhinov "Photochromic dihetarylethenes. 19. Synthesis of 1,2-dihetarylethenes on the basis of thieno[3,2-*b*]pyrroles linked by a maleimide bridge" *Russ. Chem. Bull.* **2003**, *52*, 1814. b) P. Y. Reddy, S. Kondo, T. Toru, Y. Ueno "Lewis acid and hexamethyldisilizane-promoted efficient synthesis of N-alkyl and N-arylimide derivatives" *J. Org. Chem.* **1997**, *62*, 2652. c) H. Tian, H.-Y. Tu "Synthesis and photochromic properties of new bisthienylethene derivatives and a copolymer" *Adv. Mat.* **2000**, 12, 1597. d) B. Chen, M. Wang, C. Li, H. Xia, H. Tian "New photochromic copolymers with bisthienylethene pendant groups" *Synt. Met.* **2003**, *135-136*, 491. e) X. Li, H. Tian "High-content pendant photochromic copolymer with dithienylethene/fluorene 2:1 mole ratio" *Macromol. Chem. Phys*. **2005**, *206*, 1769.

[49] K. D. Belfield, J. Wang "Modified Horner-Emmons reaction of polymeric phosphonates: versatile synthesis of pendant stilbene-containing polymers" *J. Polym. Sci., Pol. Chem.* **1995**, *33*, 1235.

[50] K. D. Belfield, M. V. Bondar, C. C. Corredor, F. E. Hernandez, O. V. Przhonska, S. Yao. "Two-photon photochromism of a diarylethene derivative enhanced by Förster's resonance energy transfer from two-photon absorbing fluorenes" *ChemPhysChem* **2006**, *7*, 1-7.

[51] a) T. Virgili, D. G. Lidzey, D. D. C. Bradley, *Adv. Mater.* **2000**, 12, 58-62. b) G. Cerullo, S. Stagira, M. Zavelani-Rossi, S. De Silvestri, T. Virgili, D. G. Lidzey, D. D. C. Bradley, *Chem. Phys. Lett.* **2001**, 335, 27.

[52] a) S. Luo, K. Chen, L. Cao, G. Liu, Q. He, G. Jin, D. Zeng, Y. Chen, "Photochromic diarylethene for rewritable holographic data storage". *Opt. Expr.* **2005**, 13, 3123. b) M. Irie, M. Ohata, K. Morimitsu, "Photochromic materials, their manufacture, and information rewritable devices". *Jpn. Kokai Tokkyo Koho* **2003**, 9 pp. c) K. Taniguchi, K. Sakamura, F. Matsui, "Rewritable photochromic optical recording mediums" *Jpn. Kokai Tokkyo Koho* **1997**, 11 pp. d) M. Irie, "Rewritable optical recording method". *Jpn. Kokai Tokkyo Koho* **1994**, 4 pp. e) F. Tatezono, T. Harada, Y. Shimizu, M. Ohara, M. Irie "Photochromic rewritable memory media: a new nondestructive readout method". *Jpn. J. App. Phys.* **1993**, 32, 3987.

[53] a) M. P. Ligocki, C. Leuenberger, J. F. Pankow "Trace organic compounds in rain - II. Gas scavenging of neutral organic compounds" *Atm. Environ.* **1985**, *19,* 1609. b) R. M. Dickhut, K. E. Gustafson "Atmospheric Washout of Polycyclic Aromatic Hydrocarbons in the Southern Chesapeake Bay Region" *Environ. Sci. Technol.* **1995**, *29*, 1518.

[54] J. Sabate, J. M. Bayona, A. M. Solanas "Photolysis of PAHs in aqueous phase by UV irradiation" *Chemosphere* **2001**, *44*, 119.

[55] a) L. Moeini-Nombel, S. Matsuzawa, *J. Photochem. Photobiol. A* **1998**, *119*, 15. b) J. T. Barbas, M. E. Sigman, R. Arce, R. J. Dabestani "Spectroscopy and photochemistry of fluorene at a silica gel/air interface" *J. Photochem. Photobiol. A: Chem.* **1997**, *109*, 229.

[56] a) J. W. Baur, M. D. Alexander, J. M. Banach, L. R. Denny, B. A. Reinhardt, R. A. Vaia, P. A. Fleitz, S. M. Kirkpatrick, *Chem. Mater.* **1999**, *11*, 2899. b) J.-D. Guo, Y. Luo, *J. Mol. Struct.*, **2003**, *635*, 1.

[57] K. D. Belfield, S. Yao, J. M. Hales, M. V. Bondar, D. J. Hagan, E. W. Van Stryland "Novel two-photon absorbing branched architectures" *Polym. Mat.: Sci. Engin.* **2004**, *91*, 340.

[58] a) K. D. Belfield, C. C. Corredor, A. R. Morales, M. A. Dessources, F. E. Hernandez "Synthesis and Characterization of New Fluorene-Based Singlet Oxygen Sensitizers" *J. Fluorescence* **2006**, *16*, 105. b) K. D. Belfield, M. V. Bondar, O. V. Przhonska, "Singlet Oxygen Quantum Yield Determination for a Fluorene-Based Two-Photon Photosensitizer" *J. Florescence* **2006**, *16*, 111.

[59] a) K. D. Belfield, M. V. Bondar, O. V. Przhonska, K. J. Schafer "Photostability of a series of two-photon absorbing fluorene derivatives" *J. Photochem. Photobiol. A: Chem.* **2004**, *162*, 489. b) K. D. Belfield, M. V. Bondar, Y. Liu, O. V. Przhonska "Photophysical and photochemical properties of 5,7-dimethoxycoumarin under one- and two-photon excitation" *J. Phys. Org. Chem.* **2003**, *16*, 69.

[60] K. D. Belfield, M. V. Bondar, I. Cohanoschi, F. E. Hernandez, O. D. Kachkovsky, O. V. Przhonska, S. Yao "Excited-state absorption and anisotropy properties of two-photon absorbing fluorene derivatives" *Appl. Opt.* **2005**, *44*, 7232.

[61] C. Eggeling, L. Brand, C. A. M. Seidel "Laser-induced fluorescence of coumarin derivatives in aqueous solution: photochemical aspects for single molecule detection" *Bioimaging* **1997**, *5*, 105.

[62] J. B. Gilbert, "Essentials of molecular photochemistry", Blackwell Science Ltd. 1991, chapters 6, 9 and 11.